Bayesian network analysis reveals MTHFD2 as a key driver of oxidized phospholipid induced amino acid reprogramming

Dissertation

zur Erlangung des Doktorgrades

der Naturwissenschaften

vorgelegt beim Fachbereich

Biochemie, Chemie und Pharmazie

der Johann Wolfgang Goethe-Universität

in Frankfurt am Main

von Frau Juliane Hitzel (geb. Stribrny)

Frankfurt am Main, 2017

vom Fachbereich Biochemie, Chemie und Pharmazie der
Johann Wolfgang Goethe-Universität als Dissertation angenommen.

Dekan	Prof. Dr. Clemens Glaubitz (Johann Wolfgang Goethe-Universität, Frankfurt)
Gutachter	Prof. Dr. Eric Geertsma (Johann Wolfgang Goethe-Universität, Frankfurt)
	Prof. Jun Zhu, PhD (Icahn School of Medicine at Mount Sinai, New York)

Datum der Disputation:

Contents

1 Introduction

1.1 Oxidized phospholipids in cardiovascular diseases

1.1.1 Membrane lipids give rise to a variety of oxidation products

A healthy endothelium maintains the vascular homeostasis and limits the development of atherosclerosis (Gimbrone & García-Cardeña, 2016). Activation and subsequent dysfunction of the endothelium leads to a vicious cycle of reactive oxygen species formation, inflammation and recruitment of monocytes. Reactive oxygen species (ROS) generated by inflammatory cells and the endothelium promote the oxidation of phospholipids contained in cellular membranes and lipoproteins (Nègre-Salvayre *et al*, 2017). Such oxidized phospholipids further promote endothelial cell activation during the development of atherosclerosis. The process of lipid oxidation is well studied for polyunsaturated fatty acid (PUFA) side chains of phospholipids in cellular membranes and lipoproteins (Bochkov *et al*, 2010). Non-enzymatic ROS-induced lipid peroxidation yields a diverse array of oxidized phospholipid (oxPL) species. OxPLs contain phosphatidylcholine, phosphatidylserine or phosphatidylethanolamine as headgroup, a saturated fatty acid of variable length at the *sn*-1 position and the polyunsaturated fatty acid chain at *sn*-2 position (Lee *et al*, 2012b). Oxidized 1-palmitoyl-2-arachidonoyl-sn-glycero-3-phosphocholine (oxPAPC) is a mixture of oxPLs which contains an arachidonate in the *sn*-2 position (Figure 1).

1.1.2 Oxidized phospholipids are associated with atherosclerosis

These oxPLs accumulate in atherosclerotic lesions and sites of chronic inflammation (Tsimikas *et al*, 2010). Furthermore, higher levels of oxPLs were oberserved in plasma from hyperlipidemic animals and levels of oxPLs in human plasma were found to be associated with increased risk for coronary artery disease (CAD) (Tsimikas *et al*, 2010; Bochkov *et al*, 2010; Podrez *et al*, 2007). Additionally, oxPLs can be enzymatically produced by myeloperoxidase and 12/15 lipoxygenase and expression of these enzymes is associated with atherosclerosis in mice (Nicholls & Hazen, 2009; Cyrus *et al*, 2001). Increased levels of oxPLs were also observed in patients with inflammatory diseases which possess impact on cardiovascular health as systemic lupus erythematosus and rheumatoid arthritis (Hahn & McMahon, 2008). Furthermore, particles in air pollutants react with oxPAPC which results in activation of pro-atherogenic pathways in endothelial cells (Gong *et al*, 2007).

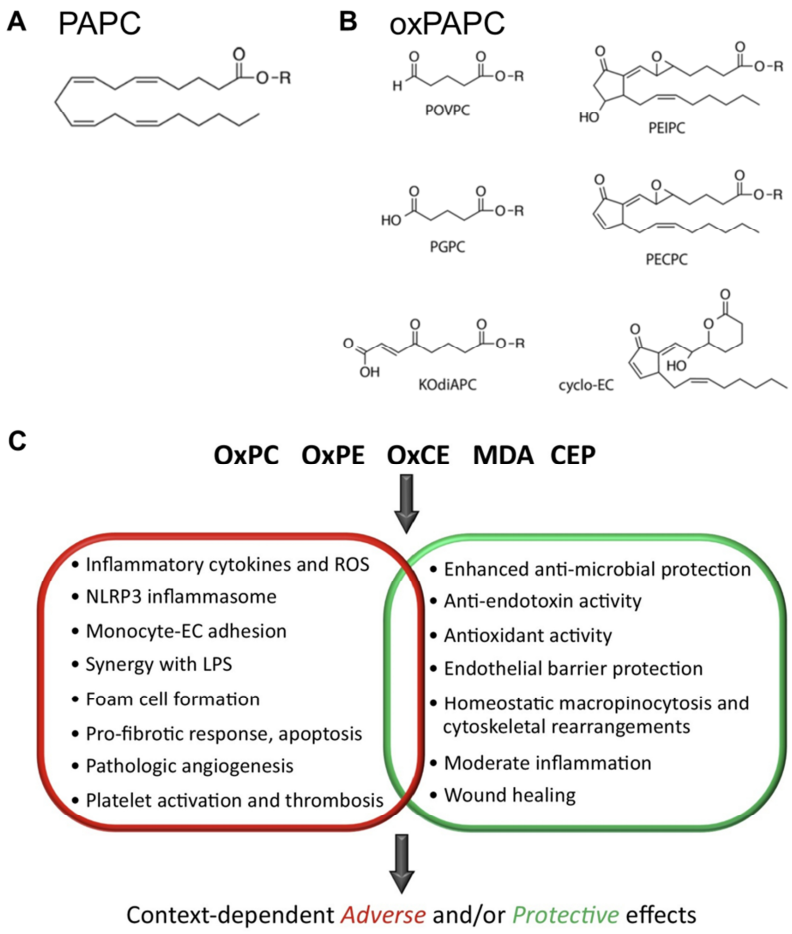

Figure 1: Chemical structure of oxPAPC and effects of oxPLs.

A: 1-palmitoyl-2-arachidonoyl-sn-glycero-3-phosphocholine (PAPC) is an arachidonic acid containing phospholipid. Only the sn-2 fatty acid is depicted and R represents the head group PAPC. B: Well characterized oxidized products of PAPC (oxPAPC). 1-palmitoyl-2-(5-oxovaleroyl)-sn-glycero-3-phospho-choline (POVPC), 1-palmitoyl-2-glutaryl-sn-glycero-3-phosphocholine (PGPC) and 1-palmitoyl-2-(5-keto-6-octene-dioyl)-sn-glycero-3-phosphocholine (KOdiAPC) are truncated oxPLs generated by the fragmentation of the arachidonic acid side chain. 1-palmitoyl-2-(5,6-epoxyisoprostanoyl)-sn-glycero-3-phosphocholine (PEIPC), 1-palmitoyl-2-(5,6-epoxyisoprostane A2)-sn-glycero-3-phosphocholine (PECPC) and epoxycyclopentenones (cyclo-EC) emerge from cyclization, rearrangement and oxidation of PAPC. Modified from (Freigang, 2016). C: The oxPLs oxidized phosphatidylcholine (OxPC), oxidized phosphatidylethanolamine (OxPE), oxidized cholesteryl ester (OxCE), malondialdehyde (MDA) and 2-(ω-car-boxyethyl)-pyrrole (CEP) exert adverse and protective effects as antagonizing Lipopolysaccharide (LPS) activity (Miller & Shyy, 2017).

Although oxPLs can activate anti-oxidant and anti-apoptotic pathways, the net effect of oxPLs on vascular cells is pro-atherogenic. OxPLs disturb endothelial cells by activating both pro- and anti-inflammatory pathways. A typical example for the latter is the oxPAPC-mediated induction of the protective stress responsive gene heme oxygenase 1 (HO1) (Furnkranz *et al*, 2005; Gargalovic *et al*, 2006b). A variety of receptors including CD36, scavenger receptor B1, Toll-like receptor 2, Toll-like receptor 4, E-type prostaglandin receptor, PAF receptor and TMEM30a are activated by oxPAPC (Lee *et al*, 2012b; Weismann & Binder, 2012). Besides receptor activation, oxPLs incorporate into the plasma membrane and change the lipid composition by depleting cholesterol from caveolin-rich

membrane fractions, which results in activation of sterol regulatory element-binding protein and induction of IL-8 (Yeh *et al*, 2004; Li *et al*, 2006; Levitan & Shentu, 2011). OxPAPC derivatives are common in oxidized low density lipoproteins (oxLDL). OxLDL derived oxPAPC binds to the CD36 scavenger receptor and is readily taken up by macrophage foam cells (Berliner *et al*, 2009; Capoulade *et al*, 2015; Miller & Shyy, 2017). Thus, oxPAPC is the most important mediator of the negative effects of oxLDL.

Summarizing the studies on oxPAPC, it is suggested that oxPAPC activates stress-protective pathways, increases anti-oxidant genes and decreases DNA replication. The long-term impact of oxPAPC is pro-inflammatory and angiogenic which contributes to plaque destabilization (Lee *et al*, 2012b). In the development of atherosclerosis, exposure to oxPAPC heavily alters the endothelial transcriptome with PEIPC as its most potent effector (Romanoski *et al*, 2011). The response of the endothelium to oxPAPC is overwhelmingly complex. To address the complexity of the oxPAPC response in endothelial cells, systems-based approaches were applied.

1.2 Network modeling of human aortic endothelial cells

1.2.1 Integrative network modeling approach

In the past decades life sciences focused on low-dimensional bi-molecular relationships. To understand biology, the system has often been reduced to elementary properties of individual components. The emergence and rapidly growing usage of high throughput techniques is changing the understanding of biology as a high dimensional complex system (Berger *et al*, 2013). The network modeling approach tries to reflect this complexity and simultaneously tries to highlight important traits underlying such a high-dimensional system (Civelek & Lusis, 2013). Networks can help to reveal relationships inside omics-data as well as to structure omics-data to understand interdependencies between molecular traits, biological process, cellular functions and physiology and pathophysiology (Figure 2).

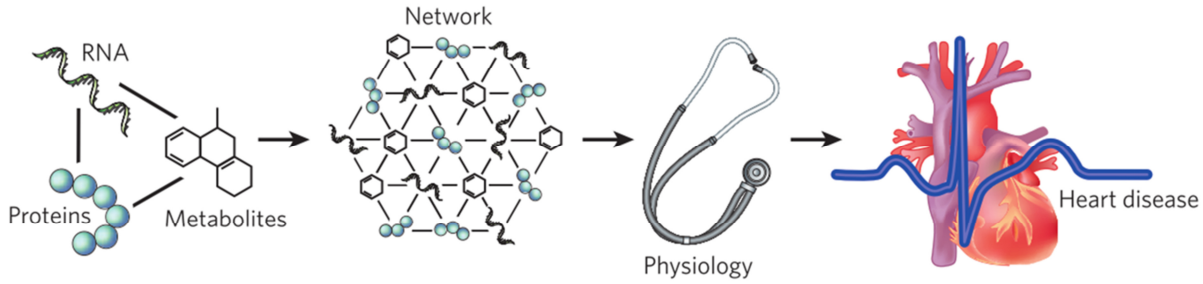

Figure 2: Network approach to link high-throughput data to physiology and pathophysiology.

Information about DNA, RNA, protein and metabolite variation can be modeled into networks of interacting molecular entities. In contrast, to directly associate changes in a given gene with changes in a disease state, the network defines physiological and disease states and links molecular biology to clinical medicine (Schadt, 2009).

Several explanatory and predictive mathematical models are being used for network modeling of biological data. These range from plain interaction networks with nodes representing proteins and edges representing physical interaction to complex networks representing directed, sequential or mechanistic relationships (Stelzl *et al*, 2005; Le Novère, 2015). Commonly used biological networks include co-expression networks, protein-protein interaction networks, gene regulatory networks, metabolic networks and signaling networks. Predominantly used network inference approaches are based on correlation, information theory, Bayesian inference and differential equations. Boolean networks provide state information by modeling nodes as binary variables and assigning them to active or inactive states (Albert & Thakar, 2014). This parameter-free model enables examining dynamic systems, but with fewer mechanistic insights than kinetic models. The appropriate model for a biological system depends on scale and dimensionality of the incorporated data as well as requirement of prior knowledge. Combination of several of these approaches can increase the accuracy of the network. However, data noise, limited sample size and squeezing complex biological systems and processes into simplified statistical models can lead to false positive results (Marbach *et al*, 2010). Therefore, experimental validation is necessary to support findings derived from systems integrative analysis.

1.2.2 Co-expression networks define connections between transcriptional entities

Co-expression networks represent a gene regulatory network model, which is based on RNA expression derived from, e.g. microarray or RNA sequencing. This model shows putative co-expression if the abundance of one RNA affects the abundance of another RNA. Nodes embody RNAs and edges between nodes embody undirected relationships between RNAs. Weighted gene co-expression network analysis (WGCNA) is a widely used approach for such co-expression modeling and applies a threshold for correlations between RNAs when defining edges between nodes (Zhang & Horvath, 2005). This model, which can be

constructed using the R package WGCNA (Langfelder & Horvath, 2008), organizes genes which correlate more with each other than other genes into a module and can offer data-defined groups for new biological interpretations (Chen *et al*, 2008; Emilsson *et al*, 2008). When two weighted gene co-expression networks from different conditions are compared and altered correlations between the two groups are analyzed, differential connectivity between the two states can be revealed. Such differentially connected gene networks have been used to characterize neurodegenerative diseases as late-onset Alzheimer's disease and Huntington's disease (Zhang *et al*, 2013; Narayanan *et al*, 2014). The advantage of weighted co-expression networks is that no pre-selected cutoff for connection is required. This network modeling approach provides information about genes which are consistently transcriptionally regulated and therefore increase the probability to find genes which share regulatory features or belong to the same biological process. However, this method does not provide information about causality and does not offer mechanistic explanations.

1.2.3 Bayesian modeling infers statistical causality between molecular entities

Probabilistic causal network models can give rise to potential mechanistic insights and among them Bayesian networks are established as the state of the art approach (Chang *et al*, 2015). Bayesian network modeling is a flexible way to model biological systems which are high-dimensional and scale free. This model improves the probability of identifying causal genes and pathways in omics-data. It presents a way to identify genes which are higher in the hierarchy and thereby suggested being vitally important for the system reflected by the network. In this model, causality, represented by directed edges between nodes, refers to statistical directional dependency between two entities, e.g. genes (Sieberts & Schadt, 2007). This statistical causality suggests a putative regulatory relationship between two genes rather than physical interaction. Bayesian inference represents a top-down data-driven and structure-based classical machine learning approach which can be applied by using packages as RimbaNET (Zhu *et al*, 2008, 2012) or Inferelator (Bonneau *et al*, 2006). Given that the applied omics-data sets are large enough, first, many candidate network models that fit the underlying data well are learned using a Monte Carlo Markov Chain (MCMC) simulation approach, and then a consensus network model is generated based on the candidate networks. Although prior knowledge is not required, known inter-relationships among genomics, transcriptomics, proteomics, metabolomics and epigenomics data can be used as prior to improve fidelity (Zhu *et al*, 2012, 2007, 2008). Such prior can also be derived protein-protein interactions, transcription factor binding sites or literature based knowledge.

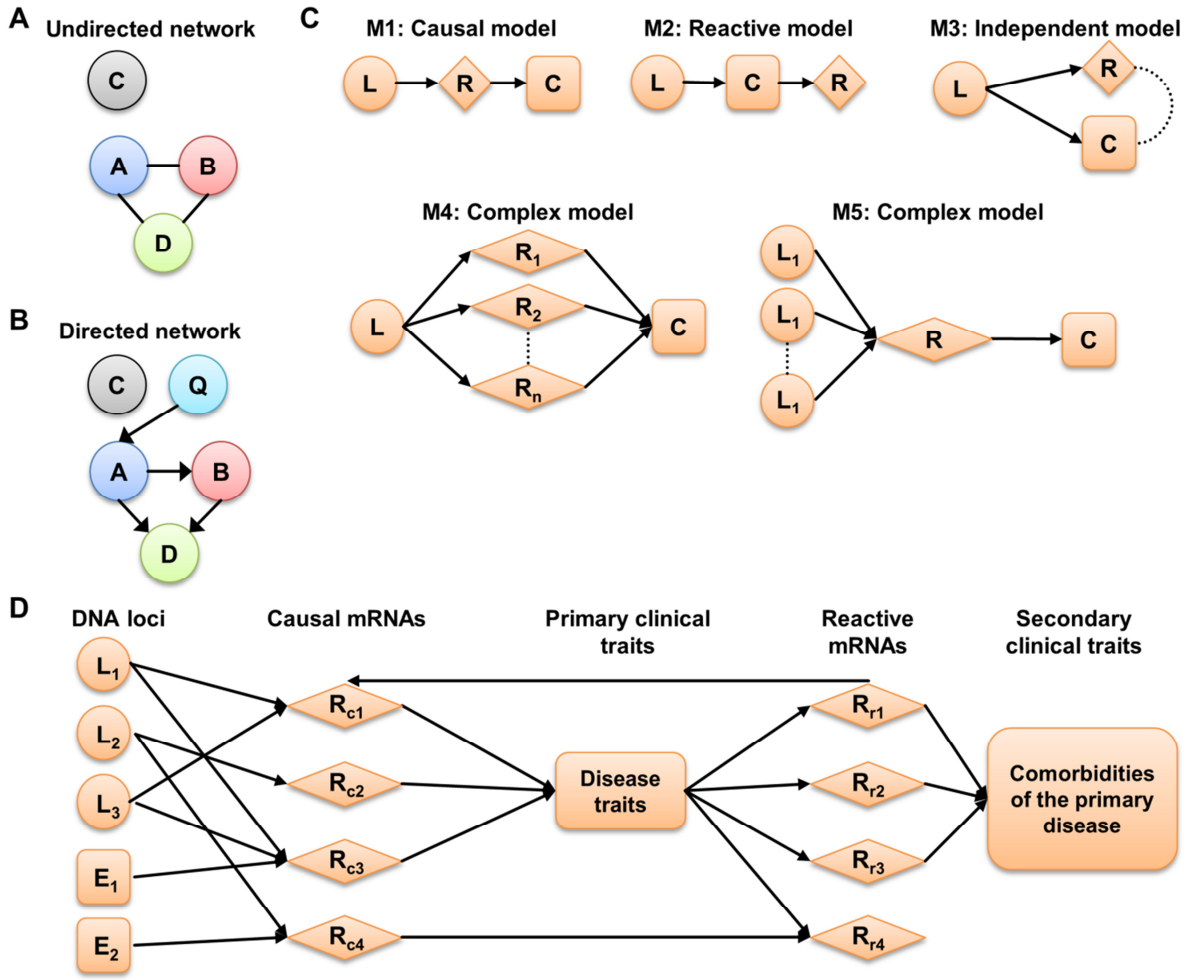

Figure 3: Infering relationships between molecular entities.

A: Undirected co-expression network. Nodes represent RNA entities and edges represent correlation between two RNAs. B: Directed Bayesian network. Nodes represent molecular entities such as genes and edges represent hierarchical relationships between genes. C: Given that the expression of a gene (R) and a complex trait (C), e.g. a disease, are influenced by a common QTL (L), the following simplified relationships are possible: the QTL affects the disease through a RNA transcript (causal model, M1); the RNA transcript is affected by the disease (reactive model, M2); the QTL affects the RNA transcript and the disease independently (independent model, M3). In slightly more complex scenarios, the QTL affects expression of several transcripts which in turn act on the disease (M4) or several QTLs affect a single transcript which affects the disease. D: QTL (L) and environmental factors (E) constitute drivers of a disease state (C) by influencing transcription (R_c). Variations in the disease state in turn influence transcription (R_r) which causes positive or negative feedback loops and comorbidities of the disease. Modified from (Schadt *et al*, 2005; Zhang *et al*, 2013).

To infer causal relationships between genes, genetic variation e.g. expression quantitative trait loci (eQTL) can be integrated with expression data to tease out causal, reactive or independent relationships between mRNA expression levels in a system, e.g. a disease state. Here, an eQTL describes a variation at a certain genetic locus which leads to a change in a quantitative trait such as mRNA expression. The relationship between genetic variations and transcriptomics is not directed, meaning that information can only flow from a change at a genetic locus to a change in gene expression or clinical traits but not the other way around (Figure 3). Causal relationships between entities can be inferred as the following (Figure 3):

(1) $$P(L,R,C) = P(L)P(R|L)P(C|R)$$

(2) $$P(L,R,C) = P(L)P(C|L)P(R|C)$$

(3) $$P(L,R,C) = P(L)P(C|L)P(R|C,L)$$

If the transcript R and a complex trait C, e.g. a physiological or pathophysiologcal state, are linked to the genetic locus L, the probability P describes the possibility that a variation in L leads to changes in R which in turn leads to changes in C (1). Variation in L can also lead to changes in C which in turn affects R (2). Furthermore, variation in L can independently affect R and C (3) (Schadt *et al*, 2005; Zhu *et al*, 2008). More complex models are possible, where one locus affects several transcript or several loci affect one transcript (Figure 3).

1.2.4 Expression trait based Bayesian networks can be solved to Non-Markov equivalent structures by incorporating genetic traits as structure prior

Since microarray and RNAseq technologies are the most common applied omics-approaches, most biological Bayesian networks are based on expression traits and use genetic information as prior.

For Bayesian networks, meaning directed cyclic graphs, conditional probabilities define the edges within the network and the probability distribution of states of a node depends on the states of its parent nodes. Each node represents the transcriptional expression of a gene. The conditional probabilities reflect the relationships between genes, stochastic nature of these relationships and data noise. The joint probability distribution $p(X)$ for the set of nodes X^i is determined by the network topology and depends on the product $\prod_i$ over the probability for X^i given the parent nodes $Pa(X^i)$:

(4) $$p(X) = \prod_i p\left(X^i \middle| Pa(X^i)\right)$$

Bayes formula gives the posterior probability of that the network model M is the true underlying model given the observed data D:

(5) $$P(M|D) \sim P(D|M) * P(M)$$

In this approach, the number of possible network models grows super-exponentially with the number of nodes. Exhaustively searching through all possible network models to find the network model which fits the observed data best constitutes a nondeterministic polynomial (NP) hard problem and is, therefore, not practicable. NP-hard problems describe problems which cannot be determined in a feasible time (a polynomial time with regard to size).

As a solution, a heuristic method based on Markov chain Monte Carlo (MCMC) (Madigan *et al*, 1995) methods can be applied to locally search for optimal structures. For this, a null network serves as the starting point for small random changes which include flipping, adding and deleting edges. Random changes which improve the fit of the network model to the observed data are accepted. Whether such a change fits more or less to the observed data,

can be determined by the Bayesian Information Criterion (BIC), also called Schwarz criterion (SBC, SBIC) (Schwarz, 1978). Increasing the likelihood to fit the network model to the observed data can be achieved by adding parameters which, however, often result in overfitting. This phenomenon occurs in excessively complex systems with too many parameters relative to the number of observations and therefore finally describes random errors or noise, but not underlying relationships. The BIC inserts a penalty for the addition of new parameters which results in a lower probability for models with a high number of parameters.

Even through a Bayesian network is a directed graph, multiple structures are Markov equivalent, which means they fit data equally well mathematically. For example, the two nodes X^1 and X^2 have the following two relationships in a network model M

(6) $$X^1 \rightarrow X^2$$

(7) $$X^2 \rightarrow X^1.$$

The probability distributions describing the two relationships are the same

(8) $$p(X^1, X^2) = (X^2|X^1)p(X^1) = p(X^1|X^2)p(X^2).$$

Thus, it is not possible to infer causal relationships from the network structure itself, as it cannot be distinguished if X^1 is causal to X^2 or X^2 is causal to X^1. Similarly, a Bayesian network which comprises three nodes X^1, X^2 and X^3, can have the following Markov equivalent models (Figure 4):

(9) $$M1\colon X^1 \rightarrow X^2, X^2 \rightarrow X^3$$

(10) $$M2\colon X^2 \rightarrow X^1, X^2 \rightarrow X^3$$

(11) $$M3\colon X^2 \rightarrow X^1, X^3 \rightarrow X^2$$

These three models possess the same conditional independent relationships since X^3 and X^1 are independent conditioning on X^2 :

(12) $$X^1 \perp\!\!\!\perp X^3 \mid X^2,$$

and are mathematically equal

(13) $$\begin{aligned} p(X) \quad &= p(M1) = p(X^2|X^1)p(X^1)p(X^3|X^2) \\ &= p(M2|D) = p(X^1|X^2)p(X^2)p(X^3|X^2) \\ &= p(M3|D) = p(X^2|X^3)p(X^3)p(X^1|X^2). \end{aligned}$$

In contrast, causal relationships can be inferred from V-shape structures which have no Markov equivalent structure:

(14) $$Mv\colon X^1 \rightarrow X^2, X^3 \rightarrow X^2$$

However, estimating the model M_v requires more parameters than estimating the models $M1$, $M2$ or $M3$ which leads to a higher BIC penalty score for the M_v model. To lower the potential impact of penalty for the number of parameters, a large sample size is necessary.

Therefore, Bayesian networks need a high number of biological experiments to be able to differentiate M_v from $M1$, $M2$ or $M3$ models.

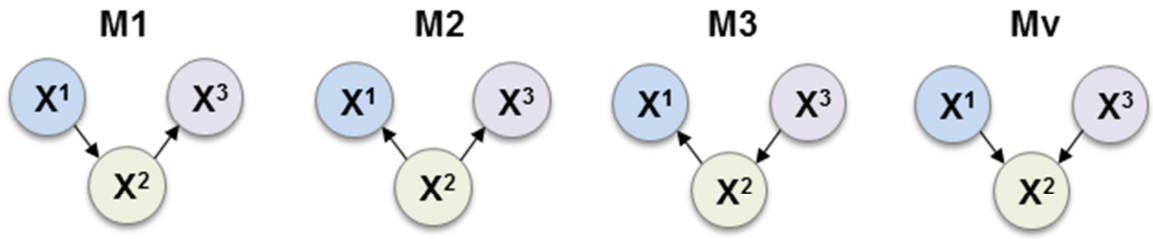

Figure 4: Different network models to fit underlying data.

M1, M2 and M3 are Markov equivalents and cannot be used to infer causal relationships. Mv represents a V-shape and Non-Markov equivalent structure, which can be used to determine a causal direction.

To break Markov equivalent structures in order to solve Bayesian networks to biological causal networks, genetic causality as structure prior can be incorporated (Zhu *et al*, 2004): a gene which has a cis-eSNP can have the cis-eSNP as one of its parent nodes (Schadt *et al*, 2008). Incorporating cis-acting eSNPs or eQTLs has been shown to improve the network reconstruction (Zhu *et al*, 2007).

The control and oxPAPC Bayesian networks (Hitzel *et al*, 2018), which were analyzed in this study, were constructed as described above. In brief, 1000 different network models were created by starting the stochastic reconstruction process from different randomly selected seeds. To decide for a consensus network from these 1000 models, edges that appeared in more than 30% of the models were defined as consensus. This process of defining a consensus network from a large number of models is called network averaging. The decision for the applied cutoff theshold of 30% for edge inclusion in this averaging process is based on former simulation studies (Zhu *et al*, 2007). Since the resulting consensus network is not necessary a directed acyclic graph, the most weakly supported edge in a loop was removed after the averaging process.

1.2.5 Network approach to complex diseases

Comprehensive multiscale network models aim to understand complex phenotypes and diseases from a systems-based perspective. Such networks can be derived from multiple omics-data and serve as a framework onto which disease signatures such as differentially expressed genes from a disease state can be projected. This approach allows extracting and defining disease specific subnetworks (Figure 5). Identification of molecular key drivers of these disease related subnetworks can help identifying causal genes for diseases.

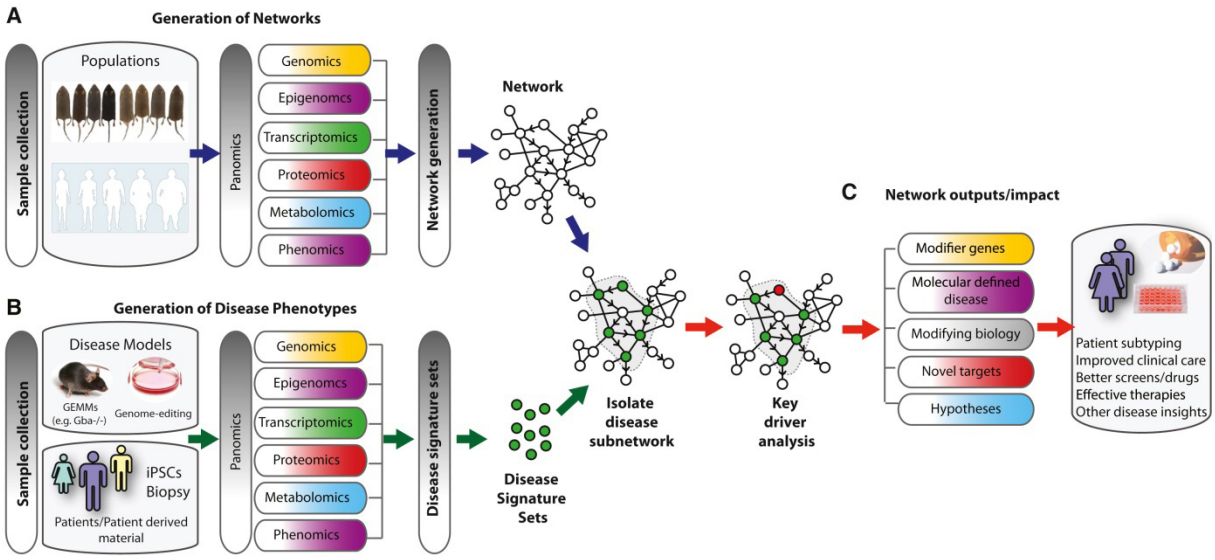

Figure 5: Network analysis of complex diseases by an integrative multiscale omics-approach.

A: Large scale de novo generation or public database usage of high troughput data of multiple omics-classes from human samples or model organisms can be used to construct a predictive reference or frame network. B: Generation of high-throughput data from disease samples can yield differentially expressed genes associated with the disease. The predictive frame network can be probed with the disease signature to extract disease associated subnetworks. Central hub proteins are identified and predicted as key drivers of the disease. C: The network-based understanding of the disease allows for the identification of novel targets and information on disease modifying genes. Modified from (Argmann *et al*, 2016).

It is important to differentiate and distinguish between causal and correlative relationships in diseases. Targeting a causal network which reflects a disease state in a way to change the network structure back into a healthy state can improve the effectiveness of disease treatment (Davis *et al*, 2009). An effective target for disrupting disease-related networks should be central and highly connected as well as in a higher order in the network hierarchy (Kidd *et al*, 2014). Due to the complexity of diseases tissue-to-tissue connections and regulations should be considered to be able to target the key tissue for the disease (Dobrin *et al*, 2009). E.g. cell type specific transcription factor regulatory networks show a similar architecture, but they are highly cell selective and shape cellular identity and function (Neph *et al*, 2012). An example of using network modeling for drug discovery is the drug topiramate, which was identified as a candidate to treat the inflammatory bowel disease (Dudley *et al*, 2011). As the expenses for genome and expression sequencing will further decrease, network modeling can be an approach for personalized medicine as it helps to tailor the drug combination for an individual.

1.2.6 Integrative network modeling in cardiovascular disease

Network modeling has identified key drivers and pathways in different physiological and disease related conditions. In mouse studies, PPARγ2 was identified as a determinant for longevity in a Bayesian subnetwork of longevity related genes in mouse adipose tissue

(Argmann *et al*, 2009). In another study, eight key drivers were identified to be causal for abdominal obesity and their association with obesity-related traits were confirmed by transgenic mouse models (Yang *et al*, 2009). In inflammatory diseases, systems genetics and co-expression modeling identified key drivers of host-microbe interactions in inflammatory bowel disease (Jostins *et al*, 2012). Additionally a recent multiscale genomics network model revealed and validated 12 key drivers of inflammatory bowel disease (Peters *et al*, 2017). Furthermore, Bayesian network modeling in eleven rodent disease models revealed an inflammatory signature and associated key drivers (Wang *et al*, 2014).

Systems genetics and network models have been also used for the identification of genes and gene clusters causal to cardiovascular pathology. Integrative co-expression and Bayesian network modeling of blood pressure associated GWAS and blood mRNA expression profiles revealed SH2B3 as a key driver for blood pressure regulation (Huan *et al*, 2015). In coronary artery disease (CAD) studies which exploits network modeling approaches integration of genome wide SNPs and blood metabolites identified SERPINA1 and AQP9 as candidate genes for atherosclerosis (Inouye *et al*, 2012). An integrative study using genomics and transcriptomics data related to CAD identified GLO1 as a key driver in a CAD associated Antigen-processing network (Mäkinen *et al*, 2014). In another study, integration of genetic and gene expression data from seven coronary artery disease (CAD)-relevant tissues from CAD patients showed 30 causal cross-tissue regulatory gene networks (RGNs) (Talukdar *et al*, 2016). Proposed key drivers were part of different pathways linked to CAD like inflammation, cholesterol and glucose metabolism which were shown to be regulated in tissue-specific and cross-tissue networks. One of the identified regulatory gene networks was enriched in RNA processing genes and silencing of the newly identified key drivers AIP, DRAP1, POLR2l and PQBP1, which were previously not linked to CAD, reduced cholesterol-ester accumulation in THP-1 foam cells. A super-network containing all CAD-causal cross-tissue regulatory gene networks was identified and shows that these networks are not isolated. Counteracting CAD therefore requires a comprehensive understanding of the concert of different tissues to understand how to treat CAD by targeting different causers rather than focusing on single targets.

Network modeling has also been attempted for endothelial cells. Integration of genome-wide methylation and gene expression in lung tissue of chronic obstructive pulmonary disease (COPD) revealed EPAS1 as a key driver regulating a hypoxia response which was validated in endothelial cells (Yoo *et al*, 2015). EQTL mapping in human aortic endothelial cells (HAEC) of 147 heart transplant donors revealed PPAP2B, GALNT4, MAPKAP5, TCTN1, SRR, SNF8 and ICAM1 as causal for susceptibility to atherosclerosis (Erbilgin *et al*, 2013). Co-expression network modeling of expression profiles of the same cohort revealed CHAC1, OKL38 and HO1 as hub-proteins in the endothelial response to oxPAPC (Romanoski *et al*,

2011). In another study, endothelial cell specific regulatory networks based on siRNA and TNFα signatures in HUVEC were constructed to compare five different software tools to infer directed networks (Hurley *et al*, 2012). This study demonstrated that these predictive network models recovered more experimentally verified relationships than by chance. However, a comprehensive data driven directed network model for endothelial cells is lacking. In this study, such comprehensive Bayesian network models, based on Bayesian inference (Zhu *et al*, 2008), for human aortic endothelial cells (HAEC) were analyzed to identify novel key drivers in endothelial cells under pro-atherogenic conditions. In a second step, these networks were used to analyze endothelial specific perturbation signatures.

1.3 Mitochondrial one-carbon metabolism

1.3.1 Compartmentalization of one-carbon metabolism

The Bayesian network modeling approach highlighted mitochondrial one-carbon metabolism as a potentially deregulated pathway in endothelial cells in an atherosclerotic context.

One-carbon metabolism constitutes a universal metabolic pathway which results in the activation and transfer of one-carbon units. Folate derivatives serve as carriers for these one-carbon units. The cycle of activated folates exists in cytosol and mitochondria and despite its apparent redundancy the flow is normally driven from mitochondria to cytosol (Figure 6) (Tibbetts & Appling, 2010).

The first active one-carbon carrier is 5,10-methylene-tetrahydrofolate (5,10-meTHF) which is synthesized by serine hydroxymethyltransferases (SHMT1/2) from tetrahydrofolate (THF). The one-carbon unit is derived from serine, which is converted into glycine. This reaction is reversible. Depending on the availability and demand of one-carbon units, serine can fuel one-carbon synthesis or serine can be produced out of one-carbon units. The activated 5,10-meTHF constitutes a cofactor for thymidine synthesis. Cytosolic 5,10-meTHF can be converted into 5-methyl-THF by methylenetetrahydrofolate reductase (MTHFR). 5-methyl-THF remethylates homocysteine to methionine in the cytosol. Methionine is the substrate for S-denosyl methionine (SAM) synthesis, which is an important cofactor for many epigenetic modifiers as well as membrane lipid synthesis.

In further steps 5,10-meTHF can be interconverted into 10-formyl-THF and subsequently hydrolyzed into formate. These reversible interconversions are carried out in the cytosol by the trifunctional enzyme methylenetetrahydrofolate dehydrogenase, cyclohydrolase and formyltetrahydrofolate synthetase 1 (MTHFD1). In the mitochondria these interconversions are split and carried out by two enzymes: bifunctional methylenetetrahydrofolate dehydrogenase / cyclohydrolase (MTHFD2/2L) and MTHFD1L. In these reactions NADPH and NADP are simultaneously interconverted. MTHFD2 is thought to be expressed

predominantly in undifferentiated cells and it was proposed that its function is taken over by MTHFD2L in adult tissue (Shin *et al*, 2014a). In that study it was shown that MTHFD2 had a 50-fold higher K_{cat}/K_M ratio than MTHFD2L. 10-formylTHF represents the most oxidized activated folate and is incorporated into the purine backbone. The synthesis of the purine backbone comprises eleven cytosolic reactions and is carried out by the enzyme-complex purinosome on the outside of mitochondria (French *et al*, 2016). Inside mitochondria 10-formylTHF is needed for the formylated inititator methionine-tRNA (Tucker *et al*, 2011). 10-formylTHF can also be oxidized into CO_2 by aldehyde dehydrogenase 1 family member L1/2 (ALDH1L1/2) (Krupenko *et al*, 2010). This irreversible reaction generates NADPH and might substantially contribute to mitochondrial redox homeostasis (Fan *et al*, 2014).

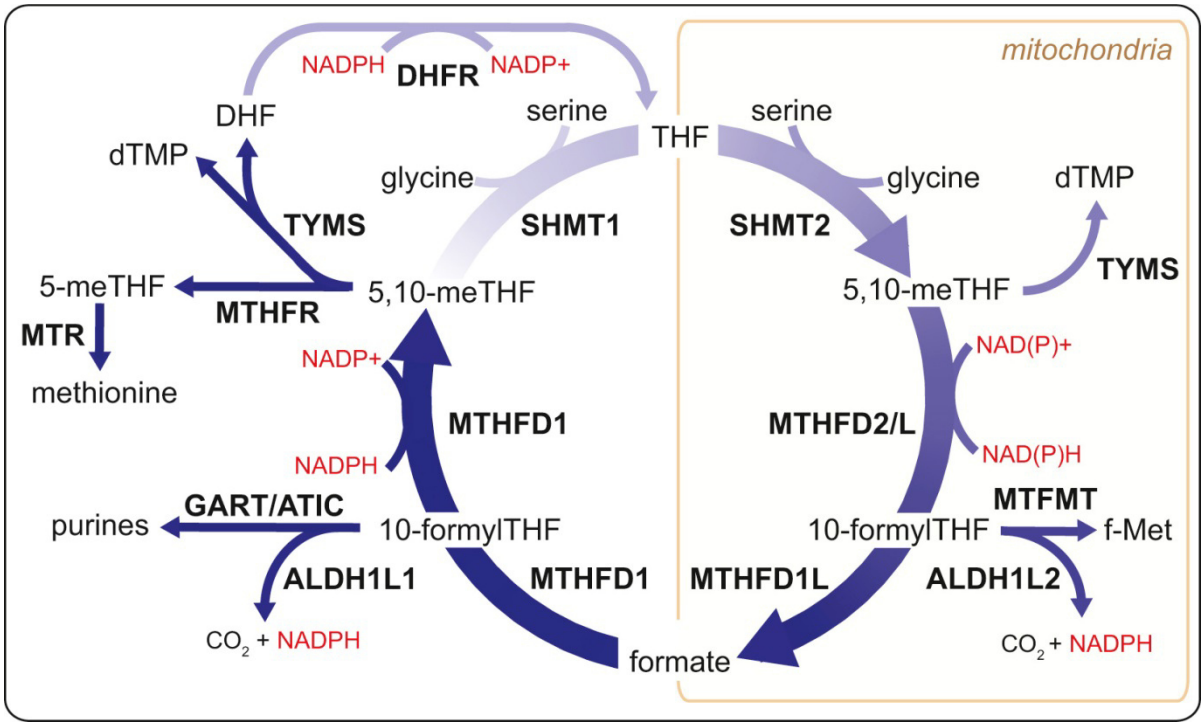

Figure 6: Compartmentalization of cytosolic and mitochondrial one-carbon metabolism.

Depicted is the flow of tetrahydrofolate (THF) and formate and its activated forms 5,10-meTHF, 5-meTHF and 10-formyl-THF. The cycle starts with mitochondrial serine hydroxymethyl transferase (SHMT2) which transfers one carbon unit from serine to THF. Activated folates are interconverted by mitochondrial bifunctional MTHFD2/MTHFD2L and MTHFD1L and cytosolic trifunctional MTHFD1. The activated one-carbons are consumed by the following pathways: purine synthesis (phosphoribosylglycinamide formyltransferase, phosphoribosylglycinamide synthetase, phosphoribosylaminoimidazole synthetase (GART)/ 5-aminoimidazole-4-carboxamide ribonucleotide formyltransferase/IMP cyclohydrolase (ATIC)); remethylation of homocysteine to methionine (methylenetetrahydrofolate reductase (MTHFR), 5-methyltetrahydrofolate-homocysteine methyltransferase (MTR)); thymidine synthesis (thymidylate synthetase (TYMS)) and coupled recycling of dihydrofolate (DHF) (dihydrofolate reductase (DHFR); N-formylmethionine synthesis (f-MET) (mitochondrial methionyl-tRNA formyltransferase (MTFMT)); or full oxidation into CO_2 (aldehyde dehydrogenase 1 family member L1/2 (ALDH1L1/2)). Modified from (Ducker & Rabinowitz, 2016).

THF and formate are transfered between cytosol and mitochondria, beacuse one-carbon loaded folates cannot cross membranes. Although no nuclear isoforms of activated folate interconverting enzmes exists, partial localization of MTHFD2 and SHMT2 in the nucleus has

been reported (Gustafsson Sheppard *et al*, 2015; Anderson & Stover, 2009). The difference in mitochondrial NADH/NADPH and cytosolic NADPH drives the cycle towards the cytosol. Serine is catabolized in the mitochondria to produce formate which is then transferred to the cytosol where it is used for purine synthesis and where the cycle synthesizes serine. Because of this direction, one-carbon units by default originate within mitochondria. This direction also results in predominantly mitochondrial produced NADPH by folate metabolism. In case of dysfunctional mitochondrial one-carbon metabolism it was shown that the cycle can switch and produce one-carbon units in the cytosol (Ducker *et al*, 2016). The mitochondrial demand for one-carbon units is low. The rationale for compartmentalization and predominant production of activated folates in the mitochondria is currently argued as uncoupling of one-carbon metabolism and glycolysis from a redox perspective since NAD^+/NADH ratio is an important regulator for glycolytic activity. Cytosolic oxidation of 5,10-meTHF to 10-formyl-THF and concomitant NADPH/NADH production could disturb this ratio and dampen cellular robustness.

1.3.2 One-carbon metabolism in physiology and pathophysiology

One-carbon metabolism directly controls the three amino acids glycine, serine and methionine and indirectly cysteine. Among these, glycine is the most important side product during the one-carbon cycle and is consumed for purine, glutathione, creatine and heme synthesis. Furthermore, glycine constitutes one third of collagen. Besides synthesis from serine, glycine can be retrieved by cellular uptake or catabolism of choline. The mitochondrial glycine cleavage system, which consists of four enzymes, oxidizes glycine into CO_2 and deaminates it to form 5,10-meTHF which in turn can enter and feed the one-carbon cycle. In quiescent adult tissues the glycine cleavage system is believed to be the predominant one-carbon source. In contrast, serine constitutes the main source of one-carbon units in stem cells, during embryogenesis and in proliferating cells in cell culture models. The one-carbon source serine is synthesized from the glycolysis intermediate 3-phospho-D-glycerate by phosphoglycerate dehydrogenase (PHGDH), phosphoserine aminotransferase (PSAT1) and phosphoserine phosphatase (PSPH).

One-carbon metabolism is indispensable for purine and thymidine synthesis. Two 10-meTHF units and one glycine are incorporated into the purine backbone (Figure 7). Purine synthesis represents the largest demand for one-carbon units in proliferating cells. Targeting one-carbon metabolism therefore blocks cell proliferation and is used for antibiotics and chemotherapeutics (Chattopadhyay *et al*, 2007). Since glycine and serine show a universally high net consumption in cancer cells, serine synthesis and mitochondrial one-carbon metabolism are overexpressed in cancers (Mehrmohamadi *et al*, 2014). In particular, MTHFD2 was identified as the most consistently overexpressed enzyme across cancers and

represents a highly sought cancer drug target and a target for selective antifolates (Nilsson *et al*, 2014; Pikman *et al*, 2016; Amelio *et al*, 2014).

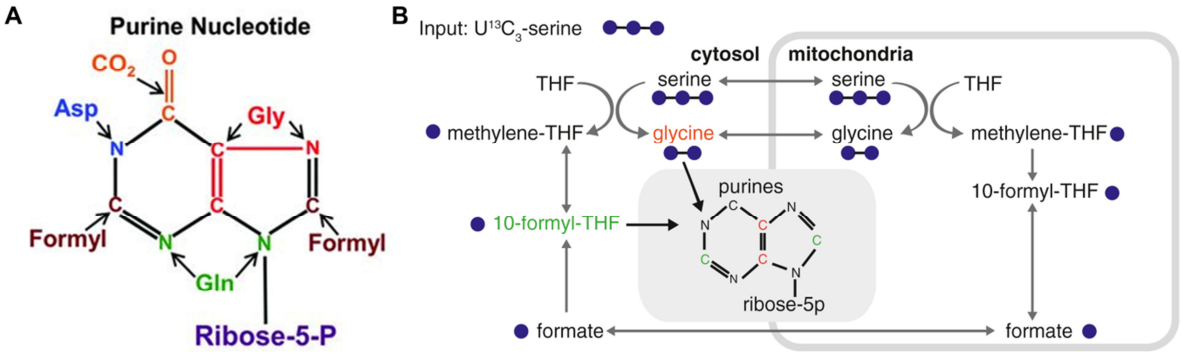

Figure 7: Composition of the purine backbone.

A: The purine backbone consists of one glycine molecule (Gly), two carbon units from 10-formylTHF (Formyl), one CO_2 molecule and nitrogen units derived from aspartate (Asp) and glutamine (Gln) (Ben-Sahra *et al*, 2016). B: The carbons of the purine backbone originate from serine and can be traced by heavy carbon labeling (Ron-Harel et al, 2016). Two carbon units from serine become glycine and are incorporated into the backbone. The third carbon unit from serine becomes the activated carbon on the THF carrier and is incorporated into the purine backbone as 10-formyl-THF.

The importance of folate coupled one-carbon metabolism in adult tissue is not well studied. The demand of one-carbon units in adult non-proliferative tissue is thought to be modest and could potentially be satisfied with formate. The function of *de novo* serine and mitochondrial one-carbon synthesis is, therefore, not clear in these tissues. Hematopoiesis and immune response are the most highly proliferative processes. Liver supported hematopoiesis was shown to be dependent on MTHFD2 (Di Pietro *et al*, 2002). Furthermore, activated and highly proliferative T-cells mobilize one-carbon metabolism and increase expression of the SHTM2-MTHFD2 axis (Ron-Harel *et al*, 2016). Serine and glycine are also important neurotransmitters and MTHFD1L contains an Alzheimer's disease associated polymorphism (Naj *et al*, 2010). Although one-carbon metabolism seems to play a role in adult tissue, the benefit of folate food intake for adult diseases as atherosclerosis or Alzheimer's disease could not be proven in clinical trials (Smith & Refsum, 2016).

Since homocysteine levels are thought to be potentially associated with atherosclerosis, folate coupled enzymes involved in methione and homocysteine interconversion have been heavily studied. However, a potential role of mitochondrial one carbon-metabolism in cardiovascular disease is not known. In this study, an unexpected association between MTHFD2 and pro-atherogenic lipids has been identified.

1.4 Bayesian network modeling of PHF histone demethylase signatures

In this study, the endothelial specific Bayesian networks were exploited to analyze signatures from PHD-finger domain containing histone demethylases in endothelial cells.

1.4.1 Transcriptional regulation by epigenetic modifiers

Epigenetics describe the influence of the chromatin structure and organization of the DNA. One major mechanism includes covalent modification of DNA and histones, which has a substantial impact on gene expression and chromosome stability, imprinting and inactivation (Dawson & Kouzarides, 2012). The most prevalent histone modifications methylation, acetylation, phosphorylation and ubiquitination constitute a histone code, which is reversibly and dynamically regulated (Bannister *et al*, 2002; Ng *et al*, 2009; Walport *et al*, 2012; Klose & Zhang, 2007; Jenuwein, 2001). The most prevalent histone methylation marks are mono-, di- and trimethylated lysine marks on histones 3 and 4: H3K4, H3K27, H3K36, H4K20 (Shi & Whetstine, 2007). Some histone marks predominantly encode a certain transcriptional outcome, e.g. H3K4me3 is considered an active or permissive mark found around transcriptional active genes whereas H3K9me3 and H3K9me2 often represent repressive marks found in transcriptional inactive regions of the genome. The combination of different histone marks at different genomic sites nearby a gene locus can fine-tune gene transcription (Kooistra & Helin, 2012). Histone methyltransferases as well as demethylases are often deregulated during cancer progression and inhibitors of these enzymes are, therefore, developed for cancer therapy (Morera *et al*, 2016). Epigenetic modifiers, and among them histone demethylases, are also important regulators of cardiovascular physiology and pathophysiology (Yan *et al*, 2010; Zhang & Liu, 2015).

1.4.2 JmjC domain containing histone demethylases

There are two classes of oxidative histone demethylases. The flavine adenenine dinocluotide dependent amine-oxidase enzyme family consists of the two histone demethylases LSD1 and LSD2 (Shi *et al*, 2004). The other family comprise the Jumonji (JmjC) domain containing histone demethylases which belong to the 2-oxoglutarate oxygenase enzyme superfamily (Figure 8) (Klose *et al*, 2006, 2007; Lee *et al*, 2007b; Tsukada *et al*, 2006; Cloos *et al*, 2006; Hong *et al*, 2007; Iwase *et al*, 2007; Lee *et al*, 2007a).

This family consists of more than 20 members and controls gene expression by modulating the epigenetic methylation code. JmjC histone demethylases are diverse and can also influence cellular signaling by demethylating and hydroxylating non-histone proteins, DNA, RNA and other metabolites (Nowak *et al*, 2016; Shen *et al*, 2014). JmjC histone demethylases demethylate their target by hydroxylating the Nε-methyl group followed by elimination of formaldehyde and producing CO_2 and succinate. This reaction requires α-ketoglutarate, molecular oxygen and iron(II) as cofactors and vitamin C to keep the iron in its reduced state. These cofactors link Jmjc histone demethylase activity and its associated chromatin remodeling to metabolism and potentially enable them as metabolic sensors (McDonough *et al*, 2010; Katada *et al*, 2012).

The state of the histone code is vitally important and the large size of the JmjC enzyme family potentially gives rise to compensation ability. However, the expression of certain JmjC family members is tissue, time and disease specific. Some JmjC enzymes have been shown to be important in the vasculature: Endothelial cells are characterized by their potential for angiogenesis. Hypoxic environments elicit endothelial angiogenesis and the hypoxia activated transcription factor HIF1α has been shown to induce expression of KDM3A, KDM4B, KDM4C and KDM4D (Beyer *et al*, 2008; Hancock *et al*, 2015). KDM2B contributes to FGF-2 controlled angiogenesis (Kottakis *et al*, 2011), JMJD6 regulates angiogenic sprouting and splicing of the vascular endothelial growth factor receptor 1 (Boeckel *et al*, 2011) and KDM5B controls angiogenesis by repressing pro-angiogenic HOXA5 and CCL14 (Fork *et al*, 2015; Li *et al*, 2011). Furthermore, JMJD8 interacts with pyruvate kinase M2 in the cytoplasm thereby promoting angiogenic sprouting of endothelial cells (Boeckel *et al*, 2016). JmjC histone demethylases therefore regulate characteristic endothelial functions. One of the JmjC subfamilies is, however, not yet well described: the KDM7 histone demethylases.

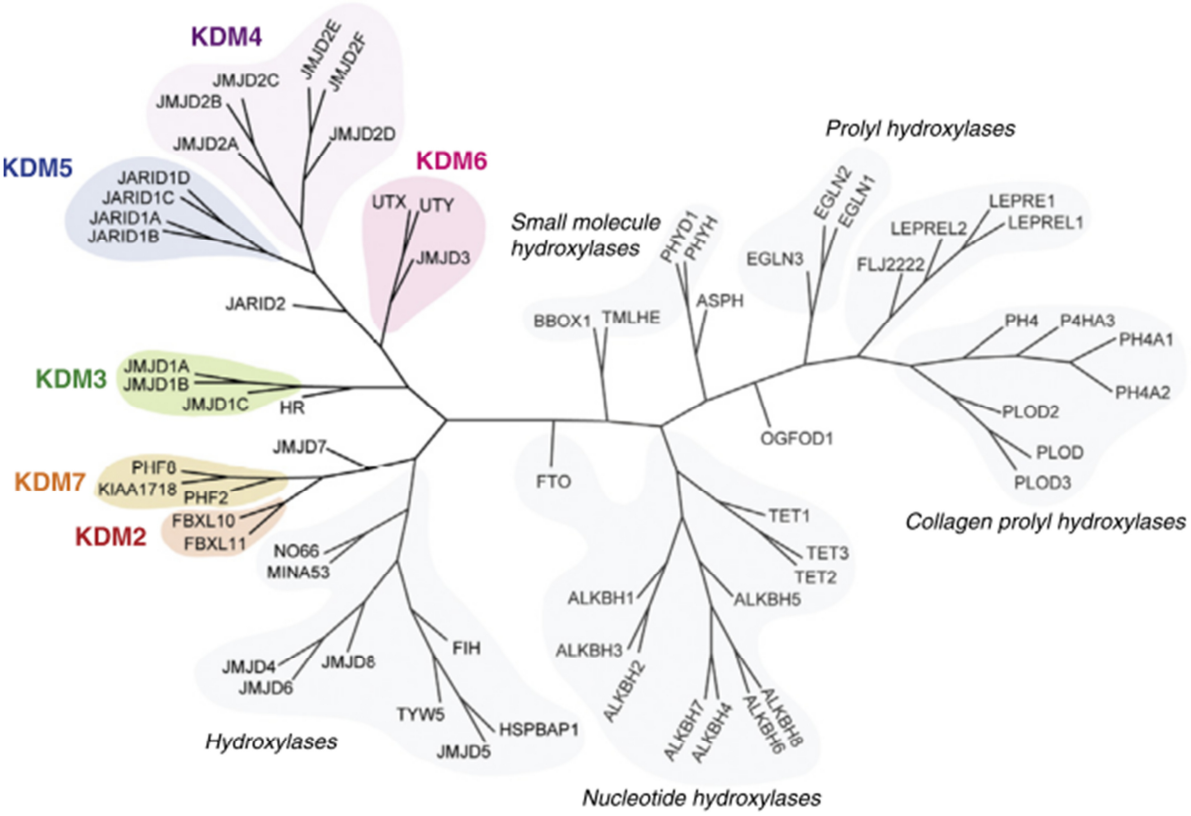

Figure 8: Family of 2-oxoglutarate oxygenases.

More than 20 histone demethylases of the KDM 2-7 subfamilies comprise a family of JmjC domain containing enzymes. Some of the enzymes of the JMJD hydroxylase family also demethylate histones. Other subfamilies of the 2-oxoglutarate oxygenase family hydroxylate prolin residues of collagen and cellular proteins (Nowak *et al*, 2016).

1.4.3 KDM7/PHD subfamily of Jmjc histone demethylases

JmjC histone demethylases are large proteins with often several domains. Among these domains the JmjC domain constitutes the eraser. Additional reader domains which can recognize other histone marks enable cross-talk between histone modifications. The complexity of these enzymes makes them therefore suitable for printing, reading and erasing the histone code as part of chromatin modifying complexes together with other histone modifiers, transcription factors and polymerases.

Among the JmjC histone demethylase family KDM7A, PHF8 and PHF2 constitute a subfamily based on the characteristic of an N-terminal plant-homeodomain (PHD) finger (Fortschegger & Shiekhattar, 2011). The PHD domain recognizes H3K4me3 and is followed by a linker and the catalytic JmjC domain (Figure 9 A).

Among the KDM7 family members, PHF8 is the so far most detailed described demethylase. PHF8 was identified as a histone demethylase which regulates neuronal development (Qi *et al*, 2010). PHF8 also acts together with Myc to influence gene expression of cytoskeletal proteins and thereby influences neurite outgrowth (Asensio-Juan *et al*, 2012). Furthermore, PHF8 is an important regulator of cell cycle progression, especially by demethylating H4K20me1 of targets of the E2F transcription factor family (Liu *et al*, 2010; Lim *et al*, 2013; Sun *et al*, 2015). PHF8 is associated with cancer progression and in the cardiovascular system PHF8 has been implicated in cardiac differentiation (Tang *et al*, 2016; Wang *et al*, 2016a).

In contrast to PHF8, KDM7A represents the most sparsely described KDM7 subfamily member and its function in the cardiovascular system is unclear. KDM7A has been shown to demethylate the repressive marks H3K9me2 and H3K27me2 (Yokoyama *et al*, 2010; Tsukada *et al*, 2010) and H3K9me1 and H3K27me1 (Tsukada *et al*, 2010). Whereas the linker of PHF8 shows flexibility, the linker between the H3K4me3 binding PHD and the JmjC domain is rigid in KDM7A (Figure 9 B,C). Due to this spatial restriction, the JmjC domain can only demethylate H3K27me2 in a *cis* mode, i.e. on the same histone, in the presence of H3K4me3 (Horton *et al*, 2010). In the absence of H3K4me3 the JmjC domain preferentially demethylates H3K9me2 in *cis.* These features lead to the dual-specificity towards H3K9me2 and H3K27me2 and suggests that KDM7A reads activated states which are marked by H3K4me3 and further promotes activation through the demethylation of the repressive marks H3K9me2 and H3K27me2 thereby promoting transcription.

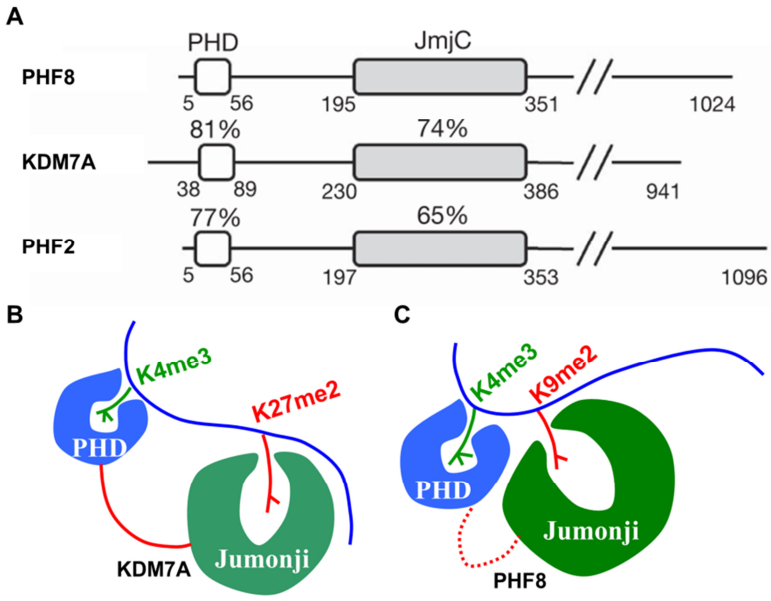

Figure 9: The jmjC histone demethylases of the KDM7/PHD subfamily.

A: PHF8, KDM7A and PHF2 constitute the KDM7 subfamily of JmjC histone demethylases. All three enzymes contain about 1000 amino acids and an N-terminal plant homeodomain (PHD) followed by a linker and the Jumonji C-domain (JmjC). The PHD and JmjC domain of KDM7A possess higher homology (indicated in percentage) to PHF8 than those domains of PHF2 compared to PHF8. Modified from (Qi et al, 2010). B: The JmjC domain of KDM7A binds to dimethylated histone 3 lysine 27 (H3K27me2) if the plant homeo domain (PHD) detects trimethylated lysine 4 on the same histone. Due to a rigid linker (red line) the JmjC domain cannot bind to dimethylated lysine 9 (H3K9me2) on the same histone. C: The flexible linker (dotted line) of PHF8 allows for the binding of the JmjC domain to H3K9me2 on the same histone. Modified from (Horton et al, 2010).

KDM7A promotes the formation of the neural plate in early chick embryos and neuronal differentiation in mouse embryonic stem cells by regulation of FGF4 expression (Huang *et al*, 2010a, 2010b) Furthermore, it was shown that KDM7A acts together in a complex with JMJD3 during HL-60 differentiation towards a macrophage-like state to promote transcriptional elongation (Chen *et al*, 2012). KDM7A negatively regulated angiogenesis in a tumor-xenograft model with KDM7A-expressing B16 and HeLa cells suggesting KDM7A being a tumor-suppressive gene (Osawa *et al*, 2011). Furthermore, long-term nutrient starvation increased expression level of KDM7A in cancer cells in this study. The function of KDM7A in the vascular system is, however, not clear.

1.5 Aim of the study

Oxidized phospholipids are associated with atherosclerosis. Despite the observation that the impact of these atherogenic lipids on endothelial cells is tremendous, the response of the endothelial cell to these lipids is overwhelmingly complex and not well understood. The aim of this work was to integrate computational analyses with experimental wet-laboratory research to increase the understanding of endothelial pathology in response to oxidized phospholipids.

The specific aims of this study were:

1. Identifying patterns in endothelial cells which are deregulated upon oxPAPC exposure by means of computational analysis of a large cohort of expression profiles
2. Detecting key drivers of deregulated patterns upon oxPAPC exposure by means of Bayesian network analysis
3. Analysing key driver associated subnetworks regarding their biological meaning by means of gene set enrichment analysis (GSEA)
4. Prioritizing of one deregulated pattern and its associated key driver upon oxPAPC exposure
5. Experimental validation of prioritized key driver in human aortic endothelial cells (HAEC) by knockdown of the key driver and oxPAPC treatment, identification of the relationship between key driver and its associated subnetwork and systematic validation of the key driver subnetwork by RNA sequencing
6. Characterization of the impact of the prioritized key driver on endothelial function as assessed by angiogenesis and migration
7. Experimental identification of the biological meaning of the deregulated subnetwork
8. Estimation of the potential disease impact of the key driver and its associated subnetwork
9. Exploiting the HAEC Bayesian networks with perturbation signatures from the KDM7 family to gain epigenetic associated endothelial cell (EC) networks

2 Materials and Methods

2.1 Materials

2.1.1 Chemicals

$^{13}C_5$-adenosine	Alsachim, Graffenstaden (France)
$^{13}C_5$-guanosine	Alsachim, Graffenstaden (France)
$^{13}C_5$-uridine	Alsachim, Graffenstaden (France)
2-Acrylamido-2-methylpropane sulfonic acid (AMPS)	AppliChem, Darmstadt
Adenosine	Sigma-Aldrich, Taufkirchen
Agar	AppliChem, Darmstadt
Agarose	Bio&Sell, Feucht bei Nürnberg
Ampicillin sodium salt	Sigma-Aldrich, Taufkirchen
Antimycin A	Sigma-Aldrich, Taufkirchen
Asparaginase	Sigma Aldrich, Taufkirchen
Asparagine	Sigma-Aldrich, Taufkirchen
bFGF, recombinant human	PeproTech, Hamburg
Bisindolmaleimide I (BIM-I)	Merck, Darmstadt
Bromophenol blue	Applichem, Darmstadt
Casyton	Roche, Bremen
Carbonyl cyanide 3-chlorophenylhydrazone (CCCP)	Sigma-Aldrich, Taufkirchen
Citric acid	Roth, Karlsruhe
Collagen Type I Rat Tail	Corning, Tewksbury, MA (USA)
Cytidine	Sigma-Aldrich, Taufkirchen
D(+)-Sucrose	AppliChem, Darmstadt
Dimethyl sulfoxide (DMSO)	Sigma-Aldrich, Taufkirchen
Dithiothreitol (DTT)	Invitrogen, Burlington (Canada)
DNase I RNase free	Promega, Mannheim
dNTPs	Bioline, London (UK)
Dulbecco`s Phosphate Buffered Saline (DPBS)	ThermoFisher, Darmstadt
ECGS-H	Promocell, Heidelberg
EGF, human recombinant	PeproTech, Hamburg
Ethidium bromide	Roth, Karlsruhe
Ethylene glycol tetraacetic acid (EGTA)	Applichem, Darmstadt
Ethylenediaminetetraacetic acid (EDTA)	Applichem, Darmstadt
EtOH absolut	Sigma-Aldrich, Taufkirchen

Fetal calf serum (FCS)	ThermoFisher, Darmstadt
Fibronectin, human	BD Biosciences, Heidelberg
Flufenamic acid	Sigma-Aldrich, Taufkirchen
Gelatine	Sigma-Aldrich, Taufkirchen
Glacial acetic acid	Roth, Karlsruhe
Glycerin 86 %	Roth, Karlsruhe
Glycine	VWR, Kelsterbach
Guanosine	Sigma-Aldrich, Taufkirchen
N-Acetyl-L-Cysteine (NAC)	Sigma-Aldrich, Taufkirchen
N-2-Hydroxyethylpiperazin-N'-2-ethansulfonsäure (HEPES)	Roth, Karlsruhe
Hydrochloric acid (HCl)	Roth, Karlsruhe
IL-1 beta, recombinant human	Peprotech, Hamburg
Isopropyl alcohol	Sigma-Aldrich, Taufkirchen
Kaliumchlorid (KCl)	Roth, Karlsruhe
L-Glutamin	ThermoFisher, Darmstadt
Lipofectamin 2000	ThermoFisher, Darmstadt
L-Histidinol	Sigma-Aldrich, Taufkirchen
Lipofectamin RNAiMax	ThermoFisher, Darmstadt
Loading Dye	ThermoFisher, Darmstadt
Methanol	Sigma-Aldrich, Taufkirchen
Methanol, Ultra LC-MS grade	Roth, Karlsruhe
My-Budget 5x EvaGreen QPCR Mix II (ROX)	Bio&Sell, Feucht bei Nürnberg
Okadaic acid (OA)	Applichem, Darmstadt
Oligo(dT)23 Anchored	Sigma-Aldrich, Taufkirchen
Oligomycin A	Sigma-Aldrich, Taufkirchen
Orthovanadate (OV)	Applichem, Darmstadt
oxPAPC	AvantiPolarLipids (USA)
1-palmitoyl-2-arachidonoyl-sn-glycero-3-phosphocholine (PAPC)	Avanti Polar Lipids
Penicillin	ThermoFisher, Darmstadt
Penicillin/Streptomycin	Corning, Manassas (USA)
Pepton from casein (pancreatic digest)	AppliChem, Darmstadt
Phenylmethanesulfonylfluoride (PMSF)	Sigma-Aldrich, Taufkirchen
PMA	EnzoLifeSciences, Lörrach
Precision Plus Protein Standard Dual Color	Bio-Rad, Munich
Random Primers	Promega, Madison (USA)
Rapamycin	Sigma-Aldrich, Taufkirchen
Reverse Transkriptase Superscript III	Life technologies, Carlsbad (USA)

Rotenone	Sigma-Aldrich, Taufkirchen
Roti-Block	Roth, Karlsruhe
Rotiphorese Gel 30	Roth, Karlsruhe
Roti-Quant	Roth, Karlsruhe
Serine	Sigma-Aldrich, Taufkirchen
Sodium chloride	Sigma-Aldrich, Taufkirchen
Sodium dodecyl sulfate (SDS)	Roth, Karlsruhe
Streptomycin	ThermoFisher, Darmstadt
Tetramethylethylenediamine (TEMED)	AppliChem, Darmstadt
TRIS	Roth, Karlsruhe
Triton X-100	Roth, Karlsruhe
Trypsin-EDTA	Sigma-Aldrich, Taufkirchen
Tween-20	Sigma-Aldrich, Taufkirchen
Uridine	Sigma-Aldrich, Taufkirchen
VEGF (165), recombinant human	R&D, Minneapolis, MN (USA)

2.1.2 Equipment

Agilent 1260 Series binary pump	Agilent Technologies, Waldbronn
Agilent 1290 Infinity LC system	Agilent Technologies, Waldbronn
Autoclave	Tuttnauer, Beit Shemesh, (Israel)
Axiovert135 microscope	Zeiss, Oberkochen
Binocular	Motic, Wetzlar
Cell Counter Case	Schärfe System, Reutlingen
Centrifuge (rotor)	Eppendorf, Hamburg
Freezer HERAfreeze basic (-80 °C)	Heraeus Instruments, Hanau
Gel documentation system, Intas Gel-Stick Imager	Royal Biotech, Frankfurt am Main
Heating block Thermomixer compact	Eppendorf, Hamburg
Heraeus Megafuge 16	ThermoFisher, Darmstadt
Herasafe HS 12	Heraeus Instruments, Hanau
Incubator Hera Cell 150i CO2 Incubator	ThermoFisher, Darmstadt
Infrared scanner, Odyssey	LI-COR, Bad Homburg
Magnetic stirrers Heidolph MR Hei-Mix L	NeoLab, Heidelberg
Micro Star 17R	VWR, Darmstadt
Microscope Axiovert 40 ETL	Zeiss, Oberkochen
Microwave 900 & Grill	Severin, Sundern
PCR device Eppendorf Mastercycler Gradient	Eppendorf AG, Hamburg
pH meter PP-50	Sartorius, Göttingen

Pipettensatz	Eppendorf, Hamburg
Power supply CS - 300V	Roth, Karlsruhe
PowerPac HC	Bio-Rad, Munich
200Pro plate reader	Tecan, Crailsheim
qPCR device PIKOREAL 96	ThermoFisher, Darmstadt
QTrap 5500 mass spectrometer	Sciex, Darmstadt
Rotor Stuart SB3	Stuart, Staffordshire (UK)
Scale Analytical Balance	Sartorius, Göttingen
Seahorse 96 extracellular flux analyzer	Agilent Technologies, Waldbronn
Shaker GFL-3013	ThermoFisher, Darmstadt
MaxQ 4000 Benchtop Orbital	ThermoFisher, Darmstadt
Spectrophotometer NanoDrop® ND-1000	Nanodrop, Rockland (USA)
Sorvall RC 6+	ThermoFisher, Darmstadt
Sterile bench Laminarflow HB 2448	Heraeus Instruments, Hanau
Supercomputer Minerva	MountSinai, New York (USA)
TIRF System LASOS77	Zeiss, Oberkochen
Transfection system Neon	Life technologies, Carlsbad (USA)
Vortex mixer Vortex Genie 2	ScientificIndustries, NY (USA)
Water purification system Milli-Q	Q-POD Millipore, Billerica (USA)
Western Blot Kammern und Zubehör	Biorad, München

2.1.3 Buffers and solutions

Triton lysis buffer

20 mM Tris/HCl pH 7,5; 150 mM NaCl; 10 mM NaPPi; 20 mM NaF; 1% Triton X-100; 2 mM sodium orthovanadate (OV); 10 nM okadaic acid (OA); protein inhibitor mix (PIM) containing Antipain, Aprotinin, Chymostatin, Leupeptin, Pepstatin and Trypsin-Inhibitor (10 nM each); 40 µg/mL phenylmethylsulfonyl fluoride (PMSF)

10x wash buffer (WB)

0.3 % tween-20; 50 mM tris/ HCl pH 7.5; 150 mM NaCl

10x transfer buffer

25 mM tris; 190 mM glycin; 20 % methanol

10x running buffer

25 mM tris; 190 mM glycine; 0.1 % SDS

50x modified TAE

242 g mM tris; 57.1 mL glacial acetic acid; 10 mL EDTA (0.5 M); pH to 8.0; to 1L ddH_2O

Methocel

6 g methocel (autoclave powder); add 250 mL endothelial basal medium (EBM) and mix at 60 °C for 20 min add 250 mL EBM and mix overnight 4 °C; centrifuge 4000 rpm, 4 °C and for 2 h

Nuclear lysis buffer C
20 mM hepes pH 7.9; 0.4 mM NaCl; 1 mM EDTA; 1 mM EGTA; 4 % triton X-100; to 10 mL ddH2O; fresh: 10 µL 0.1 M DTT; 8.7 µL PMSF, 12 µL PIM

Cytosol lysis buffer A
10 mM hepes pH 7.9; 10 mM KCl; 0.1 mM EDTA; 0.1 mM EGTA; to 10 mL ddH_2O

3x Laemmli buffer
125.3 mM tris/ HCl pH 6.8; 17 % glycerol; 4 % SDS; 40 mM DTT; 0.004 % bromphenol blue

6x DNA loading dye
30 % v/v glycerol; 0.25 % w/v bromphenol blue; 0.25 % w/v xylene cyanol; to 10 mL ddH_2O

2.1.4 Cell culture media

Endothelial basal medium (EBM) (Pelo Biotech, Planegg)
supplemented with kit supplements: glutamine

Enhanced Endothelial Cell Growth Medium (Pelo Biotech, Planegg)
supplemented with kit supplements: glutamine, bFGF, hEGF, VEGF, 8% fetal calf serum, 0.5% penicillin, streptomycin

RPMI-1640 Media without glucose, glycine and serine (Teknova, Berlin)
supplemented with 1g/L glucose, 30 µM glycine, 300 µM serine

Smooth muscle cell growth medium classic (Pelo Biotech, Planegg)
supplemented with kit supplements: glutamine, insulin, EGF, FGF, 8% FCS, 0.5% penicillin, streptomycin

Minimum Essential Medium (MEM) (ThermoFisher, Darmstadt)
Supplemented with 8 % FCS, 0.1% Gentamycine, 1% Sodium pyruvate, 1% Non-essential amino acids

Trypsin solution (10×) (Sigma Aldrich, Taufkirchen)

2.1.5 Human eukaryotic cells

Human Aortic Endothelial Cells (HAEC) (PeloBiotech, Planegg)	primary cells
Human Umbilical Vein Endothelial Cells (HUVEC) (Lonza, Basel)	primary cells
Human Aortic Smooth Muscle Cells (HASMC) (PeloBiotech, Planegg)	primary cells
HEK293T (ATCC, Manassas (USA))	cell line

2.1.6 Synthetic oligonucleotides

Gene	Forward Primer (5‘-3‘)	Reverse Primer (5‘-3‘)
ASNS	GGAAGACAGCCCCGATTTACT	AGCACGAACTGTTGTAATGTCA
ATF4	CTGCCCGTCCCAAACCTTAC	TGCTCCGCCCTCTTCTTCTG
β-Actin	AAAGACCTGTACGCCAACAC	GTCATACTCCTGCTTGCTGAT
CARS	GGTGACGTGGTATTGCTGTG	CTCTTCTCCCGATACTGCTCG
CBS	GGCCAAGTGTGAGTTCTTCAA	GGCTCGATAATCGTGTCCCC
CEBPB	ACAAGCACAGCGACGAGTACAAGA	TGCTTGAACAAGTTCCGCAGGGT
CTH	GGCCTGGTGTCTGTTAATTGT	GCCATTCCGTTTTTGAAATGCT
DDIT3	AGCTGGAAGCCTGGTATGAG	AGTCAGCCAAGCCAGAGAAG
EBNA1BP2	CTCTCGGATTCGGAGTCGGA	GCCCCTCTAGCACGACATTG
EGR1	ACCCAGCAGCCTTCGCTAAC	AGAAGCGGCGATCACAGGAC
EHHADH	AAACTCAGACCCGGTTGAAGA	TTGCAGAGTCTACGGGATTCT
F3	GGAACCCAAACCCGTCAATC	GCCAAGTACGTCTGCTTCAC
G6PD	CGAGGCCGTCACCAAGAAC	GTAGTGGTCGATGCGGTAGA
GARS	ATGGAGGTGTTAGTGGTCTGT	CTGTTCCTCTTGGATAAAGTGCT
GCLM	CATTTACAGCCTTACTGGGAGG	ATGCAGTCAAATCTGGTGGCA
GINS1	ACGAGGATGGACTCAGACAAG	TGCAGCGTCGATTTCTTAACA
GSS	GGGAGCCTCTTGCAGGATAAA	GAATGGGGCATAGCTCACCAC
IFIT1	TTGATGACGATGAAATGCCTGA	CAGGTCACCAGACTCCTCAC
IFIT3	GATTGGGTGCTGCTACAAG	ATTCCGTCTCCAGGAACTC
IFNβ	AGTGTCAGAAGCTCCTGTGGC	TGAGGCAGTATTCAAGCCTCC
IL1β	CTGTACGATCACTGAACTGC	CACCACTTGTTGCTCCATATC
JHDM1D-AS1	GTTGGAGTCTGGCTAAAGAG	CTGGGCTTCCTTCTTCATAC
KDM7A	ACCTGAATGGAGAGCGAAAG	TCATGTTCCACTCCCTCTAC
KDM7A-TSS	AGCGCCGGAAGCAGCCGAGTCTGG	CTACTCCGCTCGCCGACTGG
KDM7A-1KB	CCCTCCCTCCCTTTCCTTTC	GCAATGAGCCGAGATCACAG
LDLR	GAATGGTGTGGACATCTACTCGCTCA	GCCAACAAGTTGACATCGGAAC
MTHFD1L	CTGCCTTCAAGCCGGTTCTT	TTTCCTGCATCAAGTTGTCGT
MTHFD2	GATCCTGGTTGGCGAGAATCC	TCTGGAAGAGGCAACTGAACA
PCK2	GCCATCATGCCGTAGCATC	AGCCTCAGTTCCATCACAGAT
PFKFB3	GGGCCAAAGCTGACCAACTC	CCCTTCTTTCGCCAGGTAGC
PHF8	TGCTGACATTGACCTCTACC	TTCCAGTGGGCTTCAGAATC
PHGDH	CTGCGGAAAGTGCTCATCAGT	TGGCAGAGCGAACAATAAGGC
PSAT1	TGCCGCACTCAGTGTTGTTAG	GCAATTCCCGCACAAGATTCT
SHMT2	CCCTTCTGCAACCTCACGAC	TGAGCTTATAGGGCATAGACTCG
SLC7A1	GTCCTGCTCAACATTGGGCA	CAGGGCCTGCATTCTCACG

SLC7A5	CCGTGAACTGCTACAGCGT	CTTCCCGATCTGGACGAAGC
sXBP1	CCGCAGCAGGTGCAGG	GAGTCAATACCGCCAGAATCCA
TCF7L2	AGAAACGAATCAAAACAGCTCCT	CGGGATTTGTCTCGGAAACTT
TIPIN	AGAATGGCGTGATTGACCTACC	CCAGTGCTCCATGTGTCTGATTA
ZWILCH	AAGAAAGGAATCCGTAAAGACCC	GGTCCAACATTTTCGCCAGTAG

2.1.7 Small interfering RNAs

siRNA	Sequence (5‘-3‘)
ATF4	GCCUUCUCCGGGACAGAUU
EGR1	UCUCCCAGGACAAUUGAAAUUUGCU
MTHFD2 # 1	GAAGAGCGAGAAGUGCUGAAGUCUA
MTHFD2 # 2	UAUUCCAAAUCUGAUCACAGCAGAU
MTHFD2 # 3	AGGAUGUUGAUGGCUUUCAUGUAAU
PHF8	GCCUGCUGGCCAGUUGAGCUAUAAU
PSAT1	GAUGUCAAGGGAGCAGUACUGGUUU

2.1.8 Plasmids

FUGW empty vector	(Huang *et al*, 2010b)
FUGW-KDM7A-Flag-IRES-GFP	(Huang *et al*, 2010b)
pcDNA3.1	Christoph Schürmann
pGL3 basic	Promega, Wisconsin (USA)
pCMV6_EGR1	Origene, Herford
pCMV6_BRCA1	Olesya Kuchyrivska
pCMV6_YY1	Origene, Herford
pGL3_KDM7A_323bp	Olesya Kuchyrivska

2.1.9 Antibodies

EGR1 (rabbit, Santa Cruz, Heidelberg, primary antibody)
KDM7A (rabbit, Abcam, Cambridge (USA), primary antibody)
Topoisomerase I (goat, Santa Cruz, Heidelberg, primary antibody)
IRDye680 (donkey, LI-COR Biosciences, Bad Homburg, secondary antibody)
IRDye800 (donkey, LI-COR Biosciences, Bad Homburg, secondary antibody)

2.1.10 Reaction systems

CellTiter-Glo Luminescent Cell Viability Assay	Promega, Madison (USA)
Gel purification kit	QIAGEN, Hilden

LC-MS free amino acid analysis kit	Phenomenex, Aschaffenburg
Luciferase Assay System	Promega, Wisconsin (USA)
PeqGOLD XChange Plasmid Maxi-EF Kit	Peqlab, Erlangen
RNA Mini Kit	Bio&Sell, Feucht bei Nürnberg
truChIP Chromatin Shearing KIT	Covaris, Massachusetts (USA)

2.1.11 Software

Analyst 1.6.2	Sciex, Darmstadt
AxioVision SE64 Rel. 4.9	Zeiss, Oberkochen
Clone Manager 9	Scientific and Educational Sofware, Cary (USA)
Cytoscape	Cytoscape Consortium, http://cytoscape.org/
Gel documentation sofware	Herolab, Wiesloch
GraphPadPrism 5	GraphPad Software, San Diego (USA)
Image studio lite 5.0	LI-COR, Bad Homburg
MultiQuant 3.0	Sciex, Darmstadt
Nanodrop, Version 3.5.1	Coleman Tech., Orlando, FL (USA)
PikoReal Software 2.1	ThermoFisher, Darmstadt
Python	https://www.python.org/
R	https://www.r-project.org/
R Studio	RStudio Inc., Boston, (USA)

2.1.12 Packages

Biobase	R, biocLite (Bioconductor)
BioNet	R, biocLite (Bioconductor)
BSDA	R, CRAN
EdgeR	R, biocLite (Bioconductor)
Gplots	R, CRAN
GSEABase	R, biocLite (Bioconductor)
HTSeq	Python
Igraph	R, biocLite (Bioconductor)
Multicon	R, CRAN
Reactome FI	Cytoscape
TopHat	https://ccb.jhu.edu/software/tophat/index.shtml

2.1.13 Databases

MSigDB	http://software.broadinstitute.org/gsea/msigdb/index.jsp

HPRD	http://www.hprd.org/
STRING	https://string-db.org/

2.1.14 Geo datasets used for analysis

GSE43292	Human carotid atheroma, microarray, 64 samples
GSE21545	Biobank of human carotid plaques, microarray, 223 samples
GSE27869	HUVEC, 400 siRNAs, microarray, 400 samples
GSE72509	SLE lupus, whole blood, RNAseq, 117 samples

2.2 Methods

2.2.1 Wet-laboratory methods

2.2.1.1 Eukaryotic cell culture conditions

Human Aortic Endothelial Cells (HAEC) and pooled Human Umbilical Vein Endothelial Cells (HUVEC) were cultured in a humidified atmosphere of 5% CO_2 at 37°C on gelatin coated dishes. HAEC and HUVEC were grown in enhanced Endothelial Cell Growth Medium. Human aortic smooth muscle cells (HASMCs) were cultured on collagen in Smooth Muscle Cell Growth Medium. HEK293 cells were grown in MEM (minimal essential medium) containing 8% FCS, Gentamycin, non-essential amino acids and sodium pyruvate. HUVEC were used at passages 3-5, HAEC at passages 3-10 and HASMC at passages 6-12.

2.2.1.2 Passaging and cell counting

Dishes were pre-coated with gelatin or collagen respectively for one hour. Cells were washed with 1xDPBS once and detached with Trypsin-EDTA. Digestion of surface receptors and cell junction proteins was stopped with cell growth medium. Cells were pelleted with 1200 rpm for 4 min and the cell pellet was resuspended in growth medium. A small fraction of the cell suspension was mixed with an isotonic saline solution (Casyton) and counted (Casy Cell Counter). Cells were seeded on pre-coated dishes. Collagen coated dishes were washed twice with 1xDPBS beforehand.

2.2.1.3 Cell stimulation

Stimulation experiments were performed in basal medium lacking growth factors and supplemented with 1 %FCS. Control cells were treated with the solvent of the stimulus. For oxPAPC exposure, oxPAPC was either used from Invivogen, Avanti Polar Lipids or produced from PAPC as previously described (Watson *et al*, 1997) as the following. PAPC, which was kept in chloroform in glass tubes under nitrogen gas at -80°C, was prepared and used freshly for each experiment: PAPC was evaporated under vortexing and nitrogen flow to achieve an even lipid film on the glass wall. The lipid film was then exposed to air oxidation for 24-72 hours. For cell treatment, oxidized PAPC was dissolved in the stimulation medium by warming up to 31°C and thorough vortexing. Since the activity of oxidized PAPC varies, concentrations in the range of 40-65 µg/ml were used. After stimulus exposure, cells were washed twice with DPBS and the stimulation was stopped with lysis buffer.

2.2.1.4 siRNA knockdown

For siRNA treatment, cells were seeded out to 70-80% confluence. The siRNA as well as Lipofectamine RNAiMAX were pre-incubated with basal medium for 5 minutes, mixed together and incubated for 10 minutes. Transfection mix was added to cells in basal medium with 2% FCS for at least 8 hours. Afterwards, cells were cultured in growth medium and harvested 48-72 hours after transfection.

2.2.1.5 Electroporation-mediated overexpression

Transient overexpression was conducted by electroporation. Cells were trypsinized, washed twice with 1x DPBS. 700.000 cells were mixed with 110 µL resuspension buffer (Neon, Invitrogen) and 7µg plasmid. Electroporation was carried out with two pulses of 1150 V. Cells were seeded out on precoated dishes in medium without antibiotics. Cells were cultured in full growth medium 6 h after electroporation and harvested after 24 h.

2.2.1.6 Spheroid outgrowth assay

HUVEC were trypsinated and pelleted cells were mixed with EGM containing 20 % methocel. EGM-methocel drops were pipetted on a sterile dish and cells were incubated as hanging drops overnight. Drops were collected by rinsing off and pelleted with 1000 rpm for 3 min and incorporated with 600 µl methocel in 12 %FCS. Cells in methocel were mixed with collagen and pipetted into a 48-well plate. Angiogenesis of the spheroids were induced with 30 ng/ml VEGF-A165 over night at 37°C. Spheroid outgrowth was stopped by paraformaldehyde. Images were acquired with an Axiovert135 microscope. For quantification of the cumulative sprout length and sprout number, ten spheroids per condition were analyzed with the help of the AxioVision software (Zeiss). Treatments with VEGF-A 165 were performed for 16 hours with a concentration of 10 ng/ml.

2.2.1.7 Cell migration

HUVEC were cultured in a 24-well plate. After applying a vertical scratch to the confluent cell layer, cells were kept in basal medium supplemented with 1% FCS. Endothelial cell migration close to the scratch area was monitored by live cell imaging (Zeiss TIRF System LASOS77). The migration distance was calculated using AxioVision software (Zeiss).

2.2.1.8 RNA isolation, reverse transcription and quantitative real-time PCR

Total RNA isolation was performed with an RNA Mini Kit (Bio&Sell). Concentration of RNA was determined by NanoDrop1000 and quantified by Nanodrop 3.5.1. In order to quantify the expression of mRNAs reverse transcription polymerase chain reaction (qRT-PCR) of total cellular RNA was performed. Complementary DNA (cDNA) was synthesized with SuperScript

III Reverse Transcriptase with oligo(dT) and random hexamer primers. After annealing of primers at 65°C for 5 minutes, reverse transcription was performed at 50°C for 1 hour. To quantify cDNA PCR was performed (Sambrook et al. 1989). PCR reaction was carried out using SYBR Green Master Mix and ROX as reference dye (BioRad) in a PikoReal cycler (ThermoFisher). Relative expression of target genes was normalized to ß-Actin and analyzed by the delta-delta Ct method with the PikoReal software (ThermoFisher).

2.2.1.9 Nuclear and cytosol extraction

Cells were washed twice with ice-cold DPBS and scraped off the dish. Cells were pelleted for 1 min at 17.000 g, resuspended in hypotonic buffer and incubated for 15 min. 1 % Nonidet was added and after 1 min vortexing nuclei were pelleted at 17.000 g for 3 minutes. Nuclear pellets were washed once. The supernatant was defined as the cytosolic fraction and protein content was assessed by Bradford assay. Bradford reagent (Roti-Quant) was added to 1:100 diluted lysate and absorbance was measured. Cytosolic fraction and nuclear pellet were boiled at 95°C for 5 minutes with Laemmli buffer.

2.2.1.10 SDS-PAGE and Western blotting

Proteins were separated by sodium dodecylsulfate polyacrylamide gel electrophoresis (SDS-PAGE). First, 40 µg total protein was concentrated in a 25 mM TRIS/HCl buffered polyacrylamide gel (5% polyacrylamide, pH 6.8) containing 190 mM glycine using 10 mA / gel. Second, total protein was separated in a TRIS/HCL buffered polyacrylamide gel (8% polyacrylamide, pH 8.8) using 20 mA / gel. Separated proteins were blotted onto a methanol activated nitrocellulose membrane (NeoLab) at 250 mA in a cooled transfer buffer system. Membranes were washed with washing buffer without detergents, blocked for 1 h with 1x Rotiblock and incubated with the primary antibody. After washing with washing buffer containing 0.3 % Tween the secondary antibody was incubated for 1 h. After washing off the secondary antibody, membranes were scanned with the odyssey imaging system (LI-COR).

2.2.1.11 Amino acid profiling

For amino acid profiling, HAEC were lysed in 85% Ultra LC-MS methanol and 15% LC-MS water. Lysates were centrifuged for 10 minutes at 17,000 g and 50 µl of supernatants were processed using the EZ:faast LC-MS free amino acid analysis kit according to the manufacturer's instructions with minor modifications: An internal standard (10 µl) was applied to all samples and to the standard curve. The internal standards included homoarginine, methionine-D_3 and homophenylalanine. Analysis of metabolites was performed by LC-MS/MS using an Agilent 1290 Infinity LC system coupled to a QTrap 5500 mass spectrometer. The intensity of the measured metabolite was normalized to internal standards

and protein content of cell lysate pellets as measured by Bradford assay. Analyst 1.6.2 and MultiQuant 3.0 were used for data acquisition and analysis.

2.2.1.12 Nucleoside measurement

HAEC were lysed and centrifuged as for amino acid profiling. Additionally to cell lysate, cell culture supernatant was collected and centrifuged for 10 minutes at 17,000 g. 200 µl of samples were analyzed by liquid chromatography-tandem mass spectrometry (LC-MS/MS) as described previously (Thomas *et al*, 2015). The LC-MS/MS system consisted of an Agilent 1260 Series binary pump and a triple quadrupole mass spectrometer 5500 QTRAP. The internal standards included adenosine, guanosine, cytidine, uridine, $^{13}C_5$ adenosine, $^{13}C_5$ guanosine and $^{13}C_5$-uridine. The intensity of measured nucleosides was normalized to internal standards and protein content of cell lysate pellets for intracellular nucleoside measurement and to intracellular RNA content for extracellular nucleoside measurement. Analyst Software 1.6 was used for analysis.

2.2.1.13 ATP measurement

Extracellular ATP was measured in cell supernatants centrifuged for 3 minutes at 5000 g and then 10 minutes at 17,000 g using CellTiter-Glo Luminescent Cell Viability Assay (Promega). Equal amounts of cell supernatant and luciferase lysis-buffer were mixed and incubated for 10 minutes while shaking. Luminescence was detected using an Infinite 200Pro plate reader (Tecan) and normalized to intracellular RNA concentration.

2.2.1.14 Oxygen consumption rate

The cellular oxygen consumption rate (OCR) was analyzed using a Seahorse 96 extracellular flux analyzer. HAEC were plated in Seahorse 96-well cell culture plates 1×10^4 cells/well one day before the assay and equilibrated for 1 h in Krebs Henseleit buffer (111 mM NaCl, 4.7 mM KCl, 1.25 mM $CaCl_2$, 2 mM $MgSO_4$, 1.2 mM NaH_2PO_4 supplemented with 11 mM L-Glucose and 2 mM L-Glutamine. Cells were treated with 2.5 µM oligomycin A, 1 µM carbonyl cyanide-3-chlorophenylhydrazone (CCCP), 1 µg/ml antimycin A and 1 µM rotenone as indicated. OCR was normalized to protein content of the wells.

2.2.1.15 Luciferase Assay

HEK were transiently transfected with pGL3 basic or pGL3_KDM7A_323bp and overexpression plasmids with Lipofectamine 3000 (Thermo Fisher) according to manufacturers protocol. Luciferase activity was determined with the assay kit from Promega in a TECAN infinite M200OPro plate reader and normalized to the empty pGL3 control vector.

2.2.1.16 Chromatin immunoprecipitation

Preparation of cell extracts, crosslinking and isolation of nuclei was performed with the truCHIP™ Chromatin Shearing Kit (Covaris) according to the manufacturers instructions. After sonification of the lysates with the Bioruptur Plus (10 cycles, 30 sec on, 90 sec off, 4°C; Diagenode, Seraing, Belgium), cell debris was removed by centrifugation and the lysates were diluted 1:3 in dilution buffer (20 mmol/L Tris/HCl pH 7.4, 100 mmol/L NaCl, 2 mmol/L EDTA, 0.5% Triton X-100 and protease inhibitors). Pre-clearing was done with 20 µL DiaMag protein A and protein G coated magnetic beads slurry (Diagenode) for 45 min at 4°C. The samples were incubated as indicated over night at 4°C with the antibodies indicated. 5% of the samples served as input. The complexes were collected with 50 µL DiaMag protein A and protein G coated magnetic beads (Diagenode) for 3 h at 4°C, subsequently washed twice for 5 min with each of the wash buffers 1-3 (Wash Buffer 1: 20 mmol/L Tris/HCl pH 7.4, 150 mmol/L NaCl, 0.1% SDS, 2 mmol/L EDTA, 1% Triton X-100; Wash Buffer 2: 20 mmol/L Tris/HCl pH 7.4, 500 mmol/L NaCl, 2 mmol/L EDTA, 1% Triton X-100; Wash Buffer 3: 10 mmol/L Tris/HCl pH 7.4, 250 mmol/L lithium chloride, 1% Nonidet p-40, 1% sodium deoxycholate, 1 mmol/L EDTA) and finally washed with TE- buffer pH 8.0. Elution of the beads was done with elution buffer (0.1 M NaHCO3, 1% SDS) containing 1x Proteinase K (Diagenode) and shaking at 600 rpm for 1h at 55°C, 1h at 62°C and 10 min at 95°C. After removal of the beads, the eluate was purified with the QiaQuick PCR purification kit (Qiagen) and subjected to qPCR analysis.

2.2.1.17 Statistics for wet-laboratory experiments

Unless otherwise indicated, data are given as mean ± standard error of the mean. Calculations were performed with Prism 5.0. The latter was also used to test for normal distribution and similarity of variance. In the case of multiple testing, Bonferroni correction was applied. For multiple group comparisons, analysis of variance followed by post hoc testing was performed. Individual statistics of dependent samples were performed by paired t-test, of unpaired samples by unpaired t-test, and, if not normally distributed, by Mann-Whitney test. P values of <0.05 were considered significant. Unless otherwise indicated, n indicates the number of individual experiments.

2.2.2 Computational methods

2.2.2.1 Gene set enrichment analysis (GSEA)

Genes of interest were compared to 17,780 canonical and non canonical gene sets from the Molecular Signatures Databse (MSigDB version 6.0 or older). These included the canonical gene set collections GO, KEGG, REACTOME and BIOCARTA. The gene set collections were retrieved using the R package GSEABase (BiocLite, Bioconductor). The enrichment of the 17,780 gene sets of MSigDB in either the differentially expressed genes (DEG) compared to all genes of the RNAseq data set, a certain differential connectivity (DC) cluster compared to all DC clusters or a given Bayesian network (BN) subnetwork to whole BN, was assessed by Fisher's exact test using R. The false discovery rate (FDR) corresponding to a given p-value threshold was computed as the ratio of the number of pathways with a p-value below threshold, averaged over 50 randomized data sets, and the number of pathways with p-value below threshold. A 5% FDR based on the empirical permutation test corresponds to a Fisher's exact test p-value $<1x10^{-3}$.

2.2.2.2 Heatmap creation

Heatmaps for RNAseq data and amino acid profiles were created using the Heatmap.2 function within the R package gplot (CRAN) using R. Dendrograms were computed using the distfun function to calculate the dissimilarity (distance) between rows and between columns. The hclust function was used to calculate the hierarchical clustering when no dendrogram was applied for either rows or columns. For this, the agglomeration method Unweighted Pair Group Method with Arithmetic mean (UPGMA) was applied.

2.2.2.3 Network visualization

Networks were created in R as *.sif formate and visualized using Cytoscape version 3.5.1 or older. Node tables and edge tables were created using R. The cytoscape plugin Reactome FI was used as template to visualize the KDM7A signature within a Reactome gene set.

2.2.2.4 Differential connectivity analysis

Differential connectivity (DC) analysis of gene expression traits can detect disease associated genes that are not detected by conventional t-statistics based differential expression (DE) analysis. Differentially co-expressed gene pairs and DC clusters were computed as previously described (Narayanan *et al*, 2014). Changes in gene-gene correlation between control and oxPAPC treated groups were calculated under the assumption that gene pairs are bivariate normally distributed by a parametric meta-analysis.

Firstly, Spearman correlation coefficients r_{tij} r_{tij} ($t = 1$ for oxPAPC samples and $t = 2$ for control samples) for each gene pair (i, j) were transformed into Fisher's Z-statistics (z_{tij}):

(15) $$z_{tij} = \frac{1}{2} log\left(\frac{1+r_{tij}}{1-r_{tij}}\right)$$

This allows normal distribution with zero mean and standard deviation for a given sample size (n_t):

(16) $$SD = \frac{1}{\sqrt{n_{tij}-3}}$$

Secondly, heterogeneity statistic Q was calculated for each gene pair:

(17) $$Q = \sum_{tij} = \left(z_{tij} - \bar{z}\right)^2$$

The weights w_{tij} were used to calculate the weighted average $\bar{z}$ of z in oxPAPC and control samples:

(18) $$w_{tij} = n_{tij} - 3$$

The Q statistic follows a χ^2 distribution with a large χ^2 meaning less similar gene-gene correlation between oxPAPC and control group. Next, permutations were carried out to make differential co-expression calls from the Q-statistics: 997 permutations and applying the meta-analysis for each permutation were conducted by randomly assigning sample labels to shuffle the two groups together. The ratio of the number of gene pairs that had $Q>Q_0$ with Q_0 as global cutoff was chosen as FDR for this cutoff. A final cutoff of Q_0=22.5, which corresponds to FDR = 4.89%, for oxPAPC versus control was used to detect DC pairs. In addition a given gene pair had to be significantly co-expressed (Spearman's correlation p-value >0.01) in either control or oxPAPC group but not both to be called a differentially co-expressed DC gene pair. If the differentially co-expressed gene pair was significantly co-expressed in control group, but not oxPAPC group it was assigned to loss of connectivity (LOC) category and if the DC gene pair was significantly co-expressed in oxPAPC, but not control group it was assigned to gain of connectivity (GOC) category.

2.2.2.5 Identification of key drivers and associated subnetworks

For control and oxPAPC Bayesian network key causal regulators were computed as described previously (Zhu *et al*, 2007). For reading and analyzing the networks, the R packages BioNet and igraph (BiocLite, Bioconductor) were used. To determine key drivers, the number of N-hob downstream nodes (NHDN) for each gene was calculated. Firstly, genes which have

(19) $$\mu > \bar{\mu} + \sigma(\mu)$$

with μ = NHDN were nominated as key drivers. Secondly, nominated key drivers which have

(20) $$d > \bar{d} + 2\sigma(d)$$

with d as the outdegrees, meaning edges in outward direction, were selected as key drivers. With both criteria fulfilled, key drivers possessed a greater number of downstream nodes and

out links significantly above the average. The key drivers were ranked by the neighborhood size in outdegree direction, meaning number of downstream nodes. 29 key drivers were detected in BN_{ct} and 27 key drivers in BN_{ox}.
Next, the subnetwork associated with each key driver was defined as downstream nodes (i.e. neighbors in outdegree direction) with the key driver as the seeding point. Edges remained the same as in the complete network.

2.2.2.6 Identification of gene signature subnetworks

For the identification of KDM7A and PHF8 signature subnetworks, the R package igraph (BiocLite, Bioconductor) was used. Firstly, differentially expressed genes (DEG) of the KDM7A and PHF8 RNAseq data were identified (FDR < 0.05). Secondly, DEG which are contained within the Bayesian network, were selected. Next, directed neighbors to DEG within the network (order = 1) in indegree and outdegree direction were additionally selected. All selected genes were extracted leading to connected subnetworks of different size or non connected nodes. The resulting subnetworks were sorted by node size and the largest connected subnetwork was defined as the signature subnetwork. Next, key drivers of the signature subnetwork were defined and the subnetwork was tested for enriched biological processes (GSEA).

2.2.2.7 RNA sequencing and data analysis

RNA isolated from HAEC was treated with DNase (Qiagen, Cat# 79254). Library construction (LncRNA library, Ribo-Zero), quality assessment and sequencing (HiSeqSE50) were performed by Novogene. Differentially expressed genes were identified using the following procedure: first, sequencing reads were aligned to the human reference genome hg19 using TopHat (Trapnell *et al*, 2009). Next, the mapped sequences were aligned with htseq-count to quantify the read count for each gene (Anders *et al*, 2015). The edgeR package (Robinson *et al*, 2009) was then used to identify differentially expressed genes between control and siRNA treatment. 286 differentially expressed genes were detected at adjusted p-value of 0.005.

2.2.2.8 Assessment of Bayesian networks

To assess the accuracy of the human aortic endothelial cell Bayesian networks, the BNs were compared with several widely used databases of gene networks and gene sets: 1) 37,080 interactions covering 9,465 genes from Human Protein Reference Database (HPRD) database (Peri *et al*, 2004), 2) 195,859 high confident interactions covering 12,427 genes from STRING database (Franceschini *et al*, 2013), 3) 1,329 canonical pathways covering 8,439 genes from MsigDB databases (Subramanian *et al*, 2005), and 4) 11,174 Gene Ontology (GO) annotation sets (sets with size >=200 are excluded) covering 11,508 genes.

In particular, the percentage of inferred gene-gene connections within the BNs which were in existing protein/gene network databases, or within the same pathway in gene set databases were calculated. For comparison, 100 random networks were generated for corresponding BNs by using degree.sequence.game function within the igraph R package, and estimated accuracy of random networks was determined.

Additionally, the predictive power of the BNs was assessed by using gene sets closely regulated in endothelial cells. In particular, two independent gene sets were used: 77 gene sets related to endothelial cell from MsigDB and 400 siRNA gene signatures in HUVEC (Hurley *et al*, 2012). For siRNA gene signatures, microarray data were downloaded from Gene Expression Omnibus (GEO) (GSE27869) and preprocessed as previously described (Hurley *et al*, 2012). The R packages Biobase, BSDA and multicon were used to pre-process the data, z-transformation and z-test. Genes with a z-score >2 and <-2 were defined as significantly up-regulated and down-regulated genes respectively. Based on these gene sets, the accuracy of the BNs were compared to that of widely used gene networks including HRPD database by calculating the percentage of gene-gene connections that are within the same gene set.

2.2.2.9 Processing of Atheroma, Biobank and SLE data

Human carotid atheroma data (Ayari & Bricca, 2013) (GSE43292), biobank human carotid plaque data GSE21545 (Folkersen & Persson, 2012) and Systemic lupus erythematodes (SLE) data (Hung *et al*, 2015) (GSE72509) were downloaded from GEO. Each platform's probe ID was mapped to the corresponding gene symbol and the expression levels were averaged over multiple probes mapped to the same gene symbol. The significance level of differentially expressed genes between disease and control group was calculated by Wilcoxon rank sum test. Correlation coefficients were calculated using the cor function in R for Pearson correlation. The cumulative distribution function (CDF) was plotted using the plot function in R.

2.2.2.10 Genome-wide association studies (GWAS) of plasma metabolites and coronary artery disease

Significant single nucleotide polymorphisms (SNPs) (meta-analysis p-value < $1x10^{-4}$) associated with one of more than 400 metabolites in human blood in a genome-wide association study (http://metabolomics.helmholtz-muenchen.de/gwas/) (Shin *et al*, 2014b) were collected. Candidate SNPs were mapped to genes if their physical locations were within ± 5kb of gene bodies. Candidate SNPS in CARDIoGRAMplusC4D (Coronary ARtery DIsease Genome wide Replication and Meta-analysis (CARDIoGRAM) plus The Coronary Artery Disease (C4D) Genetics) consortium were also compared. In particular, significant SNPs

with p-value < $1x10^{-4}$ based on CARDIoGRAMplus4D 1000 Genome-based GWAS study, which is a meta-analysis of GWAS studies using 1000 genomes with 38 million variants (Nikpay *et al*, 2015), were collected. Significant SNPs whose physical location was within ±500kb of coding region of genes within the MTHFD2 subnetwork were searched.

3 Results

3.1 Integrative network analysis of human aortic endothelial cells in response to oxPAPC

In order to determine key drivers and gene clusters which shape the response of endothelial cells to pro-atherogenic lipids, an integrative network approach was applied (Hitzel *et al*, 2018). In a first step, expression profiles of HAEC obtained from 147 heart transplant donors were reused. HAEC of this cohort had been split and exposed to oxPAPC and vehicle control for 4 hours (Romanoski *et al*, 2011). Apart from canonical identification of differentially expressed genes, this dataset was exploited to identify gene pairs which show differential co-expression between control and oxPAPC treated state (Figure 10 A).

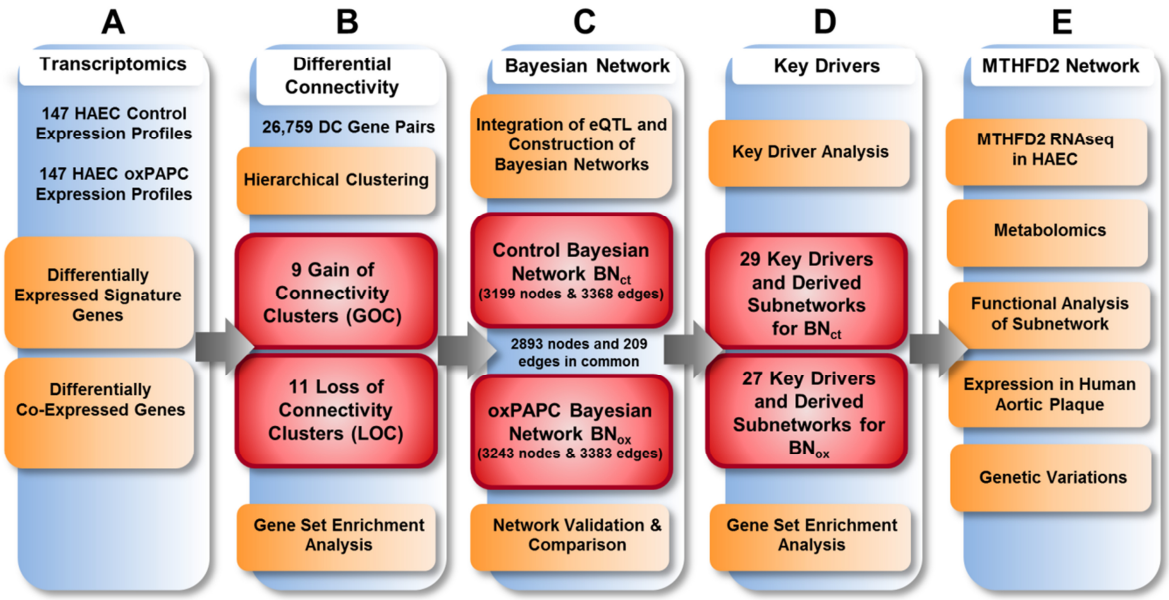

Figure 10: Integrative network approach in HAEC.

Expression profiles were used to compute differential connectivity clusters (A, B) and genotype profiles were integrated to construct Bayesian networks (C). Key drivers of the Bayesian networks were identified (D) and the subnetwork of the key driver MTHFD2 was investigated in detail (E). (Hitzel *et al*, 2018)

Hierarchical clustering of these differential connected gene pairs revealed 20 gene clusters which were characterized using gene set enrichment analysis (GSEA) (Figure 10 B). Since the data sets of the control and oxPAPC treated state are characterized by the same genotype as they originate from the same cohort of human individuals, expression quantitative trait loci of this cohort (Erbilgin *et al*, 2013) were integrated with the expression profiles to infer causal relationships between genes (Figure 10 C). The resulting Bayesing networks were assessed for their predictive power by systematically comparing them to known gene-gene relationships. Causal networks were marked by intrinsic hierarchy and therefore allowed identification of nodes which control large parts within the network. These

key drivers and their associated subnetworks were identified and the functions of these subnetworks were assessed by gene set enrichment analysis (Figure 10 D). The oxPAPC emerged subnetwork which was controlled by the key driver MTHFD2 was selected for detailed investigation which among others included RNAseq profiling, metabolomics and functional characterization (Figure 10 E).

3.1.1 Differential connectivity clusters reveal a deregulated amino acid metabolism in response to oxPAPC

Undirected gene co-expression networks have been widely used to represent more general relationships among genes. Such a weighted gene co-expression approach identified Hemeoxygenase 1 (HO1) as a hub protein in a module in oxPAPC exposed HAEC (Romanoski *et al*, 2011). Instead of focusing on co-expression modules with limited information, the analysis was extended and differential co-expression clusters were computed. This approach gives additional information about the direction of the connection between genes in control versus treated state (Narayanan *et al*, 2014) and thereby helps identifying differentially regulated biological processes upon oxPAPC exposure.

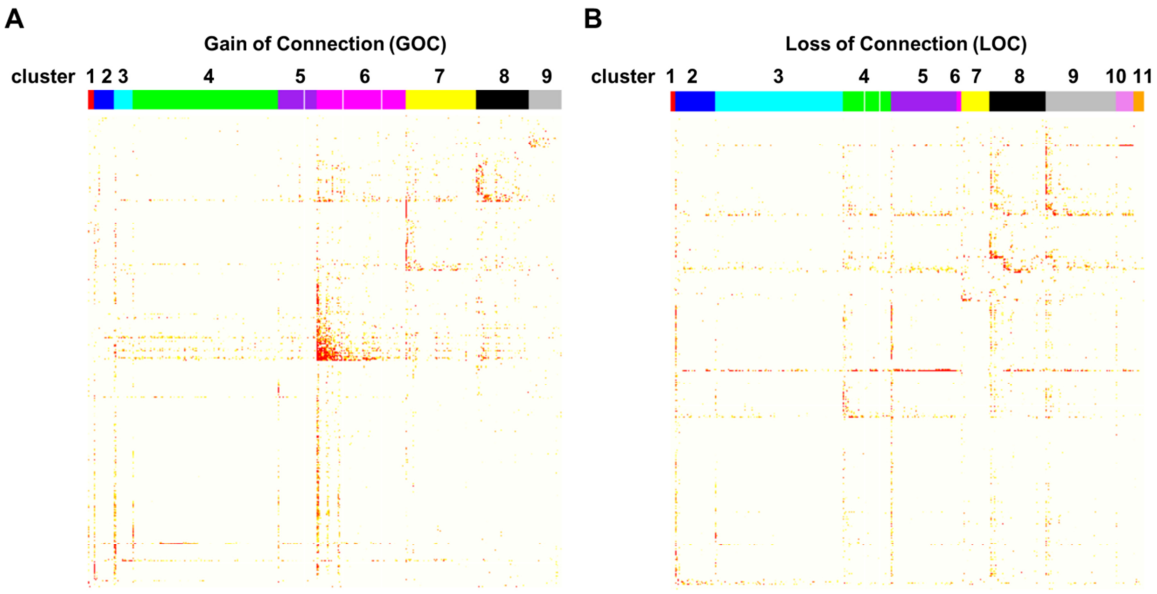

Figure 11: Differential connectivity clusters of HAEC exposed to oxPAPC.

Topological overlap matrix (TOP) of nine clusters with significant gain of co-expression (GOC) (A) and eleven clusters with significant loss of co-expression (LOC) (B) identified in a comparison of genome-wide gene-gene co-expression relations between oxPAPC treated and control HAEC. (Hitzel *et al*, 2018)

Firstly, differential connected (DC) gene pairs under the two conditions were identified (Hitzel *et al*, 2018). 26,759 DC gene pairs showed significant differential co-expression. Among these significantly co-expressed DC gene pairs 50.4% showed gain of connectivity (GOC) meaning enhanced co-regulation between genes with oxPAPC treatment. In comparison,

49.5% showed loss of connectivity (LOC), thus reduced co-regulation between genes. Secondly, hierarchical clustering was applied which yielded nine significant GOC clusters (Figure 11 A) and eleven significant LOC clusters (Figure 11 B) with co-regulations elicited by oxPAPC. Among all DC clusters, GOC cluster 6 showed the most coherent differential connectivity changes which suggest that GOC cluster 6 represents the strongest response of HAEC to oxPAPC. To dissect biological meaning of DC gene clusters, gene set enrichment analysis (GSEA) was performed.

Table 1: Significantly overrepresented canonical pathways in GOC clusters. (Hitzel *et al*, 2018)

GOC cluster	Top functional category	p–value
GOC1	GO_MACROAUTOPHAGY	2.55E-03
GOC2	GO_HOMOPHILIC_CELL_ADHESION_VIA_PLASMA_MEMBRANE_ADHESION_MOLECULES	3.22E-34
	KEGG_LYSOSOME	2.21E-10
GOC3	GO_LAMELLIPODIUM	1.81E-05
GOC4	GO_MITOTIC_CELL_CYCLE	2.12E-31
	HALLMARK_G2M_CHECKPOINT	1.11E-21
	REACTOME_CELL_CYCLE	4.35E-19
	KEGG_CELL_CYCLE	2.06E-05
GOC5	GO_NEGATIVE_REGULATION_OF_MITOTIC_CELL_CYCLE	7.74E-05
GOC6	GO_CELLULAR_AMINO_ACID_METABOLIC_PROCESS	1.63E-09
	HALLMARK_MTORC1_SIGNALING	2.66E-11
	REACTOME_CYTOSOLIC_TRNA_AMINOACYLATION	4.24E-09
	KEGG_AMINOACYL_TRNA_BIOSYNTHESIS	1.19E-08
GOC7	GO_ORGAN_MORPHOGENESIS	8.13E-08
GOC8	GO_NUCLEIC_ACID_BINDING_TRANSCRIPTION_FACTOR_ACTIVITY	6.28E-08
GOC9	GO_REGULATION_OF_CELLULAR_RESPONSE_TO_HEAT	6.33E-10

Table 2: Significantly overrepresented canonical pathways in LOC clusters. (Hitzel *et al*, 2018)

LOC cluster	Top functional category	p–value
LOC1	GO_REGULATION_OF_MESODERM_DEVELOPMENT	2.91E-05
	HALLMARK_ESTROGEN_RESPONSE_LATE	5.49E-05
LOC2	GO_POSTTRANSCRIPTIONAL_REGULATION_OF_GENE_EXPRESSION	1.96E-06
	HALLMARK_P53_PATHWAY	3.66E-07
LOC3	GO_CATABOLIC_PROCESS	6.59E-07
	REACTOME_METABOLISM_OF_RNA	9.46E-05
LOC4	GO_DNA_DEPENDENT_DNA_REPLICATION	2.49E-09
	REACTOME_CELL_CYCLE	4.18E-09
	HALLMARK_E2F_TARGETS	1.17E-08
	KEGG_DNA_REPLICATION	7.28E-05
LOC5	GO_MITOCHONDRIAL_PART	2.01E-10
	HALLMARK_MYC_TARGETS_V1	5.02E-10
	REACTOME_CELL_CYCLE	4.29E-07
LOC6	GO_SPHINGOLIPID_METABOLIC_PROCESS	1.09E-04
LOC7	GO_REGULATION_OF_CELLULAR_AMIDE_METABOLIC_PROCESS	1.81E-06
	HALLMARK_TNFA_SIGNALING_VIA_NFKB	3.01E-06

LOC8	GO_RIBONUCLEOTIDE_BINDING	2.39E-09
	HALLMARK_G2M_CHECKPOINT	9.23E-11
LOC9	GO_NCRNA_PROCESSING	2.65E-09
	REACTOME_SRP_DEPENDENT_COTRANSLATIONAL_PROTEIN_TARGETING_TO_M	3.61E-08
	EMBRANE	9.28E-07
	KEGG_RIBOSOME	
LOC10	GO_IMMUNE_SYSTEM_PROCESS	1.40E-07
	KEGG_CELL_ADHESION_MOLECULES_CAMS	1.41E-06
	REACTOME_IMMUNOREGULATORY_INTERACTIONS_BETWEEN_A_LYMPHOID_AN	8.34E-05
	D_A_NON_LYMPHOID_CELL	
LOC11	GO_CIRCULATORY_SYSTEM_DEVELOPMENT	3.90E-12
	HALLMARK_TGF_BETA_SIGNALING	1.18E-06
	KEGG_TGF_BETA_SIGNALING_PATHWAY	2.17E-06

The top functional GO category of each GOC and LOC cluster is listed in Table 1 and Table 2 respectively. Additionally the top functional category from KEGG, HALLMARK and REACTOME gene sets (MSigDB v.6) are listed if p-value ≤ 1E-05 according to Fisher's exact test (FET). Biological processes related to cell adhesion and lysosomal function (GOC2) as well as cell cycle (GOC4) and heat shock response (GOC9) showed the strongest enrichment for gain of connectivity between genes upon oxPAPC treatment (Table 1). In contrast, loss of connectivity was observed for biological processes related to development (LOC11), cell cycle (LOC4, LOC5, LOC8) and non-coding RNA (LOC9) (Table 2). Top 10 significantly overrepresented canonical gene set categories (MSigDB v.6) for cluster GOC6 are listed in Table 3. GOC cluster 6 was significantly enriched for categories related to mTOR signaling and unfolded protein response. Many of the 10 most significantly enriched canonical gene set categories were related to amino acid metabolism. Therefore, GOC cluster 6 was termed GOC-AA.

Table 3: Significantly overrepresented gene set categories in GOC-AA. (Hitzel *et al*, 2018)

GOC-AA: Top functional canonical gene set categories	p–value
MTOR_UP.N4.V1_UP	4.74E-14
ALK_DN.V1_UP	3.24E-12
HALLMARK_MTORC1_SIGNALING	2.66E-11
HALLMARK_UNFOLDED_PROTEIN_RESPONSE	1.07E-09
GO_CELLULAR_AMINO_ACID_METABOLIC_PROCESS	1.63E-09
REACTOME_CYTOSOLIC_TRNA_AMINOACYLATION	4.24E-09
GO_ORGANIC_ACID_METABOLIC_PROCESS	8.75E-09
KEGG_AMINOACYL_TRNA_BIOSYNTHESIS	1.19E-08
REACTOME_TRNA_AMINOACYLATION	1.19E-08
TGANTCA_AP1_C	3.83E-08
RCGCANGCGY_NRF1_Q6	4.61E-08
GO_NEGATIVE_REGULATION_OF_CELL_DEATH	5.55E-08

Taken together, the applied DC clustering approach suggests that amino acid metabolism experiences a massive remodeling in response to oxidized phospholipids.

3.1.2 Bayesian network modeling of HAEC exposed to oxPAPC

To explore the mechanism underlying deregulated amino acid metabolism in response to oxPAPC, Bayesian network modeling was applied (Hitzel *et al*, 2018). This approach gives hierarchical information of gene gene relationships and therefore allows for the identification of causal regulators. In order to construct directed probabilistic Bayesian networks, expression profiles of control and oxPAPC treated state, as used for computing the DC clusters, and expression quantitative trait loci of the same cohort were integrated to infer causal relationships among genes. The resulting control Bayesian network (BN_{ct}) and oxPAPC Bayesian network (BN_{ox}) were assessed, analyzed and experimentally validated.

3.1.3 Systematic assessment of HAEC Bayesian networks

Firstly, BN_{ct} and BN_{ox} were compared with widely used databases for gene sets and gene networks (Hitzel *et al*, 2018). The estimated accuracies of BN_{ct} and BN_{ox} were higher than corresponding 100 random networks for: 37,080 interactions covering 9,465 genes from Human Protein Reference Database (HPRD); 195,859 high confident interactions covering 12,427 genes from STRING database; 1,329 canonical pathways covering 8,439 genes from MsigDB databases; and 11,174 Gene Ontology (GO) annotation sets covering 11,508 genes (Figure 12 A).

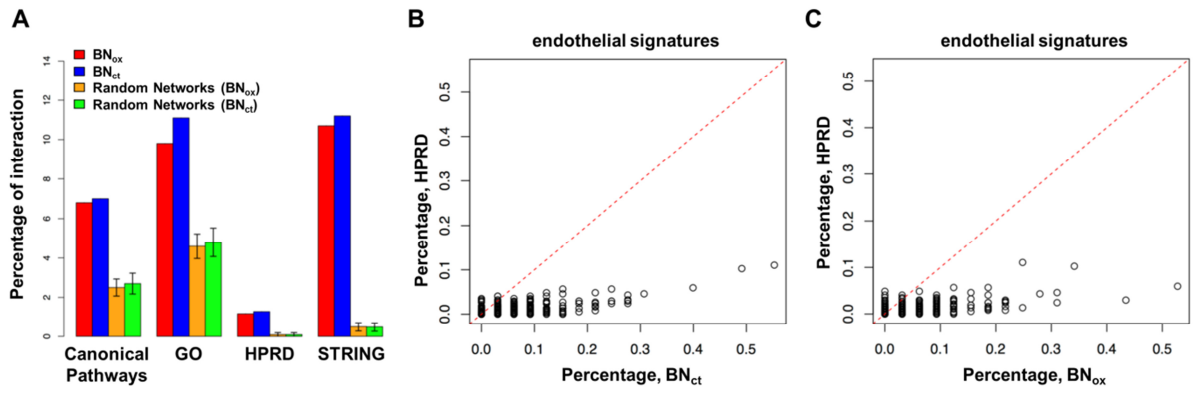

Figure 12: Validation of HAEC Bayesian networks.

A: Percentage of inferred gene gene connections in BNs and corresponding random networks within gene set and network databases. B, C: Percentage of gene gene connections in BN_{ct} (B) and BN_{ox} (C) compared to HPRD networks within endothelial signatures. (Hitzel *et al*, 2018)

Secondly, the predictive power of BN_{ct} and BN_{ox} were assessed with respect to endothelial specific signatures. The percentage of gene gene connections within BN_{ct} (Figure 12 B) and BN_{ox} (Figure 12 C) was higher than in global gene networks from HPRD for endothelial

specific signatures which consisted of 77 endothelial related gene sets (MSigDB) and 400 siRNA gene signatures in HUVEC (Hurley *et al*, 2012).

3.1.4 Key driver analysis of HAEC Bayesian networks

To identify causal regulators and their regulated biological processes, key driver analysis was performed (Zhu *et al*, 2008; Zhang *et al*, 2013). Key drivers are defined as nodes which control many downstream nodes and which influence the expression of a significant portion of the subnetwork they reside in. 73 and 72 key drivers were identified in BN_{ct} and BN_{ox} respectively. Next, the subnetwork associated with each key driver was extracted. Each key driver was used as seeding point and all downstream nodes, meaning neighbors in outdegree direction, were defined. This approach yielded 29 and 27 key drivers with associated subnetworks with more than 100 nodes in size for BN_{ct} and BN_{ox} respectively (Figure 13).

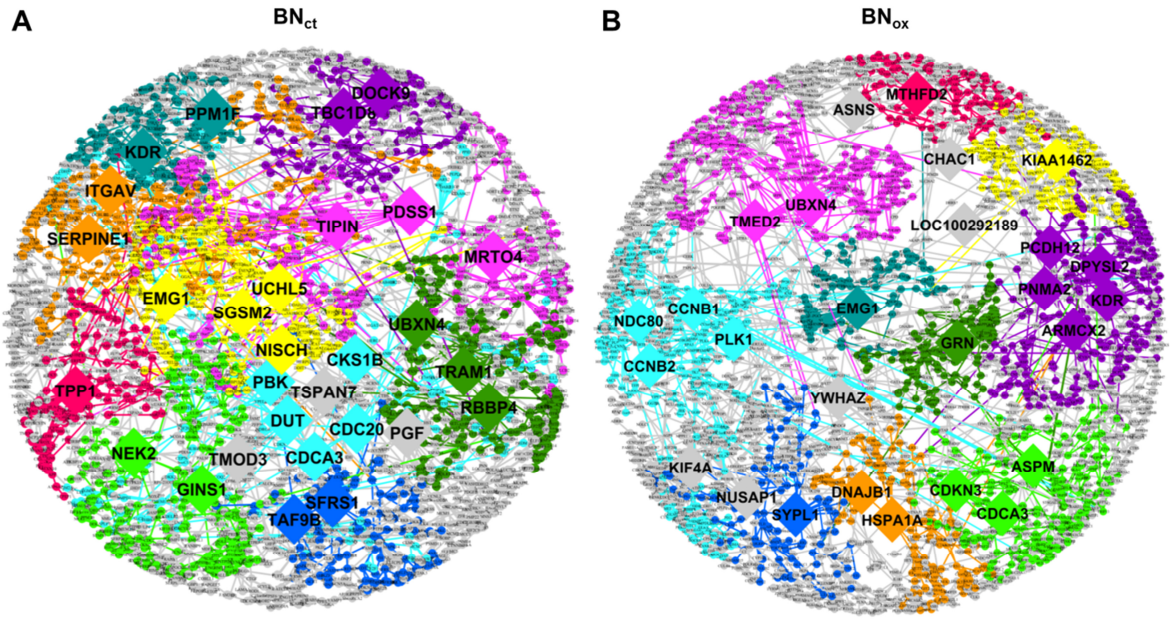

Figure 13: HAEC Bayesian networks.

Network view of HAEC Bayesian networks of control state (BN_{ct}) (A) and oxPAPC treated state (BN_{ox}) (B). Key drivers with more than 100 downstream nodes are indicated and ten selected top-ranked subnetworks are colored. Edges are colored according to source node. (Hitzel *et al*, 2018)

Gene set enrichment analysis of identified key driver subnetworks in BN_{ct} showed canonical gene set categories related to cell cycle, ribosome biogenesis, Wnt-signaling and vacuolar lumen / Lysosome related pathways as major biological processes (Table 4, Appendix).

Table 4: Most significantly overrepresented canonical gene set category (FET p-value) in key driver (KD) associated subnetworks (node size ≥ 100) in BN_{ct}. Selected top-tanked subnetworks are highlighted as in Figure 13. (Hitzel *et al*, 2018)

KD	size	Top functional canonical gene set category	p–value
CDCA3	589	GO_DNA_REPLICATION	6.58E-19
PDSS1	544	GO_RIBOSOME_BIOGENESIS	5.83E-10
DOCK9	348	GO_INORGANIC_ION_TRANSMEMBRANE_TRANSPORT	5.85E-06
NEK2	317	HALLMARK_E2F_TARGETS	5.28E-24
TRAM1	281	KEGG_WNT_SIGNALING_PATHWAY	4.73E-05
TBC1D8	268	GO_INORGANIC_ION_TRANSMEMBRANE_TRANSPORT	8.52E-05
EMG1	243	GO_TRNA_PROCESSING	1.13E-04
CKS1B	232	GO_DNA_REPLICATION	7.56E-29
ITGAV	230	HALLMARK_INFLAMMATORY_RESPONSE	1.70E-06
PBK	223	GO_DNA_REPLICATION	2.86E-19
UBXN4	210	KEGG_WNT_SIGNALING_PATHWAY	4.95E-05
TIPIN	179	GO_ANTIGEN_PROCESSING_AND_PRESENTATION_VIA_MHC_CLASS_IB	6.61E-04
TMOD3	158	GO_REGULATION_OF_RNA_SPLICING	5.72E-05
GINS1	151	GO_DNA_REPLICATION	2.67E-20
PPM1F	150	GO_MEMBRANE_REGION	1.05E-05
DUT	143	GO_L_ASCORBIC_ACID_BINDING	4.05E-04
CDC20	141	GO_PEPTIDYL_TYROSINE_MODIFICATION	4.74E-04
TPP1	140	GO_VACUOLAR_LUMEN	1.76E-06
UCHL5	139	GO_RESPONSE_TO_TOPOLOGICALLY_INCORRECT_PROTEIN	7.36E-04
TAF9B	131	GO_TRANSCRIPTION_FACTOR_COMPLEX	5.06E-05
SERPINE1	127	GO_REGULATION_OF_N_METHYL_D_ASPARTATE_SELECTIVE_GLUTAMATE_RECEPTOR_ACTIVITY	6.12E-05
KDR	125	GO_MEMBRANE_REGION	6.99E-07
SGSM2	122	REACTOME_UNFOLDED_PROTEIN_RESPONSE	3.92E-04
MRTO4	119	GO_RIBOSOME_BIOGENESIS	6.91E-07
SFRS1	112	GO_POSITIVE_REGULATION_OF_GENE_EXPRESSION	2.01E-04
PGF	111	GO_TRIGLYCERIDE_CATABOLIC_PROCESS	1.59E-04
NISCH	110	REACTOME_UNFOLDED_PROTEIN_RESPONSE	2.06E-04
RBBP4	109	GO_EXECUTION_PHASE_OF_APOPTOSIS	2.14E-04
TSPAN7	100	GO_IMPORT_INTO_CELL	2.51E-04

Biological processes related to cell cycle, golgi, lysosome and amino acid metabolism were enriched in BN_{ox} (Table 5, Appendix).

Table 5: Most significantly overrepresented canonical gene set category (FET p-value) in key driver (KD) associated subnetworks (subnetwork size ≥ 100) in BN_{ox}. Selected top-tanked subnetworks are highlighted as in Figure 13. (Hitzel *et al*, 2018)

KD	size	Top functional canonical gene set category	p–value
CCNB2	513	HALLMARK_E2F_TARGETS	1.52E-20
UBXN4	318	GO_GOLGI_ORGANIZATION	2.85E-05
KIF4A	304	GO_CELL_CYCLE_PROCESS	3.52E-14
NDC80	263	HALLMARK_E2F_TARGETS	2.72E-14
PCDH12	261	GO_ANGIOGENESIS	4.85E-05
ASPM	242	GO_ORGANELLE_FISSION	1.96E-09
CCNB1	235	GO_ANION_TRANSMEMBRANE_TRANSPORTING_ATPASE_ACTIVITY	3.76E-04
KDR	214	HALLMARK_ESTROGEN_RESPONSE_LATE	1.96E-04
CDCA3	184	KEGG_ABC_TRANSPORTERS	1.12E-05
NUSAP1	175	GO_DNA_REPLICATION	2.71E-14
PLK1	160	GO_ANION_TRANSMEMBRANE_TRANSPORTING_ATPASE_ACTIVITY	1.18E-04
CDKN3	159	GO_ANION_TRANSMEMBRANE_TRANSPORTING_ATPASE_ACTIVITY	1.16E-04
DPYSL2	155	GO_IRON_ION_HOMEOSTASIS	6.65E-04
LOC100292189	139	GO_CIRCULATORY_SYSTEM_DEVELOPMENT	2.22E-04
GRN	138	KEGG_LYSOSOME	8.22E-11
KIAA1462	136	GO_REGULATION_OF_PHOSPHORUS_METABOLIC_PROCESS	3.95E-06
TMED2	131	GO_ACTIVATION_OF_NF_KAPPAB_INDUCING_KINASE_ACTIVITY	6.07E-04
DNAJB1	129	GO_PROTEIN_FOLDING	6.55E-07
EMG1	129	GO_NCRNA_PROCESSING	3.68E-05
ASNS	121	GO_CELLULAR_AMINO_ACID_METABOLIC_PROCESS	2.38E-09
MTHFD2	114	GO_CELLULAR_AMINO_ACID_METABOLIC_PROCESS	7.32E-08
PNMA2	114	GO_CIRCULATORY_SYSTEM_DEVELOPMENT	5.13E-04
YWHAZ	113	BIOCARTA_ARAP_PATHWAY	3.92E-04
HSPA1A	111	GO_PROTEIN_FOLDING	6.34E-06
ARMCX2	109	GO_CIRCULATORY_SYSTEM_DEVELOPMENT	2.71E-04
CHAC1	107	REACTOME_CYTOSOLIC_TRNA_AMINOACYLATION	2.98E-08
SYPL1	102	GO_NEGATIVE_REGULATION_OF_ERBB_SIGNALING_PATHWAY	5.86E-05

Asparagine synthetase (ASNS) and the mitochondrial methylenetetrahydrofolate dehydrogenase/cyclohydrolase (MTHFD2) were identified as key drivers for subnetworks enriched in amino acid metabolic processes. ASNS and MTHFD2 are no key drivers in BN_{ct} and amino acid metabolism has not been identified as a significantly enriched biological process in the control state. This observation confirms the above identified emergence of an amino acid metabolism cluster in response to oxPAPC. Since folate metabolism is potentially important in the process of atherosclerosis, MTHFD2 was of particular interest.

The subnetwork regulated by MTHFD2, termed BN_{MTHFD2}, showed similar enrichment as the identified GOC-AA cluster (Table 6). Confirmatory, BNMTHFD2 significantly overlapped with the GOC-AA cluster (FET p-value=2.33E-28). Thus, MTHFD2 may facilitate a shift in amino acid metabolism in HAEC in response to oxidized phospholipids.

Table 6: Gene set enrichment analysis of canonical gene set categories (FET p-value) in BN_{MTHFD2}. (Hitzel *et al*, 2018)

BN_{MTHFD2}: Top functional canonical gene set categories	p–value
MTOR_UP.N4.V1_UP	5.35E-13
ALK_DN.V1_UP	2.23E-11
GO_CELLULAR_AMINO_ACID_METABOLIC_PROCESS	7.32E-08
KEGG_GLYCINE_SERINE_AND_THREONINE_METABOLISM	2.53E-06
REACTOME_CYTOSOLIC_TRNA_AMINOACYLATION	2.53E-06
GO_SERINE_FAMILY_AMINO_ACID_METABOLIC_PROCESS	2.53E-06
GO_TRNA_BINDING	2.53E-06
HALLMARK_MTORC1_SIGNALING	3.91E-06
GO_INTRINSIC_APOPTOTIC_SIGNALING_PATHWAY_IN_RESPONSE_TO_ENDOPLASMIC_RETICULUM_STRESS	6.39E-06
GO_ORGANIC_ACID_METABOLIC_PROCESS	7.46E-06
KEGG_AMINOACYL_TRNA_BIOSYNTHESIS	1.08E-05
REACTOME_TRNA_AMINOACYLATION	1.08E-05

3.1.5 MTHFD2 links endothelial reactions and oxidized phospholipids to an amino acid subnetwork

MTHFD2 is highly overexpressed in many cancers and constitutes a core enzyme for mitochondrial one-carbon metabolism which represents the highest scoring metabolic pathway across all human cancers (Nilsson *et al*, 2014; Tedeschi *et al*, 2015). MTHFD2 is localized to mitochondria and possesses 5,10-methylene-tetrahydrofolate (5,10-MTHF) dehydrogenase and cyclohydrolase activity. In essence, MTHFD2 catalyzes the conversion of 5,10-MTHF to 10-formyl-tetrahydrofolate (10-FTHF) which is a 1C donor indispensable for *de novo* synthesis of purines like adenine or guanine (Tibbetts & Appling, 2010). Since the function of MTHFD2 has been studied to a vast majority in undifferentiated cells, its role in adult cells and in particular in endothelial biology is, to this date, totally unknown. In particular, a link between MTHFD2 dependent amino acid metabolism and atherogenic lipid signaling is not known. Given the importance of metabolism for the endothelium, the MTHFD2 network was analyzed in greater detail.

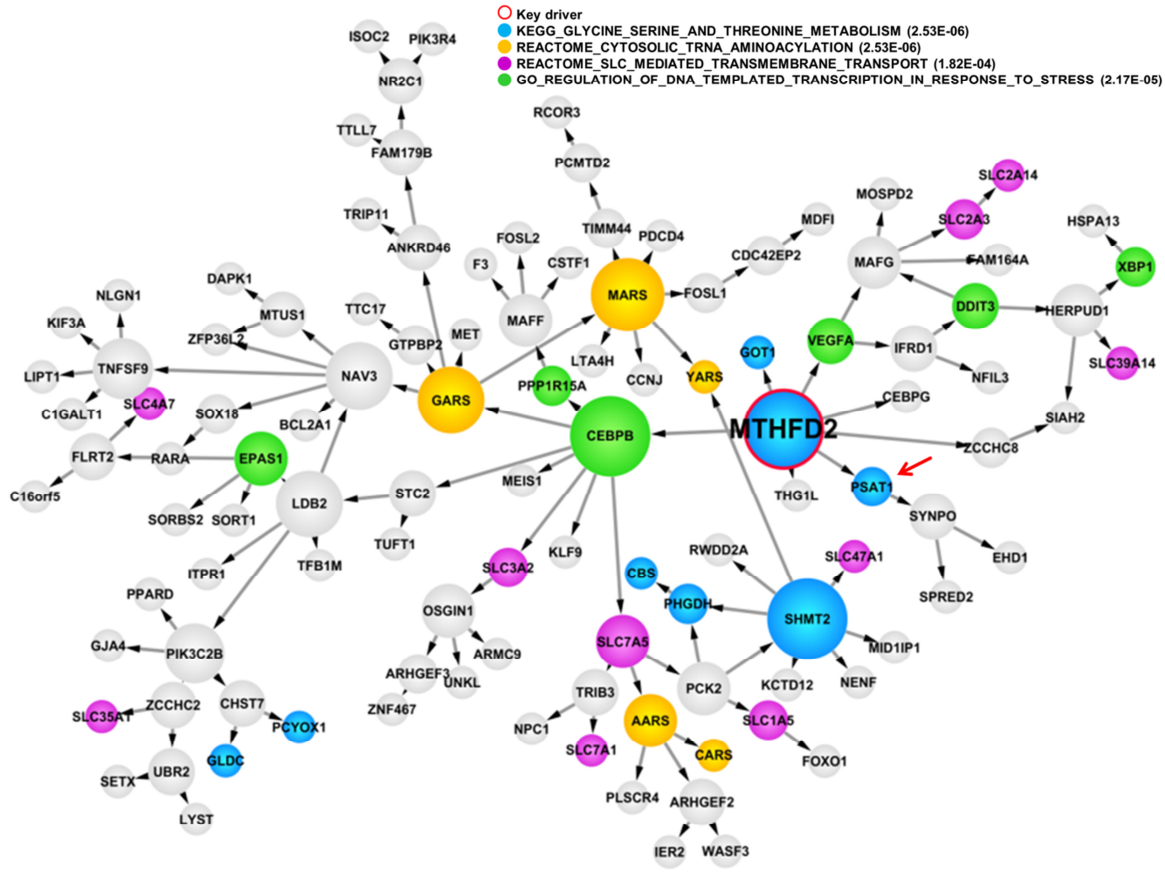

Figure 14: Network view of the MTHFD2 Bayesian network.

Nodes which belong to indicated significantly overrepresented canonical gene set categories are highlighted respectively. Node size reflects outdegree. The key driver MTHFD2 is highlighted in red and its downstream node PSAT1 is indicated (red arrow). (Hitzel *et al*, 2018)

The MTHFD2 associated subnetwork comprised 114 genes of which many constituted enzymes involved in glycine-serine metabolism (blue), solute carrier (SLC) transporters which mediate cellular uptake of sugar and mostly large amino acids (pink), aminoacyl tRNA synthetases (AARs) (yellow) and stress responsive genes (green) (Figure 14).

3.2 Experimental validation of MTHFD2 Bayesian network

3.2.1 MTHFD2 mediates the oxPAPC-dependent changes in amino acid metabolism

BN_{MTHFD2} comprises enzymes which center on cytosol-mitochondrial coupled serine-glycine synthesis (Figure 15 A). The mitochondrial folate cycle generates glycine from serine, which is catalyzed by SHMT2. In the course of this reaction the co-factor tetrahydrofolate is converted to 5,10-MTHF. The enzyme MTHFD2 then uses 5,10-meTHF to produce the highly reactive 1-C donor 10-formyl-THF, which is recycled to tetrahydrofolate by MTHFD1L.

The serine consumed for this reaction is synthesized by PHGDH and PSAT1 from glycolysis intermediates (Tedeschi *et al*, 2013).

To validate BN_{MTHFD2} and to better understand the role of MTHFD2 in endothelial cells an experimental approach was applied. HAEC were exposed to oxPAPC and MTHFD2 was silenced by siRNAs. In accordance with the above observed emergence of BN_{MTHFD2} upon oxPAPC exposure, MTHFD2 expression was induced by oxPAPC (Figure 15 B). Importantly, expression of all key enzymes of the cytosol-mitochondrial serine-glycine synthesis pathway (PHGDH, PSAT1 and SHMT2) was increased by oxPAPC. Additionally, siRNA mediated silencing of MTHFD2 induced expression of these enzymes, which was potentiated by oxPAPC. Down-regulation of MTHF2D or oxPAPC exposure also increased the expression of other genes in BN_{MTHFD2}: the aminoacyl tRNA synthetases (AARS) GARS and CARS, the transcription factor CEBPB and the transporters SLC7A5 and SLC7A1 which import large amino acids. To determine the hierarchical position of MTHFD2 within the subnetwork, its direct downstream node PSAT1 (Figure 14, arrow) was silenced. Expression of genes in BN_{MTHFD2} was affected to a lesser extent by PSAT1 knockdown than by MTHFD2 knockdown (Figure 15 B). Importantly, MTHFD1L, which contributes to formate formation within the mitochondrial one-carbon cycle but does not belong to the MTHFD2 network, was not only not affected by oxPAPC but was also unaltered in response to siRNA against PSAT1 or MTHFD2. Collectively, these results validate MTHFD2 as a key regulator of the MTHFD2 network in oxPAPC exposed HAEC. Furthermore, they indicate that oxPAPC elicits a metabolic shift promoting the cellular uptake of amino acids and the *de novo* synthesis of glycine.

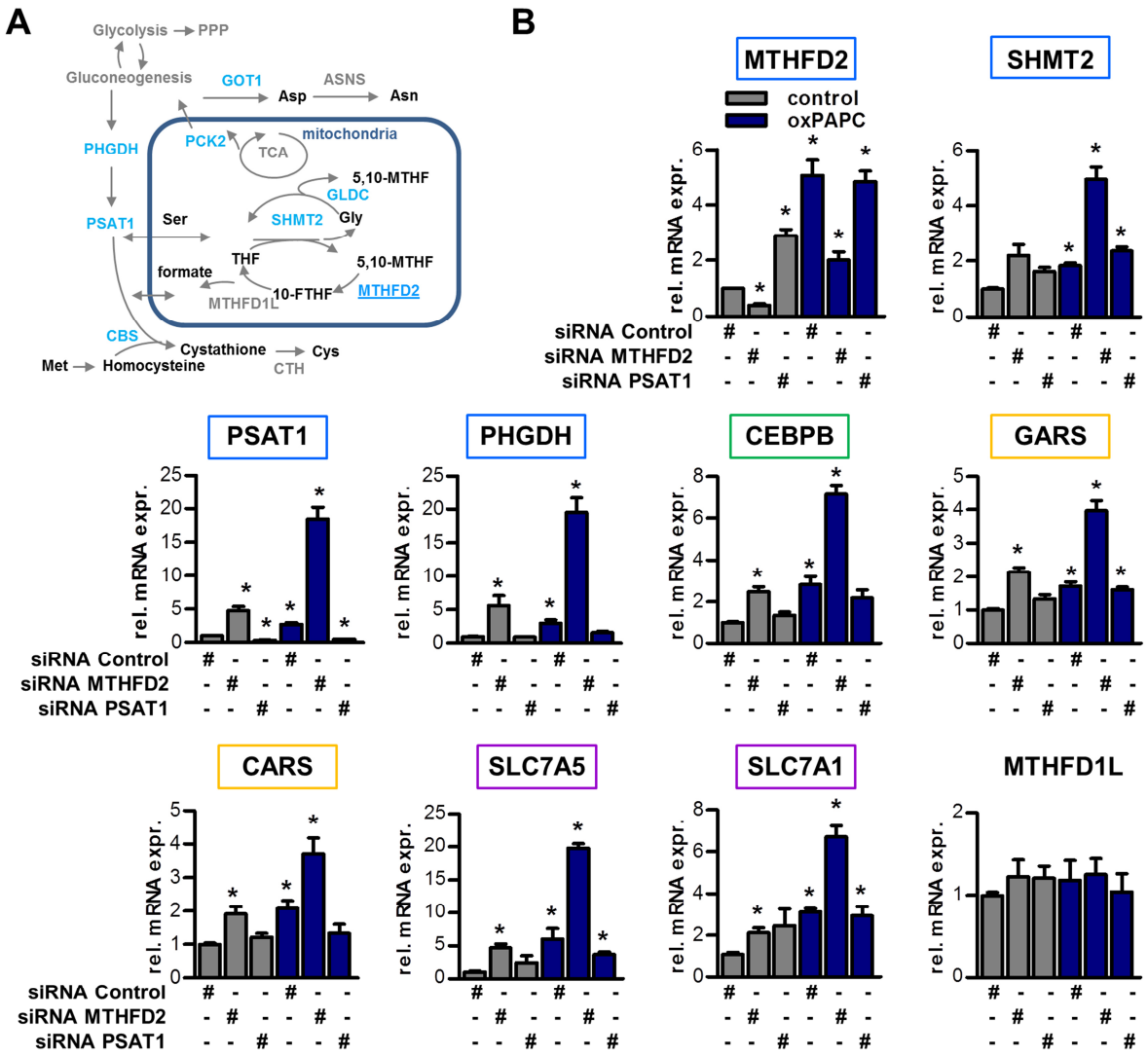

Figure 15: Key driver MTHFD2 and oxPAPC induce expression of genes in BN_{MTHFD2}.

A Schematic diagram of enzymes of BN_{MTHFD2} involved in amino acid metabolism. Enzymes of BN_{MTHFD2} (blue) are involved in serine, glycine, cysteine and aspartate interconversion. B: Experimental validation of BN_{MTHFD2} as assessed by quantitative RT-PCR. HAEC with siRNA knockdown against key driver MTHFD2, the downstream node PSAT1 or scramble control were exposed to medium (1% FCS) with or without oxPAPC for 4 hours (n≥4). Genes which belong to BN_{MTHFD2} are framed by the color of the corresponding gene set category as in Figure 14. *MTHFD2* = methylenetetrahydrofolate dehydrogenase ($NADP^+$ dependent) 2-methenyltetrahydrofolate cyclohydrolase, *SHMT2* = serine hydroxymethyltransferase 2, *PHGDH* = phosphoglycerate dehydrogenase, *PSAT1* = phosphoserine aminotransferase 1, *CEBPB* = CCAAT/enhancer binding protein beta, *GARS* = glycyl-tRNA synthetase, *CARS* = cysteinyl-tRNA Synthetase, *SLC7A5* = solute carrier family 7 member 5, *SLC7A1* = solute carrier family member 1, *MTHFD1L* = methylenetetrahydrofolate dehydrogenase ($NADP^+$ dependent) 1-like. Data are represented as ± SEM *≤0.05 (Student's t-test). (Hitzel *et al*, 2018)

3.2.2 MTHFD2 regulates 18 core genes related to amino acid metabolism

In order to directly address the importance of MTHFD2 for endothelial cell gene expression, RNAseq with siRNA-based knockdown of MTHFD2 in HAEC was performed. Differentially expressed genes were identified (FDR <0.01, Figure 16 A) and significantly overrepresented gene set categories of the RNA signature at FDR < 0.05 were determined.

Table 7: Significantly overrepresented canonical gene set categories in MTHFD2 RNAseq signature (FDR<0.05). (Hitzel *et al*, 2018)

MTHFD2 RNAseq: Top functional canonical gene set categories	p–value
HALLMARK_MTORC1_SIGNALING	9.33E-19
MTOR_UP.N4.V1_UP	5.44E-16
NFE2L2.V2	5.38E-14
GO_CELLULAR_AMINO_ACID_METABOLIC_PROCESS	7.54E-14
REACTOME_CYTOSOLIC_TRNA_AMINOACYLATION	2.44E-12
HALLMARK_UNFOLDED_PROTEIN_RESPONSE	1.29E-11
ALK_DN.V1_UP	1.10E-10
KEGG_AMINOACYL_TRNA_BIOSYNTHESIS	1.51E-10
REACTOME_TRNA_AMINOACYLATION	1.81E-10
GO_LIGASE_ACTIVITY_FORMING_CARBON_OXYGEN_BONDS	2.55E-10
GO_AMINO_ACID_ACTIVATION	8.69E-10
GO_SERINE_FAMILY_AMINO_ACID_BIOSYNTHETIC_PROCESS	1.80E-09

The majority of the most significantly enriched canonical gene sets were related to amino acid metabolism (Table 7). Additionally, categories related to mTOR, UPR and the Nrf2 response (NFE2L2) were enriched. Notably, the signature of enriched gene sets resembled that of the GOC-AA cluster and BN_{MTHFD2}. Next the MTHFD2 siRNA signature was projected onto BN_{MTHFD2}. Consistently, close neighbors of the key driver MTHFD2 were upregulated in the MTHFD2 RNAseq signature (Figure 16 B). Indeed, the MTHFD2 siRNA signature significantly overlapped with BN_{MTHFD2} as compared to whole BN_{ox} (FET p-value=8.34E-16). Finally, the siRNA signature also significantly overlapped with the GOC-AA cluster as compared to all DC clusters (FET p-value=1.19E-17).

Next, indispensable pathway genes were identified by comparing cluster GOC-AA, BN_{MTHFD2} and the RNAseq signature. This analysis yielded 18 commonly shared genes: the mitochondrial one-carbon cycle genes MTHFD2 and SHMT2, the serine synthesizing enzymes PHGDH and PSAT1, SLC transporters, AARs as well as CEBPB and the mitochondrial phosphoenolpyruvate carboxykinase 2 (PCK2) (Figure 16 C). Collectively, integrative analysis of the MTHFD2 RNAseq signature validated the MTHFD2 subnetwork and confirmed the fundamental role of MTHFD2 in amino acid metabolic reprogramming.

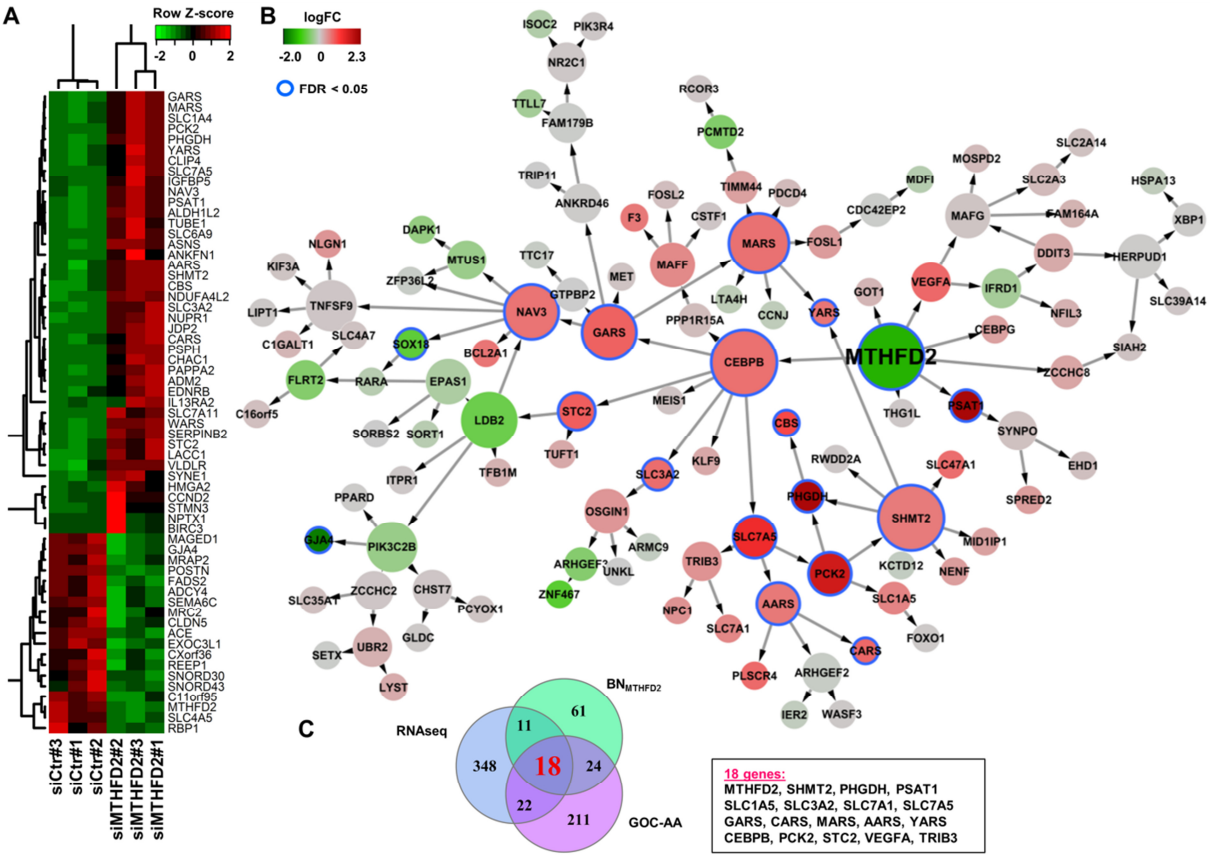

Figure 16: RNAseq validation of MTHFD2 Bayesian subnetwork.

A: Heatmap for fragments per kilobase of transcript per million mapped reads (FPKM) of significantly differentially expressed genes (FDR < 0.01). RNAseq was performed in HAEC with three different siRNAs against key driver MTHFD2 or scramble control. B: Projection of RNAseq signature (FDR < 0.05) in A onto BN_{MTHFD2}. Direction of expression of BN_{MTHFD2} nodes in RNAseq signature is indicated by node color. Node size reflects outdegree. C: Venn diagram of genes in GOC_{aa}, BN_{MTHFD2} and RNAseq signature (FDR < 0.01). Genes belonging to all three gene sets are indicated. (Hitzel *et al*, 2018)

3.2.3 MTHFD2 expression in response to oxPAPC

The MTHFD2 network was strongly enriched for mTOR signaling and MTHFD2 expression was reported to be regulated by the mTOR-ATF4 axis (Ben-Sahra *et al*, 2016). Consistently, siRNA mediated knockdown of ATF4, but not the transcription factor TCF7L2 which was a predicted transcription factor for GOC-AA, reduced expression of MTHFD2 in response to oxPAPC (Figure 17 A). Additionally, the mTOR inhibitor rapamycin abolished expression of ATF4 and MTHFD2 (Figure 17 B).

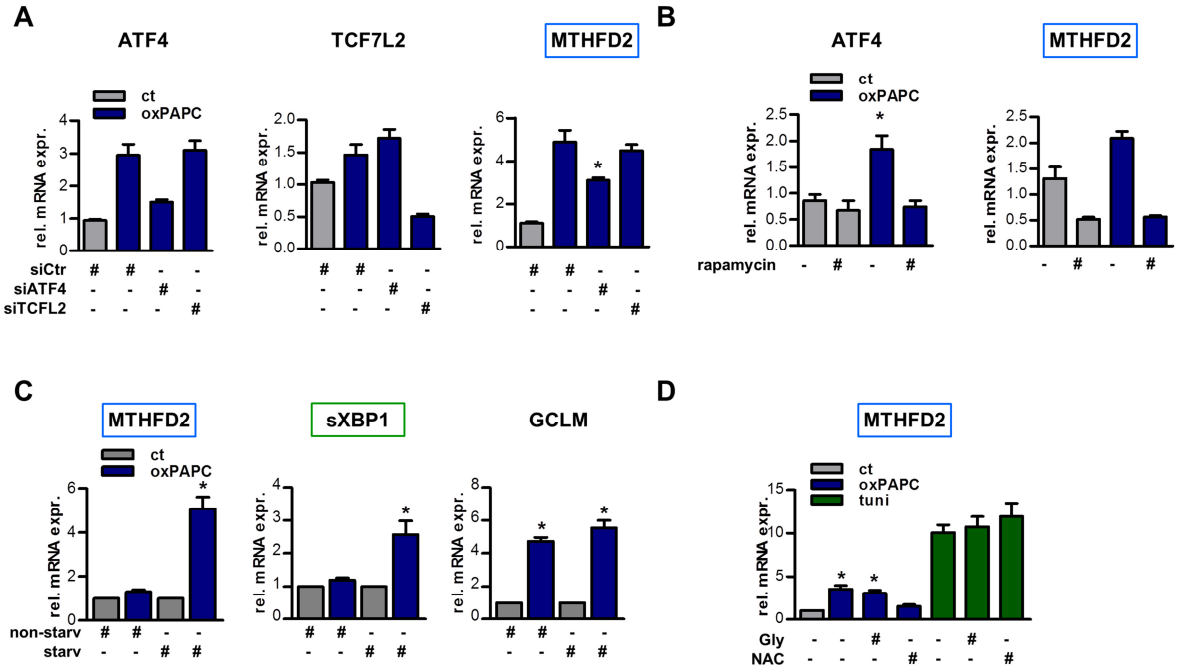

Figure 17: Induction of MTHFD2 in response to oxPAPC is dependent on ATF4.

A: Quantitative RT-PCR detection. HAEC were treated with siRNA against control, ATF4 or TCFL2 and exposed to oxPAPC for 4 h in 1% FCS (n=4). B: HAEC were treated with rapamycin (20 nM) for 16 h and exposed to oxPAPC for 4 h in 1% FCS (n=4). C: HAEC were exposed to growth medium (8% FCS) (non-starv) with or without oxPAPC or basal medium (1% FCS) (starv) with or without oxPAPC (n=4). Genes belonging to BN_{MTHFD2} are framed as above. *SXBP1* = spliced x-box binding protein 1, *GCLM* = glutamate-cysteine ligase modifier subunit. D: HAEC were pre-treated with N-acetyl-L-cysteine (NAC) (5mM) and glycine (500 µM) for 1 h and then exposed to oxPAPC for 4 h in 1% FCS (n=3). Data are represented as mean ± SEM *≤0.05 (Student's t-test). (Hitzel *et al*, 2018)

Oxidized phospholipids induce cellular oxidative stress. One of the strongest responses to oxidized phospholipids therefore constitutes the activation of the redox-defensive Nrf2-Keap1 system (Jyrkkanen *et al*, 2008). Interestingly, whereas the Nrf2 target gene glutathione synthesizing enzyme glutamate-cysteine ligase modifier subunit (GCLM) (Jyrkkanen *et al*, 2008) was induced by oxPAPC in the presence or absence of fetal calf serum in the culture medium, expression induction of genes in BN_{MTHFD2} like MTFHD2 or the active spliced form of x-box binding protein 1 (XBP1) was massively attenuated upon serum addition (Figure 17 C). This finding suggests that serum constitutes might satisfy the cellular needs of substrates otherwise generated by BN_{MTFHD2}. Supplementation of glycine, which is produced by the mitochondrial one-carbon cycle, and which is part of the redox defense peptide glutathione did not prevent induction of MTHFD2 (Figure 17 D). In contrast, the reactive oxygen species (ROS) scavenger N-acetyl-L-cysteine (NAC) prevented the induction of MTHFD2. NAC was reported to react with the oxPAPC component PEIPC thereby neutralizing its activity (Springstead *et al*, 2012). This observation therefore suggests that the oxPAPC elicited induction of MTHFD2 might be due to PEIPC activity.

3.2.4 BN_{MTHFD2} is linked to atherosclerosis

The circumstance that atherosclerosis is driven in part by oxidized lipids raises the possibility that BN_{MTHFD2} is active in atherosclerotic samples (Hitzel *et al*, 2018). Therefore, gene expression profiles which compare 32 carotid artery plaque and 32 healthy tissues from a human cohort (Ayari & Bricca, 2013) was reanalyzed. Expression changes for the 114 genes in the BN_{MTHFD2} were similar in the expression profiles of the HAEC cohort in response to oxPAPC as compared to the carotid arteries in response to atherosclerosis (Figure 18). The majority of genes in the BN_{MTHFD2} which were induced in response to oxPAPC were also increased in atherosclerosis, among them SLC transporters, AARs, PCK2 and XBP. Moreover, also an association was observed for oxPAPC- and atherosclerosis-mediated gene repression.

Table 8: Association between genes in the BN_{MTHFD2} and CAD risk loci. Genetic variances in genes in the BN_{MTHFD2} associated with CAD risk. (Hitzel *et al*, 2018)

Gene	SNP	p-value
SORT1	rs7528419, rs12740374, rs4970834, rs611917	7.05E-08, 1.25E-07, 1.04E-06, 1.45E-06
SLC7A1	rs9551751	7.93E-08
SHMT2	rs11172113	1.72E-06
DDIT3	rs11172113	1.72E-06
MARS	rs11172113	1.72E-06
CEBPB	rs6095611, rs1034056, rs6067199, rs6091031	9.14E-06, 1.38E-05, 1.59E-05, 1.75E-05
FOXO1	rs9594389, rs7323896	1.68E-05, 1.78E-05
GJA4	rs1336624	2.42E-05
CDC42EP2	rs12419237	4.82E-05
PIK3C2B	rs16854023	5.57E-05

To further investigate the possible association of the BN_{MTHFD2} with cardiovascular pathology, genetic variations linked to coronary artery disease (CAD) were re-analysized with respect to the BN_{MTHFD2}. The CARDIoGRAMplusC4D genome-wide association study (GWAS) (Nikpay *et al*, 2015) which contains genomic variations associated with coronary artery disease and myocardial infarction was searched for single nucleotide polymorphisms (SNPs) (p-value<$1x10^{-4}$) whose physical location was within ±500kb of coding region of the 114 genes of the BN_{MTHFD2}. Genes of the BN_{MTHFD2} contained several SNPs (Table 8) and CAD risk loci were enriched in the BN_{MTHFD2} (FET p-value<0.0077). Collectively, these data raise the possibility that the BN_{MTHFD2} in HAEC causally contributes to CAD development. They also demonstrate that the amino acid reprogramming response, represented by the BN_{MTHFD2}, operates in humans and is likely to be important in the atherosclerotic disease process.

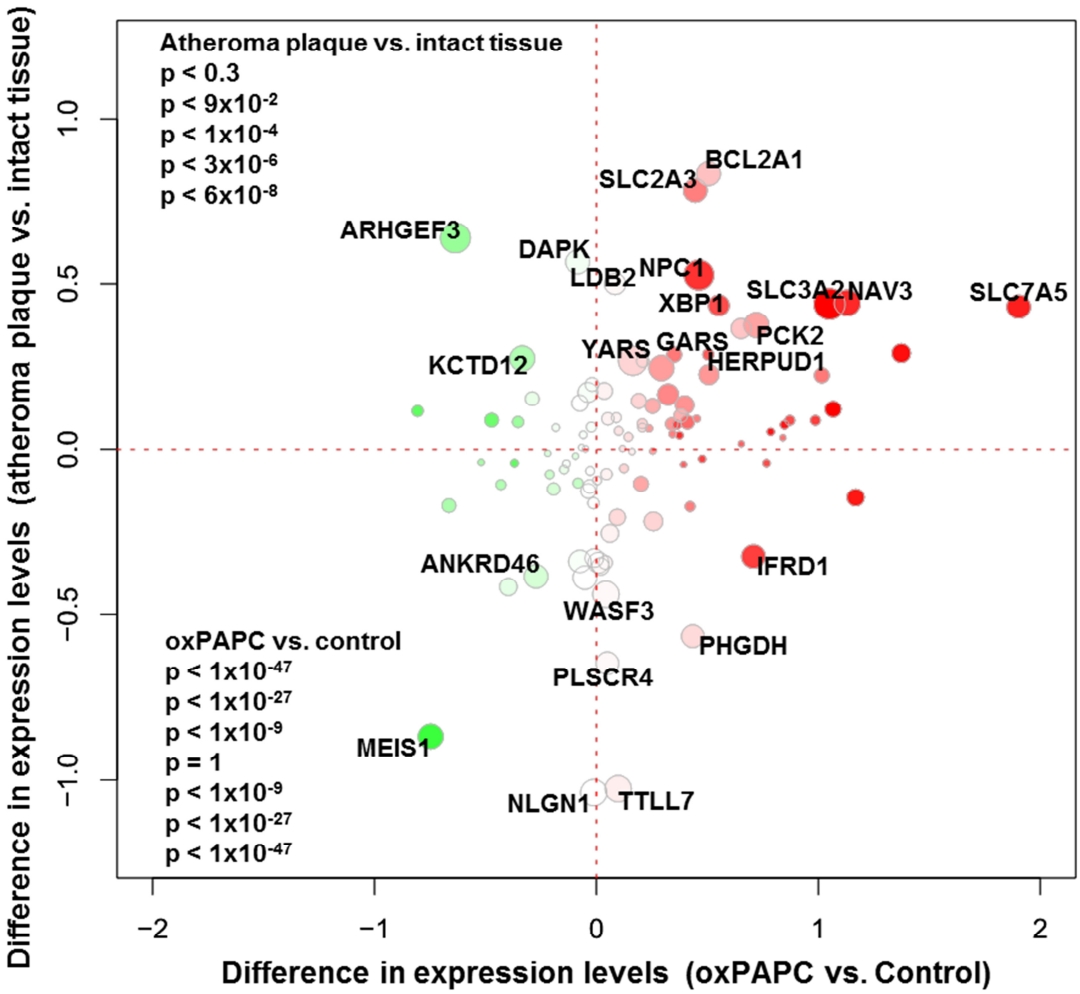

Figure 18: Expression of genes in the BN_{MTHFD2} in human aortic plaques.

Difference in expression levels of 114 genes in the BN_{MTHFD2} in 32 human atheroma plaques versus healthy tissue (y-axis) compared to expression levels of 114 genes in the BN_{MTHFD2} in 147 HAEC exposed to oxPAPC for 4 h (x-axis). (Hitzel *et al*, 2018)

3.3 Physiological function of the MTHFD2 Bayesian network

3.3.1 Short-term oxPAPC exposure and knockdown of MTHFD2 deplete intracellular glycine pools in cardiovascular cells

As shown in the previous chapters, the emergence of an MTHFD2 controlled amino module was computationally established and experimentally validated. These findings, however, do not explain the physiological function of this response. To address this experimentally, first the impact of oxPAPC and of silencing of MTHFD2 on intracellular amino acid levels in HAEC was evaluated (Figure 19). SiRNA mediated knockdown of MTHFD2 decreased the intracellular glycine concentration which suggests that the *de novo* mitochondrial glycine synthesis is highly active in endothelial cells and that it is much more important than the

cellular uptake or the cytosolic glycine synthesis. Importantly, 4 h of oxPAPC exposure decreased the intracellular glycine pool, an effect which was potentiated by knockdown of MTHFD2.

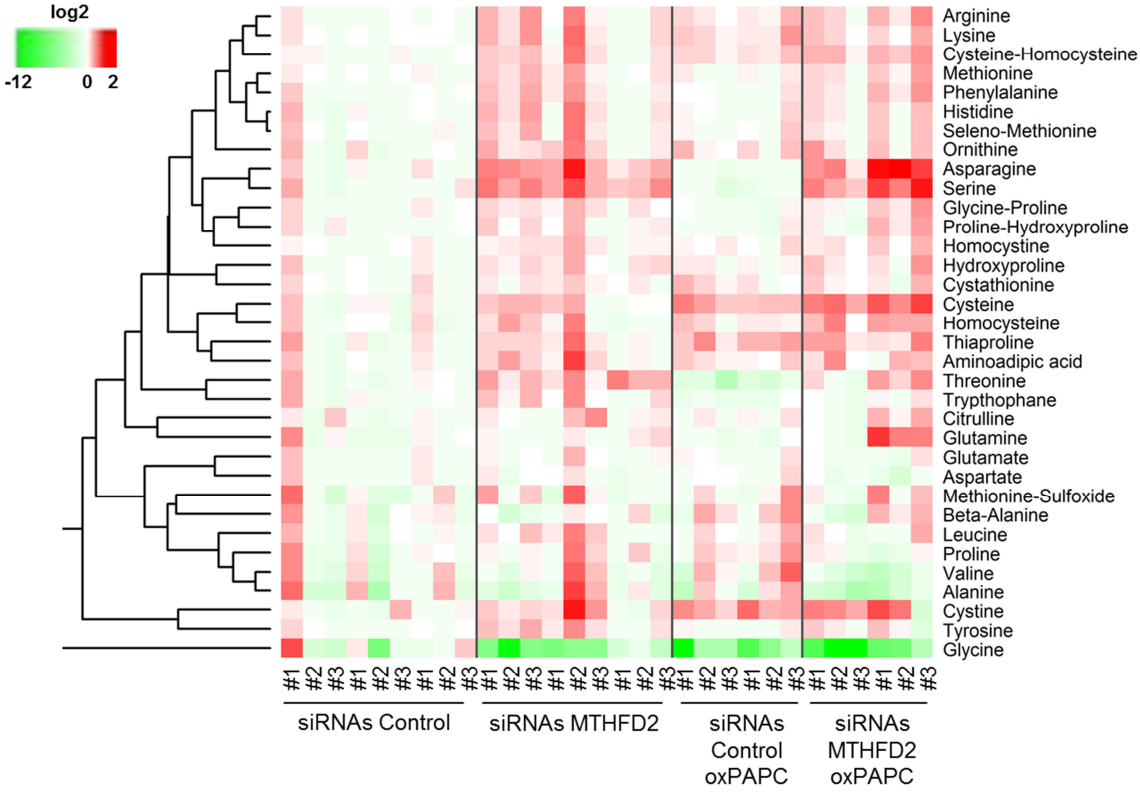

Figure 19: Heatmap of amino acid profile in HAEC.

HAEC were treated with three different siRNAs against the key driver MTHFD2 or scramble control and then exposed to medium (1% FCS) with or without oxPAPC for 4 hours. Amino acids in cell lysates were measured by mass spectrometry (n=6-9). (Hitzel *et al*, 2018)

Consistent with the observed emergence of the MTHFD2 centered amino acid metabolic response, glycine was the most markedly changed amino acid in response to oxPAPC or to MTHFD2 knockdown. Since MTHFD2 indirectly contributes to serine-to-glycine conversion, knockdown of MTHFD2 increased serine levels (Figure19). Additionally, cysteine and cystine which are linked to serine metabolism by the BN_{MTHFD2} gene cystathionine-beta-synthase (CBS) and which contribute to redox defense were increased by oxPAPC. Although cysteine and glycine are both amino acids for glutathione synthesis, they were oppositely affected, suggesting a different function and an additional consumption path for glycine upon oxidized phospholipid exposure.

MTHFD2 and short time oxPAPC caused drain of the intracellular glycine pool was also observed in human aortic smooth muscle cells (HASMC), although to a lesser extend (Figure 20 A). This suggests a general importance of the mitochondrial one-carbon metabolism for the cellular glycine pool in cardiovascular cells. In line with this, siRNA based knockdown of

MTHFD2 in HASMC increased the expression of the serine synthesizing PHGDH and PSAT1 as well as of the ER stress transcription factor ATF4 (Figure 20 B).

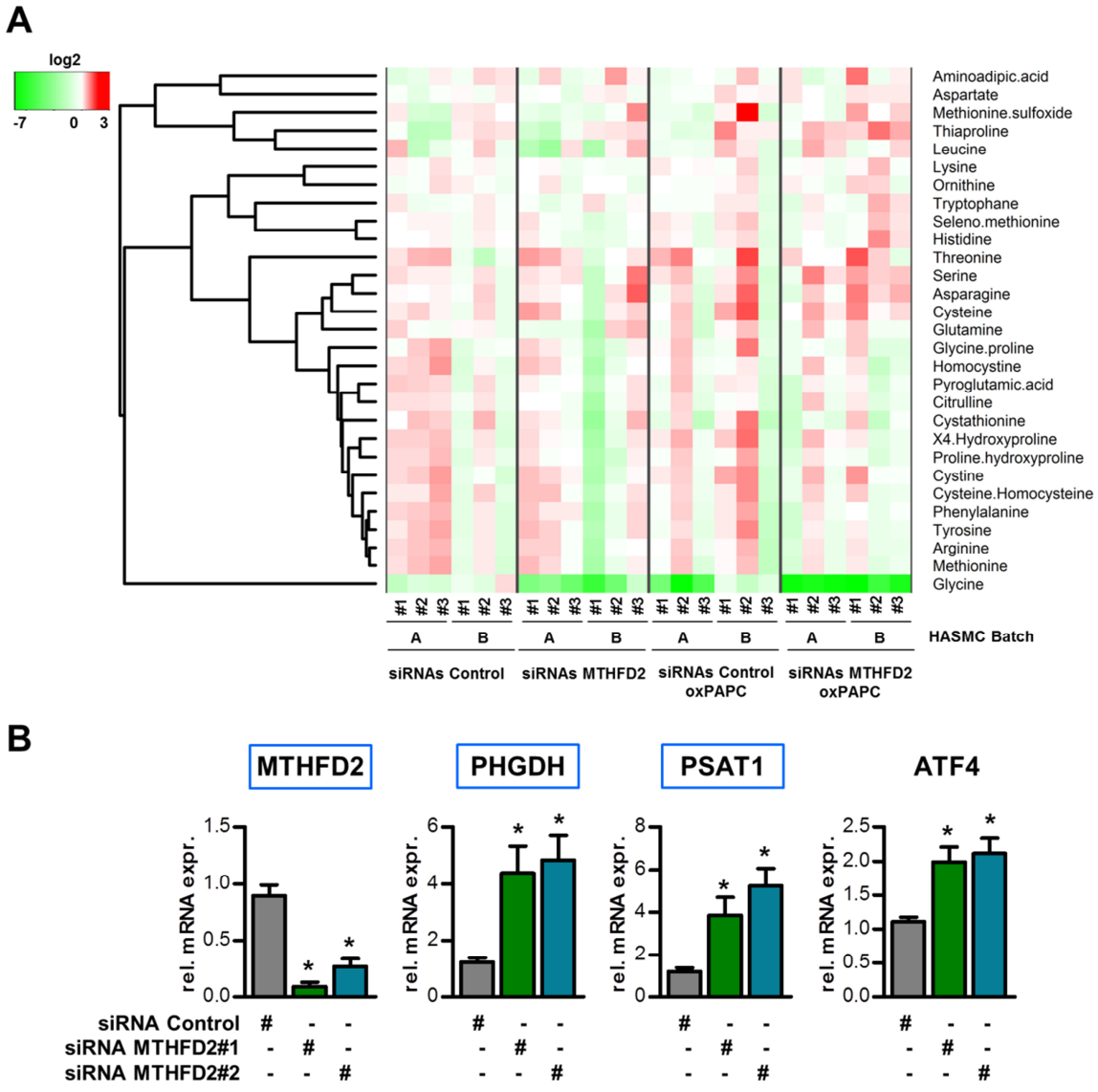

Figure 20: A: MTHFD2 is required for glycine synthesis in human aortic smooth muscle cells.

A: HASMC were treated with three different siRNAs against the key driver MTHFD2 or scramble control and then exposed to medium (1% FCS) with or without oxPAPC for 4 hours. Amino acids in the cell lysates were measured by mass spectrometry (n=6). B: Relative mRNA expression in HASMC treated with siRNAs against MTHFD2 or scramble control after exposure to oxPAPC (1% FCS) (n=4).

3.3.2 MTHFD2 impacts on plasma metabolites in humans

To further solidify the physiological importance of the BN_{MTHFD2} its association with human plasma metabolites was analyzed. For this, data from a human genome-wide association study which contained the plasma level of 400 metabolites (Shin *et al*, 2014b) was tested for SNPs (meta-analysis p-value<$1x10^{-4}$) within ±5kb of gene bodies of the 114 genes of the BN_{MTHFD2}.

Table 9: Association between genes in the BN_{MTHFD2} and plasma metabolites. (Hitzel *et al*, 2018)

Gene	Metabolite	SNP	p-value
MTHFD2	N-acetylglycine	rs10174907	1.43E-05
EPAS1	N-acetylglycine	rs1530628, rs2197698, rs1530627	8.69E-05, 9.45E-05, 9.76E-05
GLDC	glycine	rs2297442	2.94E-05
AARS	tyrosine	rs9936903	1.89E-08
LTA4H	methionine	rs12579455	4.99E-05
SETX	citrulline	rs612169, rs545971, rs674302, rs514659	5.91E-05, 6.35E-05, 6.39E-05, 6.86E-05
EPAS1	tryptophane	rs1530628	8.13E-05
PCK2	glycerol 3-phosphate	rs1062230	2.60E-05

In total, 60 SNPs in 28 genes in the MTHFD2 network were associated with plasma metabolite concentrations. A SNP rs10174907 in MTHFD2 was significantly associated with plasma N-acetylglycine concentration (Table 9) and SNPs associated with N-acetylglycine concentration were enriched for genes in the BN_{MTHFD2} (FET p-value<0.0045). This analysis suggests that the MTHFD2 network may contributes to the regulation of plasma metabolite concentrations and substantiates the functional significance for the BN_{MTHFD2} for cardiovascular amino acid metabolism.

3.3.3 Emergence of the BN_{MTHFD2} is a consequence of oxPAPC-mediated depletion of intracellular glycine

The above made observations hint that the BN_{MTHFD2} induction in response to oxPAPC is a direct consequence of oxPAPC-elicited glycine depletion. Indeed, supplementation of glycine, but not of serine or of asparagine fully prevented the induction of genes in the BN_{MTHFD2} in umbilical vein endothelial cells (HUVEC) in response to the downregulation of MTHFD2 (Figure 21 A). Furthermore, HAECs which were deprived of glycine and serine showed induced expression of MTHFD2 and PHGDH (Figure 21 B). Consistently, long-term oxPAPC exposure increased the production of glycine and led to elevated intracellular glycine levels (Figure 21 C) To substantiate these results, amino acid deprivation in response to asparaginase, which depletes cells of asparagine (Richards & Kilberg, 2006), and to the histidine analog L-histidinol (HisOH), which inhibits activation of histidine by histidyl-tRNA synthetase, was examined (Bouman *et al*, 2011). Both treatments induced the expression of genes in the BN_{MTHFD2} (Figure 21 D, E). Taken together, these findings suggest that the BN_{MTHFD2} constitutes an amino acid response which in response to oxPAPC compensates for the loss of glycine.

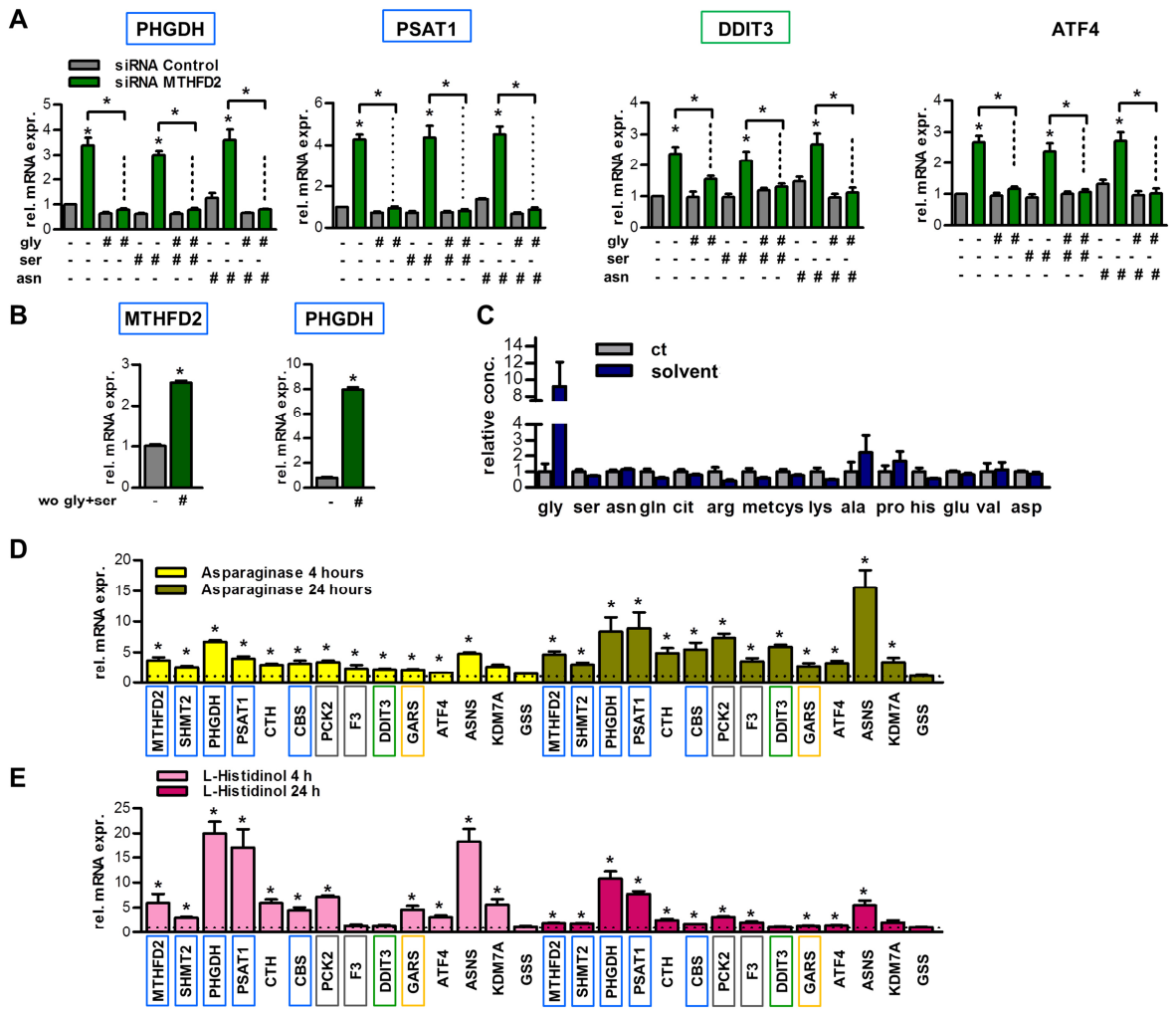

Figure 21: Glycine, but not serine or asparagine prevents the induction of the Bayesian amino acid subnetwork.

A: HUVEC were treated with siRNA against MTHFD2 or scramble control. Subsequently, the groups indicated were supplemented with glycine, serine or asparagine (500 µM) for 16 hours (n=4). Genes belonging to the BN_{MTHFD2} are framed by the color of the corresponding gene set category as above. *DDIT3* = DNA damage inducible transcript 3 (CHOP), *ATF4* = activating transcription factor 4. B: Quantitative RT-PCR detection of MTHFD2 and PHGDH in HAEC cultured in medium without serine and glycine (wo) or supplemented with serine (300 µM) and glycine (30 µM) for 16 h (n=4). C: HAEC were exposed to oxPAPC in 15 FCS for 24 h and intracellular amino acids were measured by mass spectrometry (n=4). D: HAEC were treated with 1 U/ml asparaginase (ASNase) or H_2O in growth medium for 4 and 24 hours (n≥4). Genes belonging to the BN_{MTHFD2} are framed as above. *CTH* = cystathionine gamma-lyase, *CBS* = cystathionine-beta-synthase, *F3* = coagulation factor III / tissue factor, *ASNS* = asparagine synthetase, *KDM7A* = lysine demethylase 7A, *GSS* = glutathione synthetase. E: HAEC were treated with L-Histidinol (2 µM) or H_2O in growth medium for 4 and 24 hours (n≥4). Genes belonging to the BN_{MTHFD2} are framed as before. Data are represented as ± SEM *≤0.05 (Student's t-test). (Hitzel *et al*, 2018)

3.3.4 Knockdown of MTHFD2 impairs the angiogenic capacity in a glycine-dependent manner

In order to determine the importance of the MTHFD2 response on the cellular functional level, the endothelial angiogenic capacity as determined by spheroid outgrowth in response

to vascular endothelial growth factor A (VEGFA) was measured (Hitzel *et al*, 2018). SiRNA against MTHFD2 in HUVEC strongly impaired the angiogenic function as assessed by sprout length and number of sprouts, an effect which was prevented by glycine supplementation (Figure 22 A, B, C). Additionally, silencing of MTHFD2 reduced the endothelial migration as assessed by scratch wound assay and glycine supplementation also restored the migration (Figure 22 D). Thus, MTHFD2-derived glycine is a prerequisite for VEGF-mediated angiogenic ability of endothelial cells.

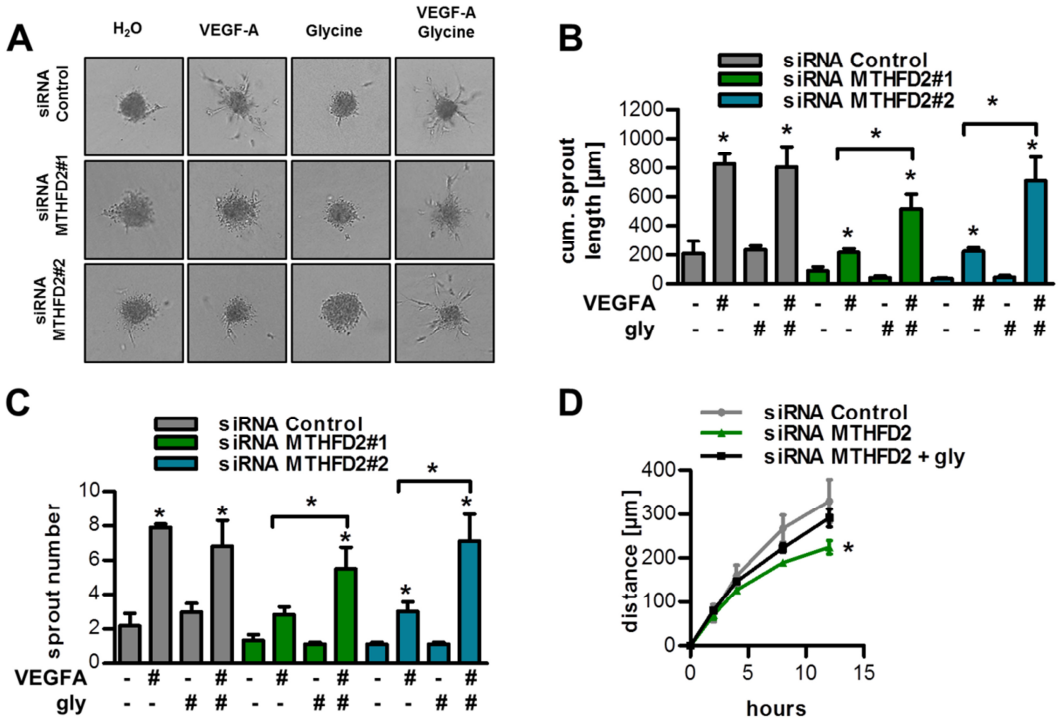

Figure 22: Glycine prevents the impairment of spheroid outgrowth in response to MTHFD2 knockdown.

A: Spheroid assay of HUVEC treated with or without the siRNAs indicated and VEGF-A165 (10 ng/ml) or glycine (500 µM) (n=3). B, C: Quantification of the cumulative sprout length (B) and sprout number (C) of the spheroid assay in A (n=3). D: HUVEC were treated with the indicated siRNAs and supplemented with or without glycine (500 µM). Migration distance after application of scratch is depicted (n=3). Data are represented as ± SEM *≤0.05 (Student's t-test). (Hitzel *et al*, 2018)

3.3.5 Oxidized phospholipids elicit endothelial purine nucleotide release

In the above chapters it was shown that oxPAPC induced endothelial glycine depletion; that the BN_{MTHFD2} was induced to compensate this response and that the BN_{MTHFD2}-dependent glycine production was essential for endothelial cell function. To get behind the biological meaning of the BN_{MTHFD2} it is necessary to understand why endothelial glycine levels decrease upon oxPAPC stimulation. Glycine is an important substrate for numerous cellular pathways including heme synthesis, glutathione synthesis and for protein *de novo* synthesis. However, glycine and 10-formyl-THF are particularly synthesized by the mitochondrial one-

carbon cycle to feed the synthesis of purines. Purines, in the form of ATP and GTP are essential for the cellular energy homeostasis and for DNA and RNA *de novo* synthesis.

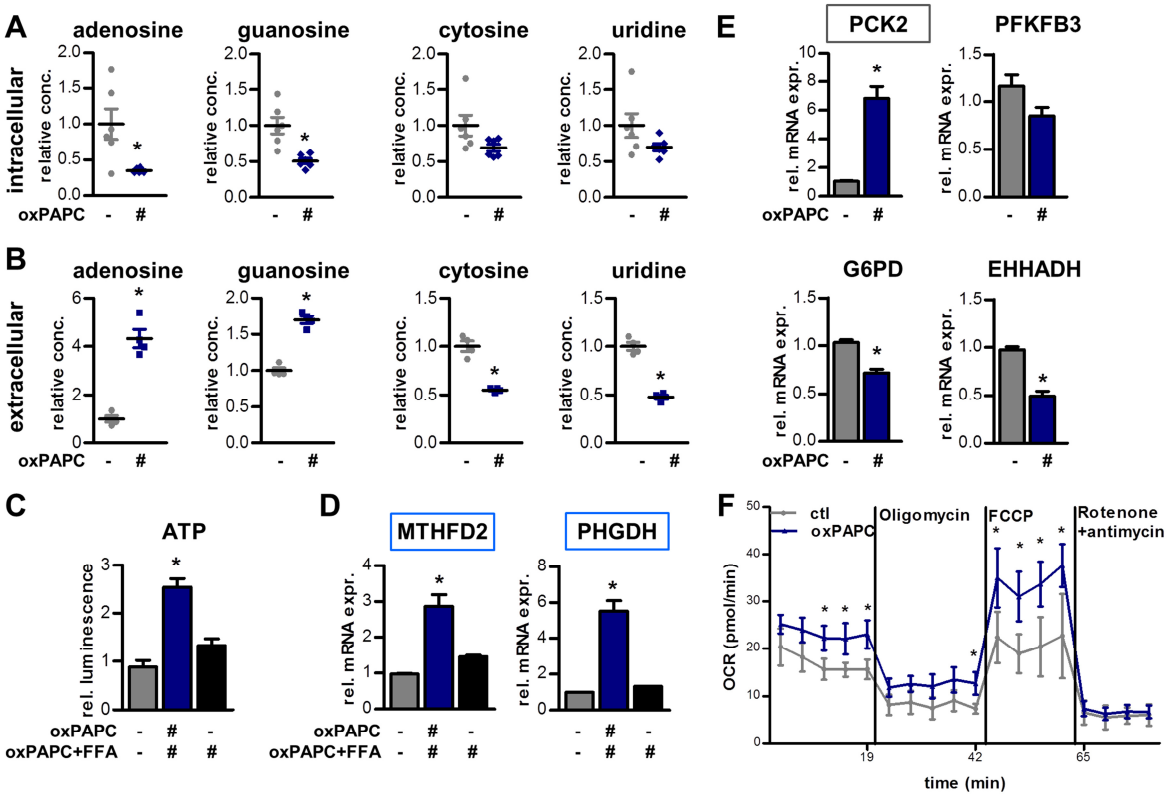

Figure 23: OxPAPC elicits ATP release.

A: Nucleoside measurement in HAEC exposed to medium (1% FCS) with or without oxPAPC for 24 hours. Cell lysates were measured by mass spectrometry (n=6). B: Nucleoside measurement in supernatants of HAEC exposed to medium (1 % FCS) with or without oxPAPC for 24 hours. Supernatants were measured by mass spectrometry (n=4). C: ATP measurement of supernatants of HAEC exposed to medium (1% FCS) with or without oxPAPC and flufenamic acid (FFA, 50 µM) for 8 hours. ATP was measured by luminescence and normalized to the intracellular RNA concentration (n=4). D: qRT-PCR detection of MTHFD2 and PHGDH in HAEC exposed to medium (1% FCS) with or without oxPAPC and flufenamic acid (FFA, 50 µM) for 24 h (n=4). E: Quantitative RT–PCR detection of metabolic enzyme markers in HAEC in medium (1% FCS) with and without oxPAPC for 24 hours (n=4). Genes belonging to the BN_{MTHFD2} are framed as before. *PCK2* = Phosphoenolpyruvate carboxykinase 2, *PFKFB3* = 6-phosphofructo-2-kinase/fructose-2,6-biphosphatase 3, G6PD = glucose-6-phosphate dehydrogenase, *EHHADH* = enoyl-CoA hydratase/3-hydroxyacyl CoA dehydrogenase. F: Oxygen consumption rate (OCR) profile as an index of mitochondrial respiration in HAEC exposed for 4 hours to medium (1% FCS) with or without oxPAPC (n≥3). HAEC were treated with the ATP synthase inhibitor oligomycin (2.5 µM), carbonyl cyanide-3-chlorophenylhydrazone (CCCP) (1 µM) for maximal mitochondrial capacity and antimycin A (1 µg/ml) and rotenone (1 µM) to inhibit mitochondrial activity (n>7). Data are represented as ± SEM *≤0.05 (Student's t-test). (Hitzel *et al*, 2018)

Purines are also important signaling transmitters and it is well known that endothelial cells release purines as signaling autacoids in response to a broad array of stimuli, including shear stress (Wang *et al*, 2016b). Through the activation of purinergic receptors, purines impact on the vascular homeostasis, coagulation, inflammation and the control of vascular tone (Lohman *et al*, 2012). Therefore, it was speculated that oxPAPC induces the release of ATP and other nucleotides from endothelial cells and thereby depletes endothelial cells of

purines and subsequently glycine. Confirming this hypothesis, exposure to oxPAPC significantly reduced the endothelial intracellular purine, but not pyrimidine nucleoside pools (Figure 23 A). In line with this, the extracellular degradation products of ATP and GTP, but not of pyrimidines as measured in the cell culture supernatant were increased in response to oxPAPC in HAEC (Figure 23 B).

If purine release was indeed the mechanism driving the cellular responses to oxPAPC, blockade of ATP release would largely attenuate the effects of oxPAPC. Indeed, flufenamic acid (Riteau *et al*, 2012) not only blocked the oxPAPC-mediated increase in extracellular ATP (Figure 23 C), but also prevented the induction of genes in the BN_{MTHFD2} in response to oxPAPC (Figure 23 D). This observation indicates that oxPAPC-redirected amino acid metabolism fuels purine synthesis to enable endothelial cells to release ATP. Next, it was tested if endothelial cells increase their metabolism to produce ATP. Expression of PCK2, the mitochondrial rate limiting enzyme for gluconeogenesis, which belongs to the identified 18 core genes, was increased whereas the endothelial glycolysis marker 6-phosphofructo-2-kinase/fructose-2,6-bisphosphatase 3 (PFKFB3) (De Bock *et al*, 2013), the pentose phosphate pathway marker glucose-6-phosphate dehydrogenase (G6DP) and the fatty acid oxidation enzyme enoyl-CoA hydratase/3-hydroxyacyl CoA dehydrogenase (EHHADH) showed decreased expression (Figure 23 E). Furthermore, oxPAPC exposure increased the mitochondrial oxygen consumption rate, indicating that oxPAPC exposure, which is accompanied by oxidative stress, does not inhibit the mitochondrial function, but rather increases mitochondrial activity (Figure 23 F).

3.3.6 Blockade of ATP release prevents impaired angiogenic ability in response to oxPAPC

Next, the effect of the blockade of the ATP release was tested on the functional level (Hitzel *et al*, 2018). Blockade of ATP release prevented the inhibitory effect of oxPAPC on the endothelial cell angiogenic capacity as assessed by the spheroid outgrowth assay (Figure 24 A, B, C). Taken together the results, oxidized phospholipids induced an amino acid metabolic reprogramming response in endothelial cells which allowed for the replenishment of the cellular nucleotide pools which became depleted as a consequence of oxPAPC-induced nucleotide release (Figure 24 D).

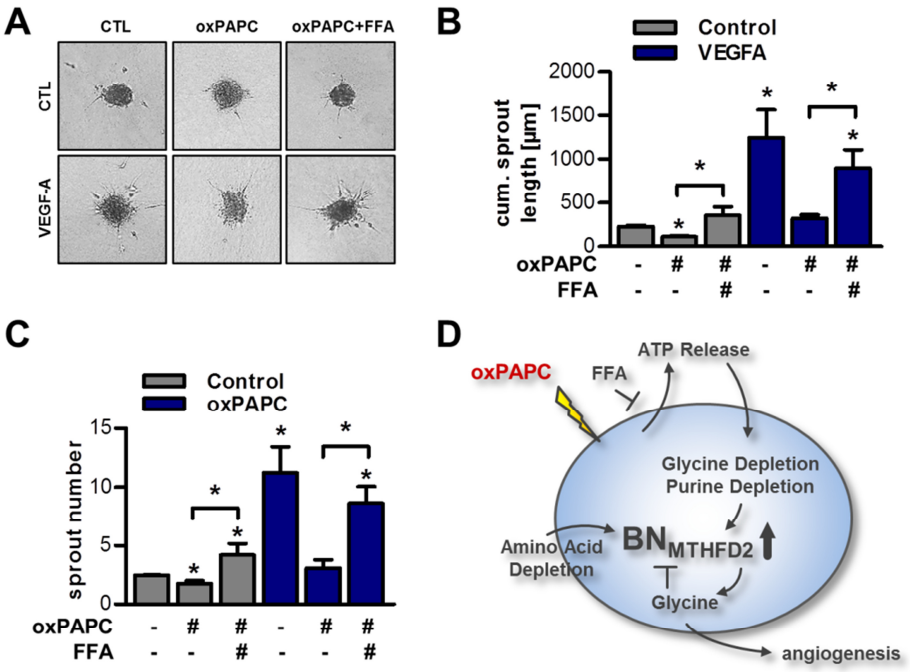

Figure 24: Flufenamic acid prevents the impairment of angiogenesis upon oxPAPC exposure.

A: Spheroid assay of HUVECs treated with oxPAPC, flufenamic acid (FFA, 50µM) and VEGF-A165 (10 ng/ml) as indicated (n=3). B, C: Quantification of the cumulative sprout length (B) and sprout number (C) of the spheroid assay in A (n=3). D: Model of findings. Data are represented as mean ± SEM *≤0.05 (Student's t-test). (Hitzel *et al*, 2018)

3.4 Signature networks of HAEC BNs

Besides analysis of the HAEC Bayesian networks themselves, the networks were exploited to define perturbation associated networks. Specifically, perturbation signatures from the KDM7 family members PHF8 (KDM7B) and KDM7A were used to obtain EC specific epigenetic associated networks.

3.4.1 PHF8 signature Bayesian network and identification of key drivers

Firstly, RNA sequencing data from HUVEC treated with siRNA against PHF8 were analysed. 726 differentially expressed genes were detected (pval < 0.05) and defined as the PHF8 signature. Secondly, the signature was projected onto the BN_{ct} and directed neighbors (order = 1) were extracted together with the signature genes. The largest connected subnetwork resulting from the signature subnetworks was defined as the PHF8 Bayesian network (Figure 25).

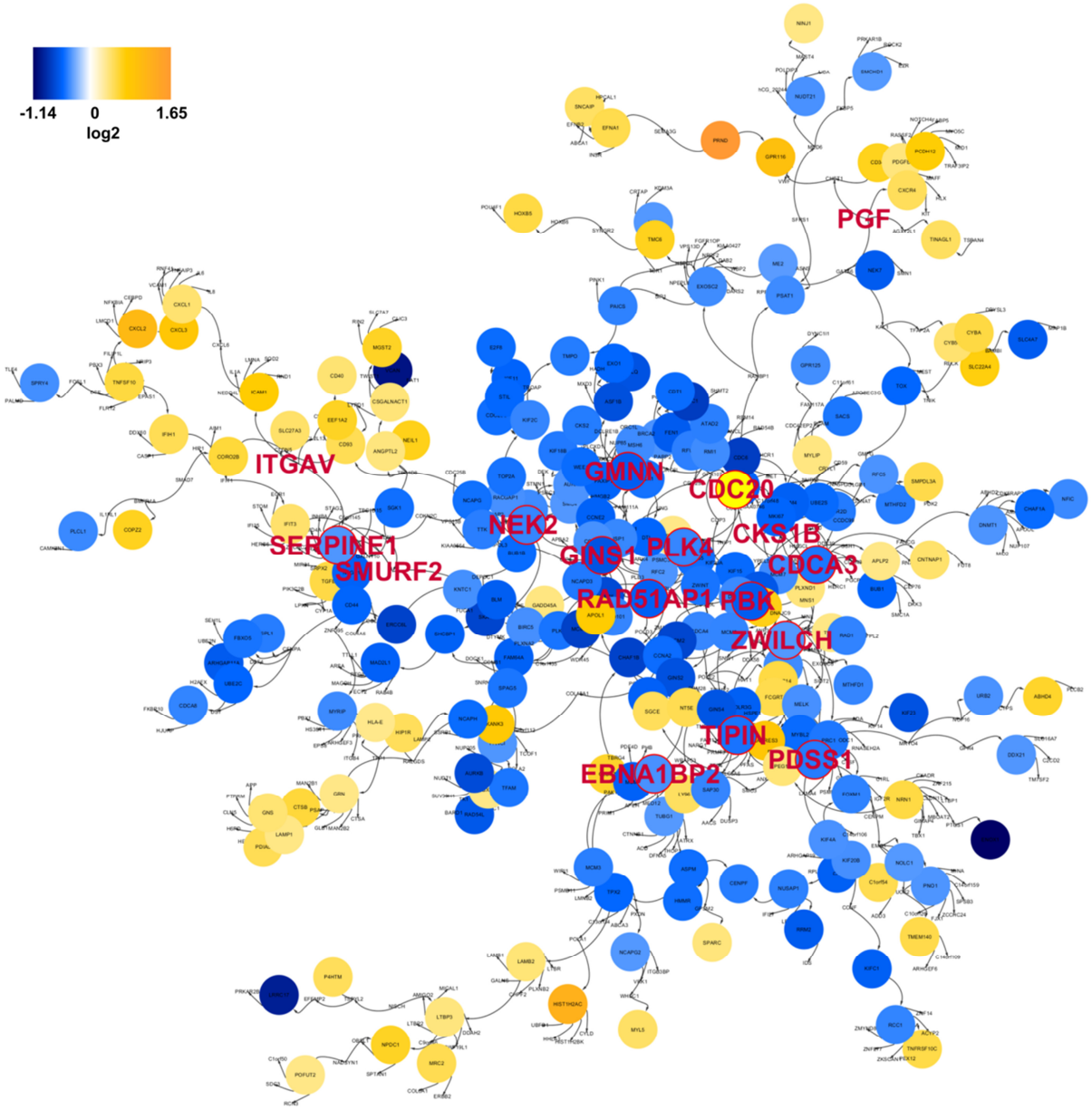

Figure 25: Network view of PHF8 Bayesian network.

The PHF8 associated Bayesian network consists of 636 nodes. Genes belonging to the PHF8 signature are indicated by a node circle and colored according to log2 fold change in the underlying RNA sequencing data set. Key drivers belonging to the PHF8 signature are highlighted by red font labelling and red borders whereas key drivers which do not belong to the PHF8 signature are not highlighted by a node circle.

The genes TIPIN, GINS1, ZWILCH, CDC20, SERPINE1, NEK2, GMNN, PLK4, CDCA3, RAD51AP1, PBK, PDSS1 and EBNA1BP2 were identified as key drivers of the PHF8 signature. In contrast, PGF, ITGAV, SMURF2 and CKS1B were detected as key drivers which were not within the PHF8 signature. The large majority of the detected key drivers were genes involved in cell cycle regulation. Gene set enrichment analysis of the PHF8 network showed strong significant enrichment for cell cycle related canonical gene set categories (Table 10).

Table 10: Significantly enriched gene set categories GSEA of PHF8 Bayesian network.

PHF8 Bayesian network: Top functional canonical gene set categories	p–value
HALLMARK_E2F_TARGETS	1.05E-43
GO_CELL_CYCLE_PROCESS	5.94E-36
GO_CELL_CYCLE	9.89E-36
REACTOME_CELL_CYCLE	1.79E-35
REACTOME_CELL_CYCLE_MITOTIC	5.33E-35
GO_MITOTIC_CELL_CYCLE	8.94E-35
REACTOME_DNA_REPLICATION	3.10E-28
GO_ORGANELLE_FISSION	1.70E-27
HALLMARK_G2M_CHECKPOINT	2.65E-27
GO_MITOTIC_NUCLEAR_DIVISION	6.62E-26
REACTOME_MITOTIC_M_M_G1_PHASES	1.41E-23
GO_CHROMOSOME_ORGANIZATION	3.14E-23

PHF8 demethylates H4K20me1 of E2F1-regulated gene promoters, thereby influencing cell cycle progression (Liu *et al*, 2010). Furthermore, PHF8 was reported to bind directly to CDC20 during mitosis and contributes to G_2/M transition (Lim *et al*, 2013). Consistently, CDC20 was detected as a key driver in the PHF8 BN. However, many of the detected key drivers are only sparsely known. Therefore, some key drivers of the PHF8 signature were experimentally validated.

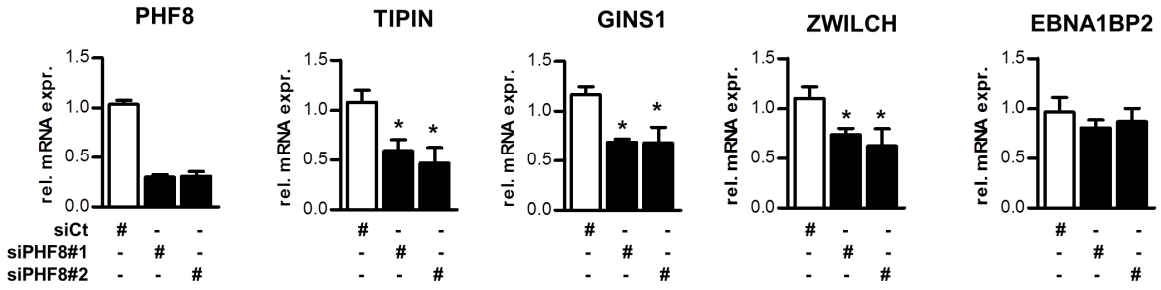

Figure 26: Experimental validation of newly identified key drivers in PHF8 BN.

HUVEC were treated with siRNA against PHF8 and qPCR was performed to test for the PHF8 BN key drivers TIMELESS interacting protein (TIPIN), GINS complex subunit 1 (GINS1), zwilch kinetochore protein (ZWILCH) and EBNA1 binding protein 2 (EBNA1BP2) (n=6). Data are represented as ± SEM *≤0.05 (Student's t-test).

SiRNA mediated knockdown of PHF8 in HUVEC led to a decreased expression of the newly identified key drivers TIPIN, GINS1 and ZWILCH (Figure 26). These are not yet well described proteins and therefore constitute potential new players in the PHF8-mediated cell cycle regulation.

3.4.2 KDM7A Bayesian network analysis

Since the function of the KDM7 subfamily member KDM7A is the least known of all three KDM7 family members, RNA sequencing was performed and the BN was exploited to describe a KDM7A associated network in endothelial cells.

3.4.2.1 RNA sequencing and canonical signature analysis of KDM7A

First, KDM7A compared to empty plasmid was overexpressed in HUVEC and RNA sequencing performed. 48 differentially expressed genes (FDR < 0.05) were detected and enrichment for canonical pathways was performed. Gene set categories related to interferon type I and II signaling, immune response and cytokine signaling were significantly enriched (Table 11).

Table 11: Significantly enriched gene set categories in KDM7A signature.

KDM7A RNAseq signature: Top functional canonical gene set categories	p–value
HALLMARK_INTERFERON_GAMMA_RESPONSE	3.36E-29
GO_RESPONSE_TO_TYPE_I_INTERFERON	3.53E-28
GO_DEFENSE_RESPONSE_TO_VIRUS	2.90E-24
REACTOME_INTERFERON_ALPHA_BETA_SIGNALING	5.04E-24
REACTOME_INTERFERON_SIGNALING	7.09E-24
GO_DEFENSE_RESPONSE	8.64E-22
GO_RESPONSE_TO_VIRUS	3.13E-21
GO_INNATE_IMMUNE_RESPONSE	3.80E-21
HALLMARK_INTERFERON_ALPHA_RESPONSE	1.93E-20
GO_IMMUNE_RESPONSE	2.48E-20
REACTOME_CYTOKINE_SIGNALING_IN_IMMUNE_SYSTEM	3.99E-20
GO_CYTOKINE_MEDIATED_SIGNALING_PATHWAY	5.90E-19

Next, the Reactome FI Plugin in Cytoscape was used to visualize KDM7A signature genes within the interferon response. The Reactome Interferon alpha/beta signaling diagram was used as template to detect KDM7A signature genes within the pathway (Figure 27). The majority of KDM7A signature genes were located in the cytosol and classified as “Expression of IFN-induced genes” in the Reactome pathway and downstream of an unknown regulator. This canonical analysis suggested that KDM7A is potentially involved in the regulation of interferon-induced genes.

3.4.2.2 KDM7A Bayesian network and key drivers

To filter out important players within the KDM7A signature, a KDM7A-specific Bayesian network was defined. The KDM7A signature (FDR < 0.05) was projected onto the BN_{ct} and the largest connected subnetwork (order = 1) was extracted and analyzed.

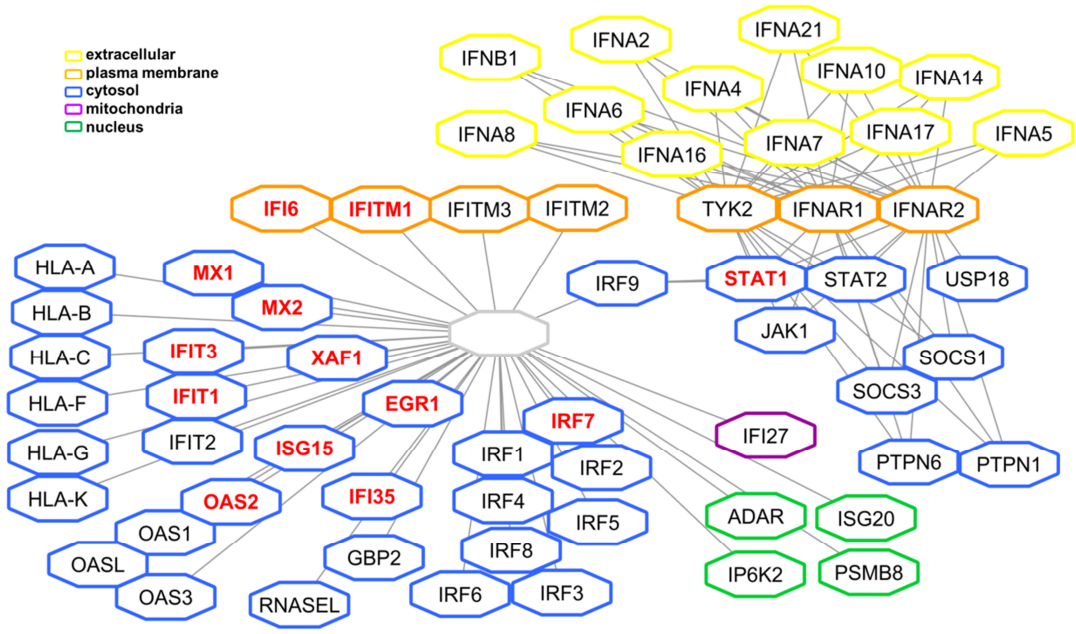

Figure 27: Visualization of KDM7A signature genes in the interferon alpha/beta Reactome pathway.

The Reactome interferon alpha/beta pathway within the Reactome FI Cytoscape plugin was used as template. Cellular localization is highlighted by border color. Genes of the KDM7A signature are highlighted by red font labeling. The grey marked node is not defined within the Reactome pathway.

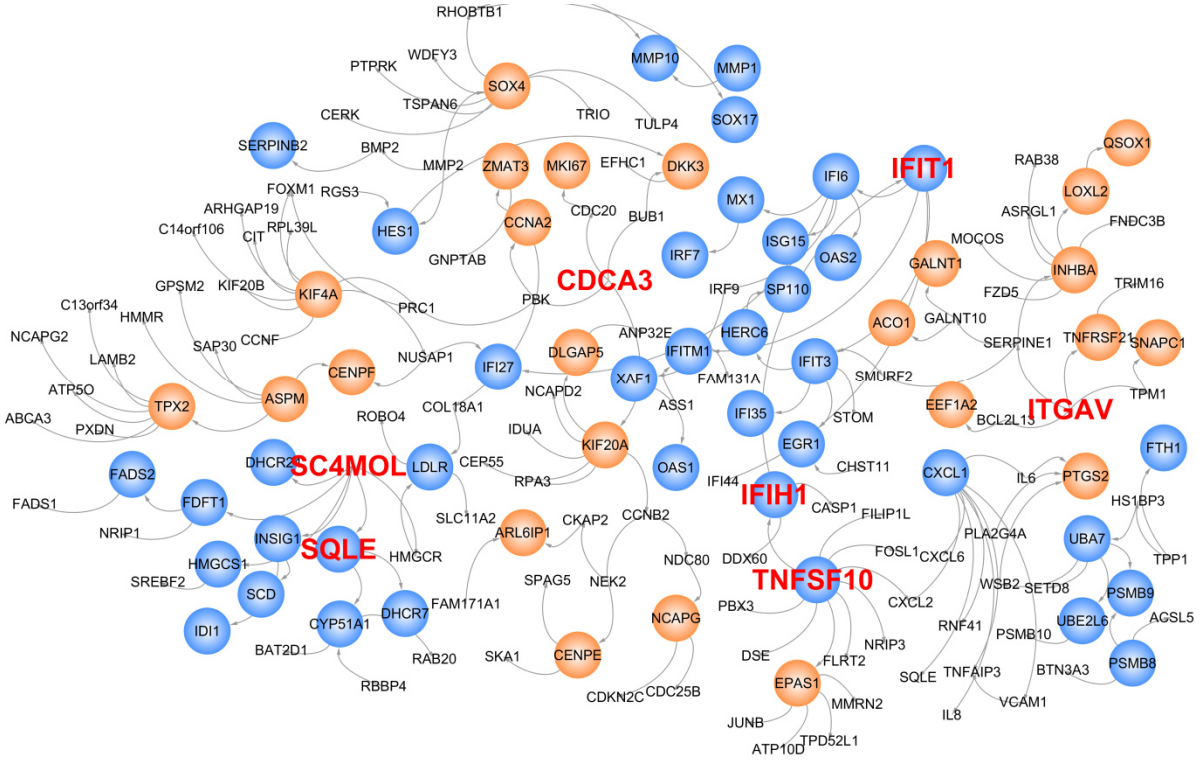

Figure 28: Network view of KDM7A Bayesian network.

The KDM7A Bayesian network consists of 168 nodes. Genes of the KDM7A signature are highlighted in blue (downregulated) and orange (upregulated) respectively. Nodes of the BN_{ct} which are not within the KDM7A signatures are not highlighted by a circle. Key drivers are highlighted by red font labeling.

The genes interferon induced protein with tetratricopeptide repeats 1 (IFIT1), interferon induced with helicase C domain 1 (IFIH1), TNF superfamily member 10 (TNFSF10) and squalene epoxidase (SQLE) were detected as key drivers of the KDM7A Bayesian network (Figure 28). The additional detected key drivers CDCA3, ITGAV and SC4MOL did not belong to the KDM7A signature. SiRNA mediated knockdown of KDM7A in HUVEC decreased expression of the key driver IFIT1 as well as IFIT3, which was part of the KDM7A BN, and the cytokines IFNβ and IL1β (Figure 29).

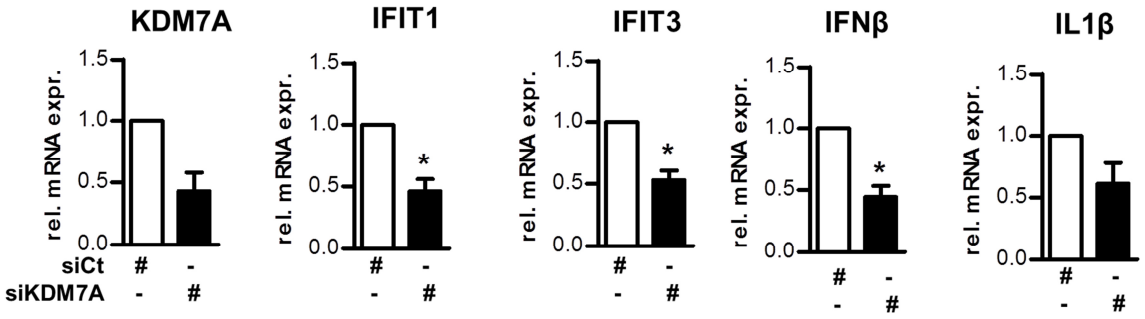

Figure 29: KDM7A affects expression of intereferon responsive genes.

HUVEC were treated with siRNA against KDM7A and relative mRNA expression of identified key drivers interferon induced protein with tetratricopeptide repeats 1 (IFIT1) as well as the KDM7A BN gene IFIT3 and the cytokines IFNβ and IL1β (n=4). Data are represented as ± SEM *≤0.05 (Student's t-test).

By means of the KDM7A signature-based network modeling, a possible association of KDM7A with the interferon response was highlighted.

3.4.2.3 KDM7A is associated with the interferon response

Next, a potential implication of KDM7A in an interferon-related disease was tested. Systemic lupus erythematosus (SLE) is an autoimmune disease, which is characterized by elevated interferon levels (Choi *et al*, 2012). Patients with SLE exhibit impaired endothelial function and excessive LDL and phospholipid oxidation and show accelerated atherosclerosis and high rates of cardiac death (Hahn & McMahon, 2008; Piper *et al*, 2007). An analysis of the whole blood RNA sequencing from 99 SLE and 18 healthy patients (GSE72509) (Hung *et al*, 2015) with regard to KDM7 family members showed a significant increased expression of KDM7A, but no increased expression of PHF2 and a decreased expression of PHF8 (Figure 30). Consistently, the histone methyltransferase for H2K27me2 G9a, which was shown to be oppositely regulated to KDM7A (Pan *et al*, 2016), was downregulated. Furthermore, KDM7A but not PHF8 expression was positively correlated with the response to virus in 32 human atheroma plaques (Ayari & Bricca, 2013), but not PHF8. These data support an association of KDM7A with the interferon response under pathophysiological conditions.

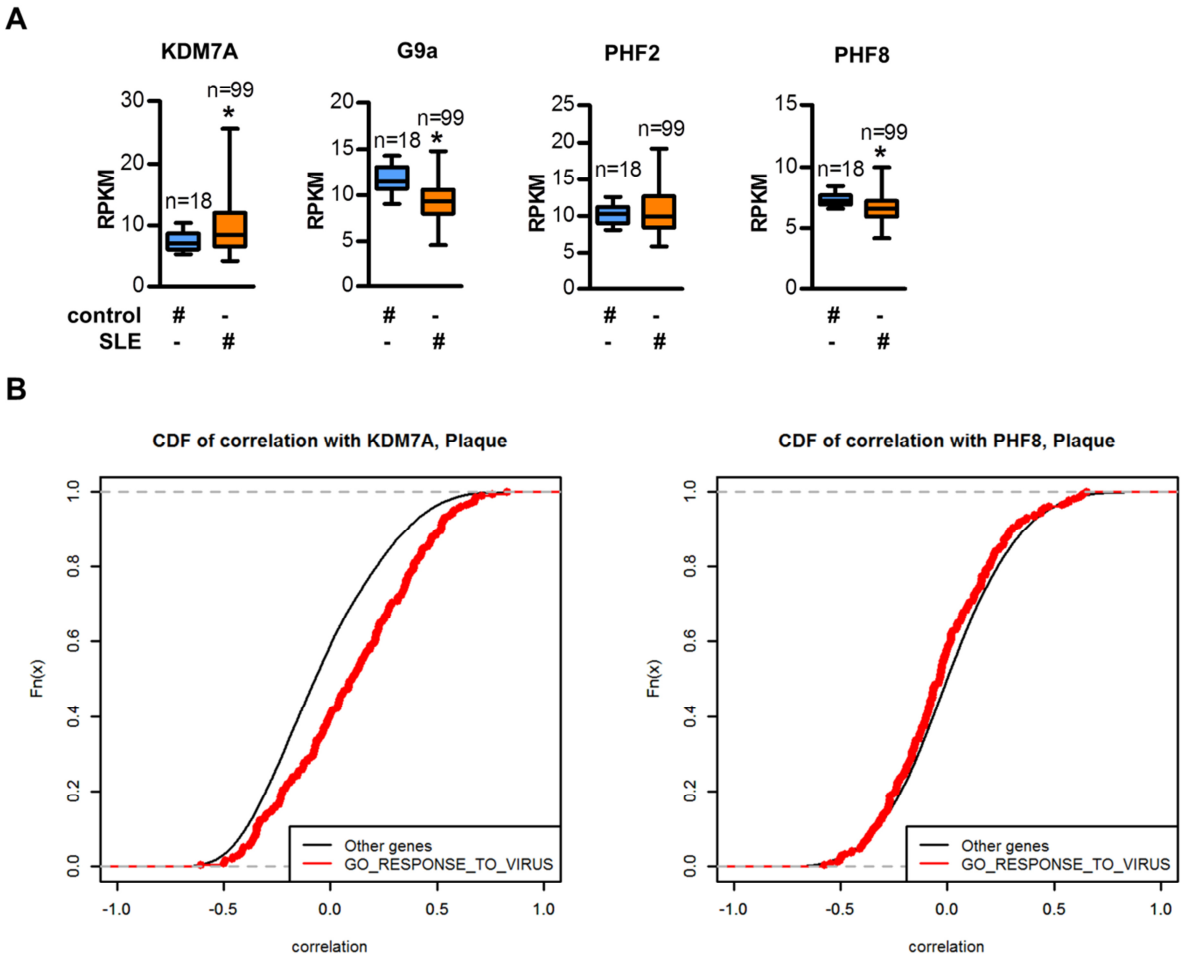

Figure 30: KDM7A is associated with interferon signaling.

A: RPKM of the KDM7 family members KDM7A, PHF2 and PHF8 as well as the histone methyltransferase G9a in whole blood RNA sequencing samples from 99 SLE and 18 healthy patients (Wilcoxon-Mann-Whitney test) B: Pearson correlation of KDM7A or PHF8 with genes within the gene set category GO-RESPONSE_TO_VIRUS compared to all other genes in 32 human atheroma plaques. Shown is the empirical cumulative distribution function (CDF).

3.4.2.4 CAD risk loci of JmjC histone demethylases

Since SLE is associated with accelerated atherosclerosis, it was tested if the locus of KDM7A is associated with coronary artery disease and myocardial infarction. The CARDIoGRAMplusC4D GWAS study (Nikpay *et al*, 2015) was searched for SNPs significantly associated with coronary artery disease (CAD) (p-value<$1x10^{-4}$) within 500kb of gene loci. Analysis of loci of previously defined 710 epigenetic modifiers (Medvedeva *et al*, 2015) revealed that among 21 JmjC histone demethylase only KDM7A, KDM2B and JMJD6 contained CAD risk loci with KDM7A having the highest association (Table 12).

Table 12: CAD risc loci in JmjC histone demethylases.

Gene	SNP	p-value
KDM7A	rs9640375, rs6945612, rs3735352, rs35586793	4.05E-07, 5.23E-07, 3.92E-07, 4.17E-07
KDM2B	rs1169288, rs1169291, rs2244608	2.75E-06, 6.22E-06, 2.86E-06
JMJD6	rs72860151	2.96E-05

3.4.2.5 KDM7A and PKC activity

The transcription factor Early growth response 1 (EGR1) was part of the KDM7A network. EGR1 is a canonical Protein kinase C (PKC) dependent early response gene (Thiel et al, 2010). EGR1 is associated with multiple cardiovascular pathological processes and associated with atherosclerotic pathogenesis as a major pathogenic transcription factor (Khachigian, 2006). Therefore, a correlation between PKC-regulated genes and KDM7A in plaque tissue was tested.

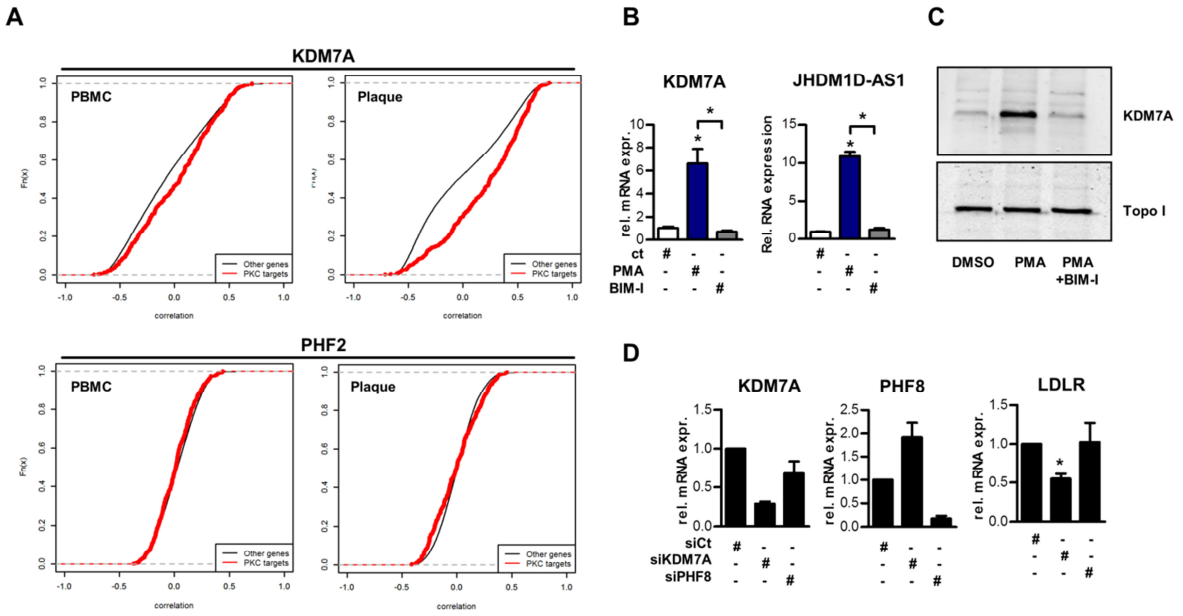

Figure 31: KDM7A is associated with PKC activity.

A: Correlation of KDM7A and PHF2 with PKC target genes in human carotid plaque tissue and peripheral blood mononuclear cells. B: Relative RNA expression of KDM7A and JHDM1D-AS1 in HUVEC treated with DMSO or PMA (50nM) or the PKC inhibitor bisindolmaleimide-I for 4 h (BIM-I) (n=3). B: Western analysis of HUVEC treated as in A. D: HUVEC were treated with siRNA against KDM7A or PHF8 and mRNA expression of LDLR was assessed (n=4). Data are represented as ± SEM *≤0.05 (Student's t-test).

KDM7A, but not PHF2 was positively correlated to previously reported upregulated genes upon activation of PKC (Caino et al, 2011) in 126 human carotid plaque tissues (Folkersen & Persson, 2012) (Figure 31 A). In contrast, no correlation was observed between KDM7A and PKC-regulated genes in peripheral blood mononuclear cells (PBMC) of 97 patients of the same cohort. Furthermore, phorbol-12-myristate-13-acetate (PMA), an activator of PKC increased the expression of KDM7A (Figure 31 B, C). The KDM7A locus contains in antisense direction a natural antisense transcript (NAT). Both share a promoter of 323 base pairs. However, the natural antisense transcript of KDM7A, the lncRNA JHDM1D-AS1, is not yet described in endothelial cells. Similar to KDM7A, JHDM1D-AS1 expression was induced by PKC activation. The selective PKC inhibitor bisindolmaleimide-I (BIM-I) prevented the induction of KDM7A and of JHDM1D-AS1. Furthermore, the low density lipoprotein receptor (LDLR), which is part of the KDM7A network and which constitutes an EGR1 target gene,

was reduced upon knockdown of KDM7A but not of PHF8 (Figure 31 D). Taken together, these data suggest that expression of KDM7A is associated with PKC activity and suggest the possibility that the EGR1-PKC-KDM7A axis is associated with atherosclerotic plaque pathogenesis.

3.4.2.6 EGR1 mediated expression of KDM7A

Since EGR1 was part of the KDM7A network and KDM7A expression correlated with PKC activity, the PKC-EGR1-KDM7A axis was further tested. SiRNA mediated knockdown of EGR1 prevented the induction of KDM7A and JHDM1D-AS1 upon PKC activation (Figure 32 A). Additionally, chromatin immunoprecipitation showed the binding of EGR1 to the shared promoter (TSS) of the KDM7A/JHDM1D-AS1 pair upon PKC activation in HEK293 cells (Figure 32 B). Next, the transcription factor activity in 126 human carotid plaque tissues (Folkersen & Persson, 2012) compared to that of PBMC of 97 patients of the same cohort was inferred as described previously (Lee *et al*, 2014). The analysis was conducted for loci of previously defined 710 epigenetic modifiers (Medvedeva *et al*, 2015). Integration of genome wide mRNA expression, DNase I hypersensitive regions in HUVEC and transcription binding affinity information of 205 transcription factors from JASPAR showed the transcription factor DNA Repair Associated (BRCA1) to have the highest association to KDM7A in plaque (Figure 32 C). BRCA1 was suggested as a target to delay atherosclerosis progression (Singh *et al*, 2013). In contrast, the transcription factor YY1, which showed a predicted binding site for the KDM7A/JHDM1D-AS1 promoter according to the Jaspar database alone, showed no binding to KDM7A. Consistently, overexpression of BRCA1 and of EGR1, but not of YY1 increased the luciferase reporter activity by binding to the KDM7A/JHDM1D-AS1 promoter in HEK293 cells (Figure 32). Collectively, the integrative analysis of KDM7A suggests that KDM7A is involved in the interferon signaling and that the PKC-EGR1-KDM7A axis is potentially active in atherosclerosis.

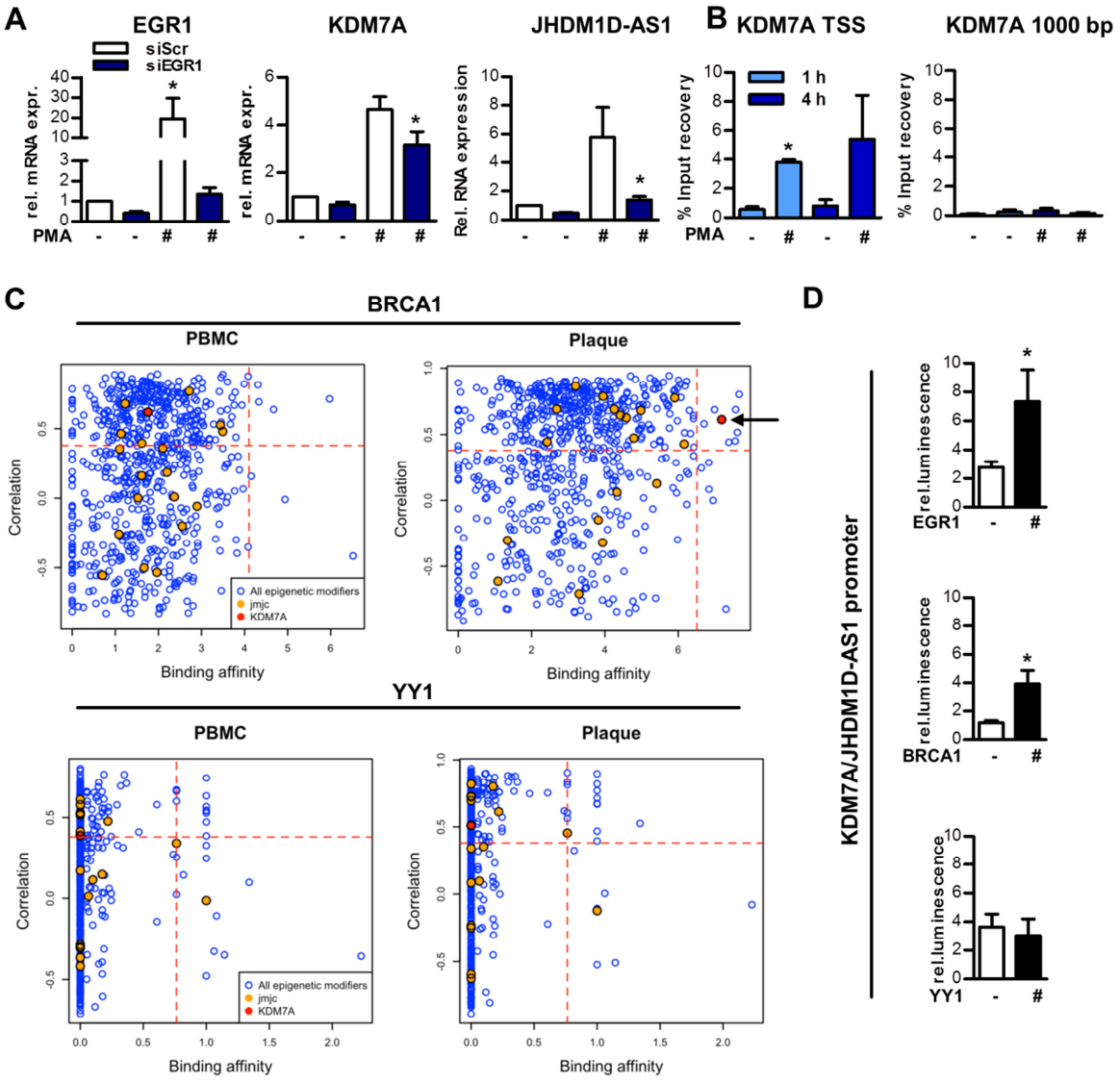

Figure 32: The PKC-EGR1-KDM7A axis.

A: Relative RNA expression of EGR1, JHDM1D-AS1 and KDM7A in HUVECs treated with scramble control siRNA or EGR1 siRNA and stimulated with PMA (50nM) for 8 h (n=3). B: ChIP for EGR1 in HEK293 cells stimulated with PMA for 1 h and 4 h for the KDM7A/JHDM1D-AS1 Promoter (TSS) or 1000 bp upstream of the TSS (n=3). C: Transcription factor activity of BRCA1 or YY1 to gene loci of 710 epigenetic modifiers in carotid plaque tissues and peripheral blood mononuclear cells (PBMC). E: HEK293 cells were transfected with the KDM7A/JHDM1D-AS1 promoter plasmid and the overexpression plasmid for EGR1, BRCA1 or corresponding empty vector. Luciferase activity was measured by luminescence (n=3). Data are represented as mean +/- SEM (*P<0.05).

4 Discussion

4.1 MTHFD2 controls an amino acid network to facilitate the ATP release in endothelial cells

4.1.1 Summary and Significance of the study

In this study a Bayesian network approach together with wet laboratory experiments and clinical data were used to uncover the reaction of human aortic endothelial cells to oxidized phospholipids (Hitzel *et al*, 2018). The application of an integrative network modeling approach resulted in the identification of deregulated gene clusters and causal regulators. Unexpectedly, an association of atherogenic lipids with the mitochondrial-one carbon metabolism was detected. Oxidized phospholipids induced a subnetwork regulating the serine-glycine metabolism with the mitochondrial methylenetetrahydrofolate dehydrogenase/cyclohydrolase (MTHFD2) as a causal regulator. The MTHFD2-controlled gene cluster redirected metabolism to glycine synthesis to replenish purine nucleotides. Endothelial cells secreted ATP as a signaling autacoid in response to oxPAPC. The MTHFD2-controlled subnetwork was necessary to maintain endothelial ATP level. Thus, MTHFD2 controlled endothelial reprogramming towards serine-glycine and mitochondrial one-carbon metabolism to compensate for the loss of ATP in response to oxPAPC. Confirming the importance of the mitochondrial one-carbon metabolism for endothelial function, MTHFD2-dependent glycine synthesis was a prerequisite for endothelial sprout formation and migration. Importantly, the MTHFD2-controlled subnetwork was activated in human atherosclerotic plaque material and single nucleotide polymorphisms within the subnetwork associated with coronary artery disease.

This study is characterized by the following principal novelty:

1) It demonstrates the power and suitability of Bayesian networks to identify and understand cellular responses.
2) It establishes metabolic reprogramming of endothelial cells as a prerequisite to facilitate ATP release.
3) It establishes a novel role of several enzymes in maintaining the endothelial amino acid and purine pool.
4) It defines a comprehensive reactome of endothelial cells to oxidized phospholipids.
5) It demonstrates that mitochondrial one-carbon related amino acid metabolism is activated in human plaques and single nucleotide polymorphisms in genes of the mitochondrial one-carbon metabolism are associated with coronary artery disease.

These findings establish MTHFD2 as a key driver with significant importance in adult cardiovascular cells. This study reveals that MTHFD2 orchestrates an amino acid response to enable endothelial cells to release ATP. Most strikingly, this by MTHFD2 driven response is elicited by pro-atherogenic lipids, thereby linking cardiovascular pathogenesis to mitochondrial metabolism.

4.1.2 Deregulated pathways in response to oxPAPC

A comprehensive characterization of gene-gene connectivity can provide significant insights and a different perspective into disease relevant processes compared to looking at single gene environments. The applied differential connectivity analysis revealed that gene-gene coregulation is drastically altered by oxPAPC in ECs. 9 GOC and 11 LOC clusters were causally related to oxPAPC. Interestingly, ECs reacted to oxPAPC with an equal proportion of disrupted (LOC) and newly connected (GOC) co-expressed DC gene pairs. In contrast, in neuronal pathological states, as in late-onset Alzheimer's disease and Huntington's disease, GOC traits were predominant (Narayanan *et al*, 2014; Zhang *et al*, 2013). It therefore should be considered, that in order to restore atherogenic lipid caused endothelial dysfunction to a healthy state not only emerging dysregulated patterns should be considered, but also healthy biological processes which are lost during disease progression.

The identified DC clusters reflect previously reported findings as well as not known processes in response to oxPAPC. The DC clusters reveal a shift in cell cycle: whereas processes related to active cell cycle and replication are disrupted (LOC4, LOC), processes related to cell cycle checkpoint activity are activated (GOC4, GOC5). Although low concentration of oxLDL can stimulate HAEC proliferation (Yu *et al*, 2011), the applied oxPAPC concentration used here rather limits cell cycle progression and induces apoptosis and thereby significantly contributes to oxPL elicited endothelial dysfunction (Li & Mehta, 2000; Li *et al*, 1998). GOC9 reflects activation of the unfolded protein response (UPR). Accordingly, oxidized phospholipids activate all three canonical branches of the UPR including nuclear translocation of ATF6, splicing of XBP1 and phosphorylation of eIF2α (Gargalovic *et al*, 2006a). Furthermore, processes related to inflammatory cell adhesion were disrupted upon oxPAPC exposure (LOC10). This supports the previously observed context-dependent anti-inflammatory activities in response to oxPAPC, which block expression of inflammatory adhesion molecules in endothelial cells (Birukov *et al*, 2004). In contrast, processes related to cell adhesion by cadherins, which form adherens junctions to mediate cell-cell contact, showed increased connectivity (GOC2). In line with this, oxPAPC showed barrier protective effects in ECs by binding to membrane localized GRP78 leading to Rac1 activation and subsequent cytosceleton reorganization (Birukova *et al*, 2014).

4.1.3 Key drivers of the HAEC oxPAPC response

The applied network modeling approach revealed hidden information stored in expression and genome profiles of the exploited HAEC cohort. Some biological processes are not obvious and can be overlooked by classical high throughput data analyses which include identification of differentially expressed genes, gene set enrichment analysis and correlation analysis. A Bayesian network approach provides comprehensive information about structures of relationships between the entities in a complex system as well as on the single gene-gene level. Furthermore, the advantage of the utility of such a network modeling approach is the possibility to provide an objective filter to rank-order genes based on network features as connectivity or hierarchy. This study utilized Bayesian inference to highlight and to prioritize genes and pathways causally related to oxPAPC in endothelial cells. With this study the first comprehensive endothelial cell Bayesian networks based on genome-wide expression and genotype data were analyzed.

Systematic validation showed that the EC Bayesian networks had higher predictive power for EC specific data sets than public databases as well as higher predictive power for public data sets than random networks. The networks therefore were questioned for the identification of novel causal regulators. GSEA of key driver associated subnetworks showed similar enrichments as the DC clusters, e.g. cell cycle and lysosome related categories, as well as new categories like ABC transporters. Within the Bayesian networks key drivers were detected which are known to be related to EC function as KDR, ITGAV and CDCA3, as well as sparsely described proteins as TRAM1, TBC1D8 or UBXN4. Also, the oxPAPC network suggests many novel key drivers like LOC100292189. Since the EC BNs have been shown to be highly predictive, they can be exploited to further investigate these potentially important genes. Interestingly, the oxPAPC Bayesian network comprised KIAA1462 as a key driver. Although the KIAA1462 gene locus contains a well known risc locus for coronary artery disease (CAD) (Deloukas *et al*, 2012), its function is sparsely known. The protein of the KIAA1462 locus, JCAD, was recently shown to contribute to angiogenesis in vivo and in vitro (Hara *et al*, 2017).

Consistent with the identified GOC-AA, the oxPAPC but not control BN contained a subnetwork with similar gene set enrichments thereby confirming amino acid metabolism as a critical response to pro-atherogenic lipids. In this study, the mitochondrial folate-cycle enzyme MTHFD2 was identified and experimentally validated as a key driver of this network. MTHFD2 was in the center of an oxPAPC-evoked response which integrated serine-glycine-synthesizing enzymes, SLC transporters and AARs. Other pathways activated by oxPAPC, and contained within the network, included elements of the redox-stress response and of the ER-stress-apoptosis machinery including DDIT3/CHOP and XBP1.

4.1.4 MTHFD2 centered amino acid metabolism in response to oxPAPC

In this study, the endothelial cell Bayesian networks revealed new processes in the reprogramming of HAEC in response to a pro-atherosclerotic stimulus (Hitzel *et al*, 2018). The HAEC Bayesian networks had high predictive power and in this study it was shown that an amino acid subnetwork emerged in response to oxidized phospholipids.

Oxidized phospholipids have not yet been linked to metabolism in HAEC. Endothelial metabolism has emerged as an important factor for endothelial function (Pircher *et al*, 2016), for controlling the angiogenic response and for the adaptation of endothelial cells to environmental conditions (Potente *et al*, 2011). In contrast, deregulated amino acid metabolism and in particular overexpression of serine-glycine-synthesizing enzymes and mitochondrial one-carbon metabolism was so far predominantly associated with fast proliferating cancer cells (Amelio *et al*, 2014; Jain *et al*, 2012). Given their high demand for purines for DNA synthesis, this reaction is expected. It also explains why knockout of MTHFD2 is lethal in the developing embryo, which also consists of rapidly dividing cells (Di Pietro *et al*, 2002). In contrast to this, MTHFD2 is weakly expressed in most postmitotic and normally proliferating cells (Nilsson et al, 2014; Ben-Porath et al, 2008). Potentially, these cells satisfy their demand for purines and glycine by uptake and salvage. Alternatively, under steady state conditions, the required de novo synthesis of these molecules is very low. Interestingly, our study suggests that MTHFD2 contributes to glycine synthesis in cultured endothelial cells under resting conditions and that this aspect might be relevant for vascular disease. We show that glycine levels were decreased upon short-term oxPAPC exposure as well as MTHFD2 knockdown. Additionally long-term induction of the MTHFD2 network in response to oxPAPC increased intracellular glycine. We thereby show that oxidized phospholipids cause a metabolic switch in mitochondrial one-carbon metabolism to facilitate the mitochondrial production of amino acids. In line with this observation, it was shown that cells barely take up glycine and rather synthesize this important amino acid on a *de novo* basis within mitochondria (Lewis *et al*, 2014). Additionally, MTHFD2 contributed to glycine levels in smooth muscle cells. Since smooth muscle cells substantially contribute to plaque development and are activated by oxidized phospholipids (Pidkovka *et al*, 2007), this observation strengthens the possible importance of MTHFD2 in the vascular system.

Plasma glycine is inversely associated with myocardial infarction risk (Ding *et al*, 2016) and our present work suggests an association between plasma amino acids, the MTHFD2 genotype and cardiovascular risk. Moreover, in our study plasma N-acetylglycine was associated with a genetic variant in the MTHFD2 gene locus. The function of N-acetylglycine and whether this modified glycine serves as a glycine donor is not known. It was shown that plasma levels of N-acetylglycine, glycine and serine negatively correlated with hepatic

steatosis (Mardinoglu *et al*, 2017). N-acetylglycine therefore might be a possible new amino acid derivative important under pathological conditions.

Knockdown of MTHFD2, the key driver of the amino acid response in the present study, reduced the angiogenic function of cultured endothelial cells. Importantly, glycine prevented this effect and also blocked the induction of the MTHFD2 network in response to MTHFD2 siRNA. Currently, MTHFD2 is tested as a potential drug target for cancer therapy (Pikman *et al*, 2016; Gustafsson *et al*, 2017). The present data suggest that in addition to a direct effect on cancer cells, MTHFD2 inhibition might also attenuate tumor angiogenesis.

The MTHFD2 network was induced by amino acid starvation as represented by MTHFD2-knockdown mediated cellular glycine-depletion as well as serine-glycine depleted medium and L-histidinol treatment. Therefore, MTHFD2-knockdown potentiated the induction of the network under oxPAPC exposure. However, glycine supplementation did not rescue the induction of the MTHFD2 network, indicating that either glycine is not sufficiently taken up by the cells or that the induction of the MTHFD2 network in response to oxPAPC is regulated by a different mechanism.

4.1.5 The MTHFD2 axis between amino acid response and mTOR signaling

The major gene ontology categories regulated by oxPAPC identified by co-expression clusters in a previous study included sterol synthesis, UPR, redox signaling and inflammation (Romanoski *et al*, 2011). In that study, CHAC1, which is the rate limiting enzme for glutathione synthesis, was identified as a hub protein regulated by ATF4 as well as HMOX1. Since our study expanded co-expression analysis to differentially co-regulated genes, new insights were gained. Unexpectedly, one of the most coherent DC clusters was GOC-AA and the corresponding BN_{MTHFD2}, which was enriched for biological processed related to mTOR activation, amino acid starvation and ER stress. This complex response pattern might be a reflection of the central position of glycine in cellular metabolism. The Ser/Thr protein kinase target of rapamycin (mTOR) is part of the two complexes mTOR complex 1 (mTORC1) and mTOR complex 2 (mTORC2) (Jewell *et al*, 2013). MTORC1 is a master regulator which promotes cell growth in the presence of amino acids and growth factors. In contrast, under starvation conditions mTORC1 is inhibited and autophagy is promoted. MTOR was shown to be activated by oxLDL in smooth muscle cells to promote proliferation (Brito *et al*, 2009) which contributes to the formation of the fibrous cap in atherosclerotic plaques. Due to the potentially beneficial effects of mTOR inhibition to induce autophagy, mTOR inhibition was suggested as a promising approach to stabilize atherosclerotic plaques (Mueller *et al*, 2008; Martinet *et al*, 2014). It was shown that oxPAPC remodels the cytoskeleton and leads to the assembly of the signalosome S1PR1-Akt-mTOR (Birukova *et al*, 2014). However, a link between mTOR, amino acid metabolism and oxidized phospholipids is not known. In this

study we show that MTHFD2 expression is dependent on mTOR activity and dependent on ATF4. In contrast to previous findings, in embryonic fibroblasts where the mTOR-ATF4-MTHFD2 axis was necessary for DNA and RNA purine nucleotide synthesis (Ben-Sahra *et al*, 2016), we hypothesize that the MTHFD2 network was activated for ATP purine synthesis for nucleotide release. Several universal transcription factors have shown to regulate de novo serine and mitochondrial folate cycle, predominantly ATF4, c-myc and p53 (Bao *et al*, 2016). Therefore, it is possible that oxPAPC induces the MTHFD2 network by different transcription factors besides ATF4.

The universal transcription factor ATF4 regulates a branch of the UPR, the amino acid starvation response as well as the growth response downstream of mTORC1 (Wu & Kaufman, 2006; Ben-Sahra *et al*, 2016). It therefore seems that the MTHFD2 network constitutes a universal response, which is activated under different conditions: under amino acid starvation as it contains SLC transporters to take up amino acids and serine-glycine related amino acid synthesizing enzymes to synthesize amino acids *de novo*. The MTHFD2 network contains a variety of transporters of the solute carrier family. Among them are the glucose transporters SLC2A14 and SLC2A3, the neutral amino acid transporter SLC1A5, the large neutral amino acid transporters SLC7A5 and SLC3A2 and the cationic amino acid transporter SLC7A1. On the other hand, the network can be activated downstream of mTORC1, which represents growth conditions. Under such conditions the cell activates serine-glycine metabolism, SLC transporters as well as AARs to increase purine synthesis and nutrient uptake for growth and protein translation.

In vitro depletion of any amino acid activates the amino acid response (AAR). Consistently, the histidine antagonist histidinol as well as asparagine depletion induced the MTHFD2 network. Asparagine synthetase (ASNS) constitutes a canonical amino acid response gene (Siu *et al*, 2002). Therefore, asparagine synthetase was together with MTHFD2 network genes strongly induced upon amino acid deprivation and additionally asparagine was together with serine strongly increased upon MTHFD2 knockdown. In line with this, asparagine synthetase was identified as a key driver close to MTHFD2 within BN_{ox}.

The presence of uncharged tRNAs activates the serine threonine kinase GCN2 which phosphorylates the translation initiation factor eIF2α leading to increased transcription of ATF4 (Dong et al, 2000; Hao, 2005; Harding et al, 2000). ATF4 can act together with ATF6 and XBP1 to induce genes involved in protein folding, maturation, and degradation (Lee *et al*, 2003; Okada *et al*, 2002). Furthermore, ATF4 upregulates apoptosis genes like CHOP, ER redox control genes like ERO1 and glucose metabolism involved genes (Ma *et al*, 2002). Additionally, ATF4 can upregulate amino acid metabolism, glutathione biosynthesis and resistance to oxidative stress (Harding *et al*, 2003). ATF4 can be induced by Nrf2 and links ER stress to the anti-oxidative defense system by orchestrating transcription of antioxidant-

response-element containing genes like HO1 and TXNRD1 (Cullinan & Diehl, 2006). Oxidized phospholipids were shown to increase ATF4 and VEGF expression through NRF2 thereby inducing the unfolded protein response and angiogenic reactions (Afonyushkin *et al*, 2010). oxPAPC treated HAECs show induction of ATF4 and ATF4 mediated IL8, IL6 and MCP-1 induction linking the ATF4 branch of UPR to inflammatory gene expression (Gargalovic *et al*, 2006a). ATF4 was also found to be a top hub gene in co-expression networks in HAECs in the UPR module (Gargalovic *et al*, 2006b). Also oxLDL triggers ATF6 mediated UPR (Sanson *et al*, 2009). Furthermore, homocysteine activate UPR and changes ATF4 expression (Outinen *et al*, 1999). ATF4 regulates this diverse array of pathways to balance amino acid metabolism under starvation, growth and redox stress conditions and unsurprisingly its target MTHFD2 orchestrates a network, which is enriched for exactly these pathways.

The function of the MTHFD2 axis in adult cells and tissues is barely known. Interestingly ATF4 is independently of the AAR pathway upregulated in response to insulin maybe to regulate insulin mediated protein synthesis which will lead to accumulation of uncharged tRNAs (Malmberg & Adams, 2008). In the presence of dexamethasone, insulin induced not only ATF4 but also ASNS, PSAT1, MTHFD2, and the transporters SLC7A1 and SLC7A5 in mouse L cells. There is evidence that insulin resistance and hyperglycemia promote, however by unknown mechanisms, atherosclerosis (Bornfeldt & Tabas, 2011). In another study, metabolic changes from fatty acid to glucose oxidation as energy use in heart resulting in hypertrophy was accompanied by mTOR dependent induction of genes which also belong to the MTHFD2 Bayesian network: mthfd2, Trib3 and Slc7a5 (Schisler *et al*, 2015).

4.1.6 MTHFD2 axis and the redox defense

In the enzymatic reaction of MTHFD2, NADPH is produced for nucleic acid and lipid synthesis and to recycle antioxidants like glutathione and thioredoxin (Fan *et al*, 2014). Glycine is also involved in redox-defense since it is used for glutathione synthesis. Therefore, it is unsurprising that MTHFD2 also contributes to redox defense. In line with this, siRNA against MTHFD2 induced an oxidative stress response with upregulation of Nrf2 target genes. The MTHFD2 network was, however, distinct from the Nrf2-dependent network. Nevertheless, MTHFD2 induction was rescued by the ROS scavenger NAC. Since NAC reacts with the oxPAPC component PEIPC (Springstead *et al*, 2012), the MTHFD2 network is possibly activated by PEIPC rather than by the Nrf2-Keap1 system. Nevertheless, we cannot exclude that reprogramming towards mitochondrial one-carbon metabolism could serve to produce NADPH as well as glycine for glutathione synthesis. Consistently, MTHFD2 was shown to contribute to NADPH production (Fan *et al*, 2014). Interestingly, MTHFD1L, which recouples 10-formyl-THF back to formate, was neither part of the MTHFD2 network

nor affected on expression level by oxPAPC or MTHFD2 knockdown. This could indicate that 10-formyl-THF not only fuels formate synthesis by MTHFD1L but is also oxidized to CO_2 by ALDH1L2 to contribute to NADPH production. Furthermore, the mitochondrial cleavage system enzyme GLDC which recycles glycine to produce additional 5,10-meTHF, the substrate for MTHFD2, was part of the network. In this glycine cleavage system additional NADPH is produced. Therefore, it is possible that the MTHFD2 network contributes not only to glycine and folate but also NADPH production.

4.1.7 Amino acid and folate metabolism in atherosclerosis

Beneficial effects of amino acids in the development of atherosclerosis have not been shown. Also, the association of amino acids and atherosclerosis is not clear. Analysis of the plasma of CAD patients suggested branched-chain and aromatic amino acids as biomarkers for cardiovascular disease (CVD) development (Magnusson *et al*, 2013).

The most studied amino acid pathways in cardiovascular diseases are arginine and cysteine metabolism. Although eNOS produced NO shows atheroprotective effects inducing smooth muscle cell relaxation, inhibition of endothelial inflammation, enhancing anit-oxidant and anti-apoptotic properties it is still controversial if dietary arginine intake is atheroprotective or atherogenic as there is still no clinical evidence (Tousoulis *et al*, 2007).

In contrast to arginine metabolism, the MTHFD2 network is indirectly linked to homocysteine metabolism via serine metabolism as well as associated folate metabolism. Many enzymes of the MTHFD2 network, which are directly and indirectly involved in serine-glycine metabolism use pyridoxal phosphate (PLP, Vitamin B6) as a cofactor. A beneficial effect of vitamin B6 and folate food intake for prevention of CAD has not been proven (Debreceni & Debreceni, 2012; Antoniades *et al*, 2009). Homocysteine is being considered a risk factor and potentially causal for CVD (Schnabel *et al*, 2005). The enzyme cystathionine β-synthase (CBS) of the reverse transsulfuration pathway, which is part of the MTHFD2 network, was with the second transsulfuration pathway enzyme cystathionine gamma-lyase (CTH) induced with the other MTHFD2 network genes under amino acid deprivation conditions. Furthermore, cysteine and homocysteine levels were increased in oxPAPC exposed HAEC with MTHFD2 knockdown. CBS condensates homocysteine and serine into cystathionine and CTH converts the latter into cysteine. Homocysteine is synthesized from methionine (Marinou *et al*, 1995) and this reaction is coupled to the folate cycle via the cofactor 5-meTHF as described in the introduction. The mitochondrial folate cycle is, therefore, indirectly coupled to homocysteine levels via serine and additionally via folates. Although homocysteine gives rise to elevated ROS burden and eNOS uncoupling through different mechanisms leading to endothelial dysfunction, classical antioxidant treatment or antioxidant vitamin intake, could so far not modifiy the clinical outcome of atherosclerosis (Antoniades *et*

al, 2009; Thomson *et al*, 2007). Administration of folate was shown to have beneficial effects on the vascular wall, however, additional folate supplement showed no benefit in countries with already high folate loaded diet (Shirodaria *et al*, 2007). Furthermore, high folate intake increases the transsulfulration pathway to methionine leading to high levels of SAM, which may has proatherogenic properties by hypermethylating DNA, uncoupling eNOS and increasing proliferation (Loscalzo, 2006; Mittermayer *et al*, 2006).

4.1.8 MTHFD2 axis and UPR in atherosclerosis

Chronic ER stress and ATF6 mediated UPR has been linked to atherosclerosis susceptibility regions of the arterial endothelium, where the role of ATF4 remains unclear (Civelek *et al*, 2009). OxPAPC and knockdown of MTHFD2 induced ATF4 and several ER stress response genes like CHOP, sXBP1 which were also members of the MTHFD2 network. This observation is in line with the fact that ER stress is present in atherosclerotic plaques and promotes the atherosclerotic process through apoptosis (Thorp *et al*, 2011; Zhou *et al*, 2005; Dong *et al*, 2010; Myoishi *et al*, 2007; Gargalovic *et al*, 2006a). Important pro-atherosclerotic lipids like 7-ketocholesterol fuel the atherosclerotic process through this mechanism (Scull & Tabas, 2011). This and the inflammatory activation of the endothelium in the atherosclerotic process explain why we observed an activation of the MTHFD2 network in atherosclerotic plaques. Moreover, our finding that decreasing MTHFD2 expression induces endothelial cell dysfunction could serve as an explanation of why genetic variations in genes of the MTHFD2 network were associated with CAD risk.

4.1.9 MTHFD2 response and ATP release

Purines are products of glycine in the intermediate metabolism and our data suggest that induction of the MTFHD2 network facilitates the endothelial production of purines in response to oxPAPC. In fact, purine nucleotides are important autacoids which, if released from endothelial cells, elicit a plethora of responses. The local release of purine nucleotides from atherosclerotic plaques and the subsequent activation of cellular purinergic receptors, for example, is thought to promote the development of atherosclerosis (Ferrari *et al*, 2015). Nucleotide release is a well-known stress reaction of endothelial cells and occurs in response to thrombin and shear stress (Godecke *et al*, 2012; Wang *et al*, 2016b). Although endothelial purine nucleotide release in response to oxPAPC has not been reported, copper-oxidized LDL (oxLDL) has been shown to induce this effect (Seye *et al*, 2002). The mechanism of thrombin and mechanical stress induced release of purine nucleotides is not fully understood but a role of gap junctions in this process has been suggested (Godecke *et al*, 2012; Lohman & Isakson, 2014). In keeping with this concept, the gap junction blocker flufenamic acid prevented ATP release in response to oxPAPC in the present study.

Flufenamic acid also prevented the induction of the MTHFD2 network in response to oxPAPC which suggests that the induction of the network is a compensatory reaction to the loss of purines.

In conclusion, by taking advantage of an integrative network modeling approach we unveiled a new reaction pattern of endothelial cells. On the basis of Bayesian network analysis we discovered that oxPAPC induced ATP release from endothelial cells results in glycine depletion. Subsequently, a network containing MTHFD2 as a key driver was activated to replenish amino acids and purines in endothelial cells. Our work not only demonstrates the power of Bayesian network analysis to uncover novel signaling mechanisms in vascular disease, it also illustrates the enormous secretory capacity of endothelial nucleotide release in the signaling context (Hitzel *et al*, 2018). It appears that endothelial cells prioritize autacoid release to such an extent that they would rather become deprived of vital metabolic components than neglect their signaling function.

4.1.10 Signature associated Bayesian networks

Exploiting the Bayesian network for retrieving epigenetic associated networks for the KDM7 A and B family members yielded two networks.

PHF8 is not well described in endothelial cells. It was shown that PHF8 contributes to proliferation and migration by maintaining E2F4 expression in endothelial cells (Gu *et al*, 2016). Consistently, the PHF8 HUVEC signature derived Bayesian network was strongly enriched for cell cycle related genes. The majority of central nodes within the network were downregulated by PHF8 whereas peripheral nodes were upregulated, which strengthens the importance of PHF8 for endothelial proliferation. However, although PHF8 had a strong impact on cell cycle gene expression, its mechanistic action in ECs is not known. The PHF8 Bayesian network suggested the new key drivers TIPIN, GINS1 and ZWILCH as candidates for PHF8 dependent endothelial cell cycle regulation. The PHF8 Bayesian network therefore confirmed the predictive power of the in this study presented HAEC Bayesian network for the identification of new key drivers in endothelial cells for specific perturbation signatures.

In contrast to PHF8, the KDM7A signature-derived Bayesian network highlighted an association of KDM7A with the endothelial interferon response. Many KDM7A signature genes are known interferon induced genes. The identified key drivers, which were part of the KDM7A signature, belonged predominantly to viral sensing and immune response pathways: IFIT1, IFIH1 and TNFSF10. KDM7A, but not the other KDM family members PHF8 and PHF2, was induced in SLE patients which strengthens the possible importance of KDM7A under pathological conditions. The potential clinical importance of KDM7A is highlighted by the observation that among all JmjC histone demethylases KDM7A contained loci with the strongest association with CAD.

KDM7A was shown to mediate TNFα induced ICAM expression by modulating its protein stability via the lysosomal pathway (Choi & Jo, 2016). However, other functions of KDM7A in the immune response are not known. Interestingly, the KDM7A interferon network contained genes known to contribute to the pathology of atherosclerosis: EGR1 and LDLR. The KDM7A Bayesian network therefore suggests that KDM7A links the inferferon response to atherosclerosis. Confirming, expression of LDLR was dependent on KDM7A, but not PHF8. Additionally, we show that KDM7A expression was regulated by the PKC-EGR1 axis. KDM7A was shown to act together with JMJD3 in PMA activated HL60 cells to promote transcriptional elongation (Chen *et al*, 2012). However, the transcriptional regulation of KDM7A is not known. We show that EGR1 binds to the promoter upstream of KDM7A. The observation that EGR1 was not a predicted transcription factor for the KDM7A locus in a human plaque cohort may contribute to the fact that EGR1 is an early responsive genes. Furthermore, since KDM7A was reported to be induced by TNFα, PMA as well as under nutrient starvation hints that KDM7A expression is regulated by different pathways and transcription factors in a context dependent manner (Choi & Jo, 2016; Chen *et al*, 2012; Osawa *et al*, 2011). Interestingly, the lnc-RNA JHDM1D-AS1, which is antisense to KDM7A, was similar to KDM7A regulated by the PKC-EGR1 axis. This lncRNA was reported to promote angiogenesis in starved tumors by increasing tumor-derived FDF-1 and stimulates tumor growth (Kondo *et al*, 2017). However, its expression regulation and function is not known.

Taken together, the KDM7A subnetwork highlighted an associated of KDM7A to the interferon response and atherosclerotic genes.

5 MTHFD2 and HAEC Bayesian networks: an outlook

5.1 MTHFD2 is a new player in atherosclerosis

In this study MTHFD2 was identified as a potential regulator of the induction of genes of the serine-glycine metabolism in endothelial cells in response to oxidized phospholipids. This study proposes that the MTHFD2-axis is activated to maintain cellular ATP, which is released upon oxPAPC treatment.

To further investigate glycine-serine metabolism and the involvement of MTHFD2 in response to oxPAPC, flux analyses can be carried out. Tracing of heavy labeled glycine can help to determine whether endothelial cells take up extracellular glycine or not. Since glycine and activated carbons are synthesized from serine, tracing of heavy labeled serine will reveal the flow of carbons upon oxPAPC treatment and its disturbance when MTHFD2 is downregulated by siRNAs. Measurement of intra- and extracellular heavy labeld ATP, purine intermediates and glutathione can confirm that the activated MTHFD2-axis contributes to synthesis of ATP. It will also help to determine whether glycine is, besides for ATP synthesis, also consumed for glutathione synthesis. Furthermore, to confirm the association between MTHFD2 and N-acetylglycine, amounts of this glycine-derivative can be measured intra- and extracellularly. It would also be important to know, whether not only oxPAPC, but also more naturally occurring oxidized lipids as in oxLDL or LDL from CAD patients activate the MTHFD2 network and reshape serine-glycine metabolism.

In a next step, the proposed mechanism can be assessed in an *in vivo* model. The folate pathway was investigated by inhibitors in a zebrafish model, where also a zebrafish ortholog of mthfd2 was identified (Lee *et al*, 2012a). However, a zebrafish knockout of mthfd2 has not been studied yet. A morpholino based knockout in an endothelial reporter zebrafish can give new insights into the importance of MHTFD2 for angiogenesis and the development of the vasculature. Furthermore, a high cholesterol diet, which has been proposed as an attractive *in vivo* model of atherosclerosis (Fang *et al*, 2014) and which results in lipoprotein oxidation and hypercholesterolemia, can serve as an *in vivo* approach to study the contribution of the mitochondrial folate pathway to the atherosclerotic process. Since MTHFD2 is embryonic lethal in mice, a conditional endothelial specific knockout can be created. A conditional mthfd2 knockout in an ApoE background can serve to study whether in such an atherosclerosis model mthfd2 contributes to plaque formation and plaque angiogenesis.

5.2 EC Bayesian networks as a platform to understand EC pathology

Since the HAEC Bayesian networks have been validated in this study, other key drivers and their associated subnetworks can be studied as they possibly consitute new potential targets

for disease treatment in atherosclerosis related endothelial pathology. The most promising key driver is KIAA1462. This key driver emerged as such upon oxPAPC treatment and although the KIAA1462 locus is associated with coronary artery disease (Peden *et al*, 2011; Erdmann *et al*, 2011) its function is marginally known (Hara *et al*, 2017). The here presented HAEC Bayesian KIAA1462 subnetwork represents an ideal model to shed light on the role and function of KIAA1462.

Since atherosclerosis is a complex disease involving different cell types acting in concert and influencing each other, the here presented endothelial networks can be integrated into cross-tissue networks containing atherosclerosis relevant cell types (Talukdar *et al*, 2016). Such a super-network can comprise endothelial and smooth muscle cells, immune cells as well as metabolic tissues contributing to CAD like liver and blood. Since more and more large scale consortium based CAD studies like STARNET (Franzén *et al*, 2016) provide RNAseq data, more information, as compared to microarray-based studies, like the non-coding transcriptome can be integrated.

Bayesian networks constitute flexible models and can therefore incorporate a large variety of such different high throughput data. The HAEC Bayesian networks could therefore be interrogated in further studies with a different focus to predict endothelial behavior. For instance, high-throughput data of blood metabolites in CAD patients (Wurtz *et al*, 2012) could be a valuable layer of information to be integrated into the HAEC Bayesian networks to more comprehensively understand endothelial behavior in CAD pathology.

6 Deutsche Zusammenfassung

In der vorliegenden Arbeit wurde ein integrativer Netzwerkmodellierungsansatz gewählt, um die Rolle des Endothels im Kontext der Arteriosklerose zu untersuchen. Hierbei wurden bioinformatische Analysen, laborexperimentelle Versuche und klinische Daten vereinigt und aus dieser Synthese neue klinisch relevante Gene identifiziert und beschrieben.

Das Endothel trägt maßgeblich zur Homöostase des vaskulären Systems bei und eine Dysfunktion des Endothels fördert die Entstehung der Arteriosklerose. Im Zuge der Atherogenese entstehen vermehrt reaktive Sauerstoffspezies, die Lipide in der Membran von Plasma-Lipoprotein-Partikeln und in der zellulären Plasmamembran oxidieren. Eine Gruppe solcher oxidierter Membranlipide ist oxPAPC, das in erhöhter Konzentration in arteriosklerotischen Plaques und lokal an Orten chronischer Entzündung im vaskulären System vorkommt. Weitherhin findet sich diese Gruppe von oxidierten Phospholipiden in oxidierten LDL-Partikeln, in denen oxPAPC die Bindung an Makrophagen vermittelt und hierdurch maßgeblich zur Bildung der Schaumzellen und damit zum arteriosklerotischen Prozess beiträgt. Die durch oxPAPC verursachte Veränderung der Endothelzelle ist bisher wenig erforscht. Es ist jedoch bekannt, dass oxPAPC die Transkriptionslandschaft in Endothelzellen tiefgreifend verändert. Um der Komplexität der Endothelzellveränderung gerecht zu werden, wurde ein bayesscher Ansatz angewendet.

In einem ersten Schritt wurden Expressionsprofile von humanen Aortenendothelzellen (HAEC) aus 147 Herztransplantatspendern verwendet. Diese Expressionprofile enthalten Transkriptionsinformationen der 147 HAEC, die mit oxPAPC oder Kontrollmedium behandelt worden waren. Es wurden signifikant koexprimierte Gene identifiziert und hiervon Gen-Paare berechnet, die einen differentiellen Vernetzungsgrad zwischen Kontroll- and oxPAPC-Status aufweisen. Dieses Netzwerkmodell gibt darüber Aufschluss, welche Gene miteinander in Verbindung stehen. 26759 Gene-Paare, die differentiell verbunden und signifkant koexprimiert waren, wurden hierarchisch gruppiert. Es wurden neun Gen-Gruppen mit einer erhöhten und elf Gen-Gruppen mit einer verminderten Konnektivität nach oxPAPC identifiziert. Gruppe 6 der erhöhten Konnektvitäts-Gruppen wies hierbei die höchste kohärente Konnektivität von allen Gruppen auf. Eine Analyse signifikant überrepräsentierter kanonischer Gensätze ergab, dass diese Gruppe insbesondere Serin-Glycin-Aminosäuremetabolismus, tRNA- und mTOR-Aktivierung wiederspiegelte. Der hier gewählte Netzwerkmodellierungsansatz zeigte auf, dass der Aminosäuremetabolismus durch oxidizerte Phospholipide massiven Veränderungen unterworfen ist.

Um den Mechanismus der Veränderung des Aminosäuremetabolismus näher zu untersuchen, wurden bayessche Netzwerkmodelle verwendet. Dieses Netzwerkmodell

enthält im Gegensatz zum differentiellen Koexpresssionsmodell gerichtete Informationen innerhalb des Netzwerkgraphes. Die Gen-Gen Verbindungen sind kausal, wodurch sich eine Hierarchie bildet und Schlüsselfaktoren innerhalb des Netzwerks bestimmt werden können. Durch die Integrierung von Expressionsprofilen und Genomprofilen derselben HAEC-Kohorte und der Inferenz von kausalen Gen-Gen-Verbindungen ergaben sich zwei bayessche Netze: Kontroll- und oxPAPC-Netzwerk. Permutationsuntersuchungen und systematische Beurteilung im Vergleich zu Gen-Gen-Verbindungen in Online-Datenbanken zeigten eine erhöhte Prognosefähigkeit der beiden HAEC bayesschen Netze. Es wurden die Schlüsselfaktoren und deren Teilnetzwerke berechnet und auf biologische Wege hin untersucht. Hierbei wurde das mitochondriale Protein MTHFD2 als ein Schlüsselfaktor für ein Teilnetzwerk des oxPAPC bayesschen Netzes identifiziert. Dieses Teilnetz zeigte eine ähnliche Gensatzanreicherung wie GOC-AA und überlappte mit diesem signifikant.

MTHFD2 ist Teil des 1C-Metabolismus und katalysiert im Mitochondrium die Umwandlung von 5,-10-mTHF zu 10-fTHF, einem reaktiven 1C-Donor. Diese Reaktion ist Teil des mitochondrialen Folat-Zyklus, der Serin in Glycin umwandelt und gleichzeitg 1C-Donoren synthetisiert, die in Form von Format ins Cytosol gelangen. Glycin und Format werden im Cytosol in das Purin-Rückgrat eingebaut. Serin speißt diesen Zyklus und wird aus dem Glykolysezwischenprodukt 3-Phosphoglycerat synthetisiert. Es konnte experimentell validiert werden, dass oxPAPC den Schlüsselfaktor MTHFD2 und weitere Gene des Teilnetzes induziert: SHMT2, das Serin in Glycin umwandelt, PHGDH und PSAT1 die Serin aus der 3-Phosphoglycerat synthetisieren, die tRNA-Aktivatoren CARS und GARS und die Aminosäuretransporter SLC7A5 und SLC7A1. Eine siRNA vermittelte Herunterregulierung des Schüsselfaktors MTHFD2 induzierte die Expression der Gene des Netzwerks während die Herunterregulierung von PSAT1, das in der Hierarchie des bayesschen Netzes weiter unten stand, einen deutlich geringeren Einfluss hatte. Somit konnte anhand des bayesschen Netzes MTHFD2 als Schlüsselfaktor für ein Teilnetzwerk identifiert werden, das für eine metabolische Verlagerung zur Aminosäure-Aufnahme und Glycin-*de-novo*-Synthese der Endothelzelle codierte. RNA-Sequenzierung nach Herrunterregulierung von MTHFD2 ergab eine signifikant differentiell exprimierte Gensignatur, die mit dem MTHFD2 bayesschen Netz und dem GOC-AA signifikant überlappte. 18 Gene des Serin-Glycin-Metabolismus, der Aminosäureaktivatoren und SLC-Transporter wurden hierbei als Kern-Gene der Antwort identifiziert.

Massenspektrometrische Untersuchungen des Aminosäure-Profils zeigten eine intrazelluläre Depletion von Glycin nach kurzzeitiger oxPAPC-Behandlung und nach Herrunterregulation von MTHFD2. Die Expressions-Induktion von Genen des MTHFD2-Netzes nach Herrunterregulierung von MTHFD2 konnte durch Glycin wieder normalisiert werden. Glycin

stellte ebenfalls die nach MTHFD2-Herunterregulation reduzierte endotheliale Angiogenese und Migration wieder her. In dieser Stude wurde hierdurch herausgestellt, dass das MTHFD2 bayesssche Netz maßgeblich zur Glycinsynthese in Endothelzellen beiträgt und die angiogene Funktion der Endothelzellen hiervon abhängt. Es konnte weiterhin gezeigt werden, dass MTHFD2 vom Transkriptionsfaktor ATF4 abhängig ist und dass die Induktion der Gene des MTHFD2-Netzes durch mTOR-Inhibierung gehemmt wird. Um zu ergründen, warum oxPAPC das Netzwerk induziert, wurden Purin-Nukleoside massenspektrometrisch gemessen. Es konnte gezeigt werden, dass Purin-Nukleoside extrazellulär angereichert waren. Durch weitere Untersuchungen wurde bestätigt, dass oxPAPC zur ATP-Sezernierung führt. Die ATP-Freisetzung durch Endothelzellen trägt maßgeblich zur Aktivierung von purinergen Signalwegen im vaskulären System bei. Die ATP-Freisetzung nach oxPAPC wurde durch den ATP-Freisetzungsinhibitor FFA verhindert. Übereinstimmend hemmte FFA auch die Expressionsinduktion der Gene des MTHFD2-Netzes. Auf physiologischer Ebene blockierte oxPAPC die Angiogenese, welche durch FFA wiederhergestellt wurde.

Die physiologische Bedeutung des MTHFD2-Netzes wurde durch die Untersuchung einer GWAS-Studie über die Plasmakonzentration von Metaboliten unterstrichen. Die genomische Variante rs10174907 im MTHFD2-Lokus war signifikant mit der N-Acetylglycin-Konzentration im Plasma assoziiert. SNPs assoziiert mit N-Acetylglycin waren angereichert in Genen des MTHFD2-Netzes. Weiterhin ergab die Untersuchung der CARDIoGRAMplus4CD GWAS-Studie eine Anreicherung von kardiovaskulär krankheitsrelevanten Genvariationen in Loci des MTHFD2-Netzwerks. Auch waren Genexpressionsänderungun von Genen des Teilnetzes in 32 humanen atheromen Plaques im Vergleich zu gesunden Proben ähnlich wie Genexpressionsänderungen in oxPAPC exponierten HAEC.

In dieser Arbeit wurde die Aktivierung des mitochondrialen 1C-Metabolism und damit assoziiertem Aminosäuremetabolism durch pro-atherogene Lipide aufgezeigt. MTHFD2 wurde als Schlüsselfaktor dieser Aminosäure-Reprogrammierung anhand eines endothelspezifischen bayessches Netzes identifiziert. Das Netzwerk wurde durch den Verlust von ATP, das als Signalautakoid freigesetzt wurde, aktiviert.

Das bayessche Netz erwies sich als prädiktiv und wurde daher verwendet, um epigenetische Signaturen der Endothelzelle näher zu untersuchen. Epigenetik beschreibt den Einfluss der Chromatin-Struktur und der DNA-Modifizierung auf die Expression und das Verhalten der Zelle. Eine große Gruppe der epigenetischen Enzyme mit über 20 Mitgliedern sind Histondemethylasen mit einer Jumonji (JmjC) Domäne. Diese Enzyme entfernen Methylgruppen von Histonen und aktivieren oder reprimieren hierdurch die Genexpression. KDM1-7 sind Untergruppen dieser Familie und viele dieser KDM-Histondemethylasen spielen eine wichtige Rolle im vaskulären System. Die drei Enzyme der KDM7, auch Plant-

Homeodomain-Finger (PHF)-Familie genannt, PHF2, PHF8 und KDM7A, sind jedoch noch unzureichend im kardiovaskulären System untesucht. Daher wurde das Endothelzell-Netzwerk verwendet, um endothelzellspezifische Netzwerkstrukturen der Signaturen von KDM7A und PHF8 zu untersuchen. Diese beiden Enzyme demethylieren die Lysine 9 und 27 des Histons 3 und beeinflussen, meist aktivieren, hierdurch die Genexpression.

Zunächst wurde eine endothelzellspezifische PHF8-Signatur, die durch RNA-Sequenzierung in HUVEC nach siRNA-Behandlung gewonnen und als differenziell exprimierte Gene definiert wurde, auf das Netzwerk projiziert und mit den direkten Nachbarn des Netzwerks extrahiert. Die Analyse des sich hieraus ergebenden größten PHF8-spezifischen Teilnetzwerks ergab eine signifikante Anreicherung von Gensätzen der Zellzyklus-Regulation. Weiterhin wurden zentrale Schlüsselgene des PHF8-Netzwerks identifizert und experimentell validiert. Hierzu zählten die bisher wenig beschriebenen Gene TIPIN, GINS1 und ZWILCH. Durch diesen Ansatz wurden daher neue potenziell durch PHF8-regulierte Gene identifiziert.

In einem analogen Analyseweg wurde ein KDM7A-spezifisches Teilnetz identifiziert und analysiert. Dieses Netzwerk zeigte Wege der Interfon-, Stimulus- und Immun-Antwort als signifikant angereichert. Als Schlüsselfaktor wurde IFIT1 identifiziert und experimentell verifiziert. Hiermit übereinstimmend korrelierte die Expression von KDM7A in humanen Plaques mit Genen der Virus-Antwort. Die Untersuchung der CARDIoGRAMplus4CD GWAS-Studie zeigte, dass von allen JmjC Histondemethylasen der KDM7A-Locus die signifikantesten Genvariationen mit Assoziation zu kardiovaskulären Krankheiten aufwies. Weiterhin war die Expression des LDL Rezeptors, der Teil des KDM7A-Netzes war, durch die Herunterregulation von KDM7A, aber nicht durch PHF8, vermindert. Die KDM7A-Expression war auch in humanen Blutproben von Patienten mit der Autoimmunkrankheit Lupus erythematodes, die durch erhöhte Interferon-Werte gekennzeichnet ist, erhöht. Es wurde gezeigt, dass die Expression von KDM7A und deren sich im KDM7A-locus befindlichen lncRNA JHDM1D-AS1 PKC-abhängig ist. Die Expression wurde durch die Transkriptionsfkatoren EGR1, der Teil des KDM7A-Netzes war und durch PKC aktiviert wird, und BRCA1 beeinflusst. In dieser Teilstudie wurde KDM7A als potenzieller Regulator in der interferon-abhängigen Immunantwort und der Arteriosklerose identifiziert.

Zusammenfassend wurden in dieser Arbeit die ersten umfassenden endothelzellspezifischen Bayesschen Netze analysiert. Das Bayessche Netz wurde erfolgreich verifiziert und ein neuer deregulierter biologischer Weg nach oxPAPC-Aktivierung entdeckt. Weiterhin wurde anhand der Gensignatur-basierten Anwendung des Bayesschen Netzes gezeigt, dass dieses auch als Filter für *Omics*-Daten verwendet werden kann, um in Gen-Signaturen krankheitsrelevante Wege und Gene zu identifieren.

7 References

Afonyushkin T, Oskolkova O V., Philippova M, Resink TJ, Erne P, Binder BR & Bochkov VN (2010) Oxidized phospholipids regulate expression of ATF4 and VEGF in endothelial cells via NRF2-dependent mechanism: Novel point of convergence between electrophilic and unfolded protein stress pathways. Arterioscler. Thromb. Vasc. Biol. 30: 1007–1013

Albert R & Thakar J (2014) Boolean modeling: A logic-based dynamic approach for understanding signaling and regulatory networks and for making useful predictions. Wiley Interdiscip. Rev. Syst. Biol. Med. 6: 353–369

Amelio I, Cutruzzolá F, Antonov A, Agostini M & Melino G (2014) Serine and glycine metabolism in cancer. Trends Biochem. Sci. 39: 191–198

Anders S, Pyl PT & Huber W (2015) HTSeq-A Python framework to work with high-throughput sequencing data. Bioinformatics 31: 166–169

Anderson DD & Stover PJ (2009) SHMT1 and SHMT2 are functionally redundant in nuclear de novo thymidylate biosynthesis. PLoS One 6: e5839 1-9

Antoniades C, Antonopoulos AS, Tousoulis D, Marinou K & Stefanadis C (2009) Homocysteine and coronary atherosclerosis: From folate fortification to the recent clinical trials. Eur. Heart J. 30: 6–15

Argmann CA, Houten SM, Zhu J & Schadt EE (2016) A Next Generation Multiscale View of Inborn Errors of Metabolism. Cell Metab. 23: 13–26

Argmann C, Dobrin R, Heikkinen S, Auburtin A, Pouilly L, Cock T-A, Koutnikova H, Zhu J, Schadt EE & Auwerx J (2009) Pparγ2 Is a Key Driver of Longevity in the Mouse. PLoS Genet. 5: e1000752 1-7

Asensio-Juan E, Gallego C & Martínez-Balbás MA (2012) The histone demethylase PHF8 is essential for cytoskeleton dynamics. Nucleic Acids Res. 40: 9429–9440

Ayari H & Bricca G (2013) Identification of two genes potentially associated in iron-heme homeostasis in human carotid plaque using microarray analysis. J. Biosci. 38: 311–315

Bannister AJ, Schneider R & Kouzarides T (2002) Histone methylation: dynamic or static? Cell 109: 801–806

Bao XR, Ong S, Goldberger O, Peng J, Sharma R, Thompson DA, Vafai SB, Cox AG, Marutani E, Ichinose F, Goessling W, Regev A, Carr SA, Clish CB & Mootha VK (2016) Mitochondrial dysfunction remodels one-carbon metabolism in human cells. Elife 5: 1–24

Basso K, Margolin AA, Stolovitzky G, Klein U, Dalla-Favera R & Califano A (2005) Reverse engineering of regulatory networks in human B cells. Nat Genet 37: 382–390

Ben-Porath I, Thomson M, Carey V & Ge R (2008) An embryonic stem cell–like gene expression signature in poorly differentiated aggressive human tumors. Nature Genetics 40: 499–507

Ben-Sahra I, Hoxhaj G, Ricoult SJH, Asara JM & Manning BD (2016a) mTORC1 induces purine synthesis through control of the mitochondrial tetrahydrofolate cycle. Science. 351: 728–733

Berger B, Peng J & Singh M (2013) Computational solutions for omics data. Nat. Rev. Genet. 14: 333–346

Berliner JA, Leitinger N & Tsimikas S (2009) The role of oxidized phospholipids in atherosclerosis. J. Lipid Res. 50: S207–S212

Beyer S, Kristensen MM, Jensen KS, Johansen JV & Staller P (2008) The histone demethylases JMJD1A and JMJD2B are transcriptional targets of hypoxia-inducible factor HIF. J. Biol. Chem. 283: 36542–36552

Birukov KG, Leitinger N, Bochkov VN & Garcia JGN (2004) Signal transduction pathways activated in human pulmonary endothelial cells by OxPAPC, a bioactive component of oxidized lipoproteins. Microvasc. Res. 67: 18–28

Birukova A a, Singleton P a, Gawlak G, Tian X, Mirzapoiazova T, Mambetsariev B, Dubrovskyi O, Oskolkova O V, Bochkov VN & Birukov KG (2014) GRP78 is a novel receptor initiating a vascular barrier protective response to oxidized phospholipids. Mol. Biol. Cell 25: 2006–16

Bochkov VN, Oskolkova O V., Birukov KG, Levonen A-L, Binder CJ & Stöckl J (2010) Generation and Biological Activities of Oxidized Phospholipids. Antioxid. Redox Signal. 12: 1009–1059

De Bock K, Georgiadou M, Schoors S, Kuchnio A, Wong BW, Cantelmo AR, Quaegebeur A, Ghesquière B, Cauwenberghs S, Eelen G, Phng LK, Betz I, Tembuyser B, Brepoels K, Welti J, Geudens I, Segura I, Cruys B, Bifari F, Decimo I, et al (2013) Role of PFKFB3-driven glycolysis in vessel sprouting. Cell 154: 651–663

Boeckel J-N, Guarani V, Koyanagi M, Roexe T, Lengeling A, Schermuly RT, Gellert P, Braun T, Zeiher A & Dimmeler S (2011) Jumonji domain-containing protein 6 (Jmjd6) is required for angiogenic sprouting and regulates splicing of VEGF-receptor 1. Proc. Natl. Acad. Sci. U. S. A. 108: 3276–81

Boeckel JN, Derlet A, Glaser SF, Luczak A, Lucas T, Heumüller AW, Krüger M, Zehendner CM, Kaluza D, Doddaballapur A, Ohtani K, Treguer K & Dimmeler S (2016) JMJD8 Regulates Angiogenic Sprouting and Cellular Metabolism by Interacting with Pyruvate Kinase M2 in Endothelial Cells. Arterioscler. Thromb. Vasc. Biol. 36: 1425–1433

Bonneau R, Reiss DJ, Shannon P, Facciotti M, Hood L, Baliga NS & Thorsson V (2006) The Inferelator: an algorithm for learning parsimonious regulatory networks from systems-biology data sets de novo. Genome Biol. 7: R36 1-16

Bornfeldt KE & Tabas I (2011) Insulin resistance, hyperglycemia, and atherosclerosis. Cell Metab. 14: 575–585

Bouman L, Schlierf a, Lutz a K, Shan J, Deinlein a, Kast J, Galehdar Z, Palmisano V, Patenge N, Berg D, Gasser T, Augustin R, Trümbach D, Irrcher I, Park DS, Wurst W, Kilberg MS, Tatzelt J & Winklhofer KF (2011) Parkin is transcriptionally regulated by ATF4: evidence for an interconnection between mitochondrial stress and ER stress. Cell Death Differ. 18: 769–782

Brito PM, Devillard R, Nègre-Salvayre A, Almeida LM, Dinis TCP, Salvayre R & Augé N (2009) Resveratrol inhibits the mTOR mitogenic signaling evoked by oxidized LDL in smooth muscle cells. Atherosclerosis 205: 126–134

Caino MC, Von Burstin VA, Lopez-Haber C & Kazanietz MG (2011) Differential regulation of gene expression by protein kinase C isozymes as determined by genome-wide expression analysis. J. Biol. Chem. 286: 11254–11264

Capoulade R, Chan KL, Yeang C, Mathieu P, Bossé Y, Dumesnil JG, Tam JW, Teo KK, Mahmut A, Yang X, Witztum JL, Arsenault BJ, Després JP, Pibarot P & Tsimikas S (2015) Oxidized phospholipids, lipoprotein(a), and progression of calcific aortic valve stenosis. J. Am. Coll. Cardiol. 66: 1236–1246

Chang R, Karr JR & Schadt EE (2015) Causal inference in biology networks with integrated belief propagation. Pac. Symp. Biocomput.: 359–70

Chattopadhyay S, Moran RG & Goldman ID (2007) Pemetrexed: biochemical and cellular pharmacology, mechanisms, and clinical applications. Mol. Cancer Ther. 6: 404–417

Chen S, Ma J, Wu F, Xiong L -j., Ma H, Xu W, Lv R, Li X, Villen J, Gygi SP, Liu XS & Shi Y (2012) The histone H3 Lys 27 demethylase JMJD3 regulates gene expression by impacting transcriptional elongation. Genes Dev. 26: 1364–1375

Chen Y, Zhu J, Lum PY, Yang X, Pinto S, MacNeil DJ, Zhang C, Lamb J, Edwards S, Sieberts SK, Leonardson A, Castellini LW, Wang S, Champy M-F, Zhang B, Emilsson V,

Doss S, Ghazalpour A, Horvath S, Drake T a, et al (2008) Variations in DNA elucidate molecular networks that cause disease. Nature 452: 429–35

Choi J-Y & Jo SA (2016) KDM7A histone demethylase mediates TNF-α-induced ICAM1 protein upregulation by modulating lysosomal activity. Biochem. Biophys. Res. Commun. 478: 1355–1362

Choi J, Kim ST & Craft J (2012) The pathogenesis of systemic lupus erythematosus-an update. Curr. Opin. Immunol. 24: 651–657

Civelek M & Lusis AJ (2013) Systems genetics approaches to understand complex traits. Nat. Rev. Genet. 15: 34–48

Civelek M, Manduchi E, Riley RJ, Stoeckert CJ & Davies PF (2009) Chronic endoplasmic reticulum stress activates unfolded protein response in arterial endothelium in regions of susceptibility to atherosclerosis. Circ. Res. 105: 453–461

Cloos PAC, Christensen J, Agger K, Maiolica A, Rappsilber J, Antal T, Hansen KH & Helin K (2006) The putative oncogene GASC1 demethylates tri- and dimethylated lysine 9 on histone H3. Nature 442: 307–311

Cullinan SB & Diehl JA (2006) Coordination of ER and oxidative stress signaling: The PERK/Nrf2 signaling pathway. Int. J. Biochem. Cell Biol. 38: 317–332

Cyrus T, Praticò D, Zhao L, Witztum JL, Rader DJ, Fitzgerald G a & Funk CD (2001) Lipid Peroxidation and Atherogenesis in. Circulation 103: 2277–2283

Davis JC, Furstenthal L, Desai A a, Norris T, Sutaria S, Fleming E & Ma P (2009) The microeconomics of personalized medicine: today's challenge and tomorrow's promise. Nat. Rev. Drug Discov. 8: 279–86

Dawson MA & Kouzarides T (2012) Cancer epigenetics: From mechanism to therapy. Cell 150: 12–27

Debreceni B & Debreceni L (2012) Why Do Homocysteine-Lowering B Vitamin and Antioxidant E Vitamin Supplementations Appear To Be Ineffective in the Prevention of Cardiovascular Diseases? Cardiovasc. Ther. 30: 227–233

Deloukas P, Kanoni S, Willenborg C, Farrall M, Assimes TL, Thompson JR, Ingelsson E, Saleheen D, Erdmann J, Goldstein BA, Stirrups K, König IR, Cazier J-B, Johansson Å, Hall AS, Lee J-Y, Willer CJ, Chambers JC, Esko T, Folkersen L, et al (2012) Large-scale association analysis identifies new risk loci for coronary artery disease. Nat. Genet. 45: 25–33

Ding Y, Svingen GFT, Pedersen ER, Gregory JF, Ueland PM, Tell GS & Nygard OK (2016) Plasma glycine and risk of acute myocardial infarction in patients with suspected stable angina pectoris. J. Am. Heart Assoc. 5: 1–10

Dobrin R, Zhu J, Molony C, Argman C, Parrish ML, Carlson S, Allan MF, Pomp D & Schadt EE (2009) Multi-tissue coexpression networks reveal unexpected subnetworks associated with disease. Genome Biol. 10: R55 1-13

Dong J, Qiu H, Garcia-Barrio M, Anderson J & Hinnebusch a G (2000) Uncharged tRNA activates GCN2 by displacing the protein kinase moiety from a bipartite tRNA-binding domain. Mol. Cell 6: 269–279

Dong Y, Zhang M, Liang B, Xie Z, Zhao Z, Asfa S, Choi HC & Zou M-H (2010) Reduction of AMP-Activated Protein Kinase 2 Increases Endoplasmic Reticulum Stress and Atherosclerosis In Vivo. Circulation 121: 792–803

Ducker GS, Chen L, Morscher RJ, Ghergurovich JM, Esposito M, Teng X, Kang Y & Rabinowitz JD (2016) Reversal of Cytosolic One-Carbon Flux Compensates for Loss of the Mitochondrial Folate Pathway. Cell Metab. 23: 1140–1153

Ducker GS & Rabinowitz JD (2016) One-Carbon Metabolism in Health and Disease. Cell Metab. 25: 27–42

Dudley JT, Sirota M, Shenoy M, Pai RK, Roedder S, Chiang AP, Morgan AA, Sarwal MM, Pasricha PJ & Butte AJ (2011) Computational Repositioning of the Anticonvulsant Topiramate for Inflammatory Bowel Disease. Sci. Transl. Med. 3: 96ra76 1-6

Emilsson V, Thorleifsson G, Zhang B, Leonardson AS, Zink F, Zhu J, Carlson S, Helgason A, Walters GB, Gunnarsdottir S, Mouy M, Steinthorsdottir V, Eiriksdottir GH, Bjornsdottir G, Reynisdottir I, Gudbjartsson D, Helgadottir A, Jonasdottir A, Jonasdottir A, Styrkarsdottir U, et al (2008) Genetics of gene expression and its effect on disease. Nature 452: 423–428

Erbilgin A, Civelek M, Romanoski CE, Pan C, Hagopian R, Berliner JA & Lusis AJ (2013) Identification of CAD candidate genes in GWAS loci and their expression in vascular cells. J. Lipid Res. 54: 1894–905

Erdmann J, Willenborg C, Nahrstaedt J, Preuss M, König IR, Baumert J, Linsel-Nitschke P, Gieger C, Tennstedt S, Belcredi P, Aherrahrou Z, Klopp N, Loley C, Stark K, Hengstenberg C, Bruse P, Freyer J, Wagner AK, Medack A, Lieb W, et al (2011) Genome-wide association study identifies a new locus for coronary artery disease on chromosome 10p11.23. Eur. Heart J. 32: 158–168

Fan J, Ye J, Kamphorst JJ, Shlomi T, Thompson CB & Rabinowitz JD (2014) Quantitative flux analysis reveals folate-dependent NADPH production. Nature 510: 298–302

Fang L, Liu C & Miller YI (2014) Zebrafish models of dyslipidemia: Relevance to atherosclerosis and angiogenesis. Transl. Res. 163: 99–108

Ferrari D, Vitiello L, Idzko M & la Sala A (2015) Purinergic signaling in atherosclerosis. Trends Mol. Med. 21: 184–192

Folkersen L & Persson J (2012) Prediction of ischemic events on the basis of transcriptomic and genomic profiling in patients undergoing carotid endarterectomy. Mol. Med. 18: 669-675

Fork C, Gu L, Hitzel J, Josipovic I, Hu J, Wong MS, Ponomareva Y, Albert M, Schmitz SU, Uchida S, Fleming I, Helin K, Steinhilber D, Leisegang MS & Brandes RP (2015) Epigenetic regulation of angiogenesis by JARID1B-induced repression of HOXA5. Arterioscler. Thromb. Vasc. Biol. 35: 1645–1652

Fortschegger K & Shiekhattar R (2011) Plant homeodomain fingers form a helping hand for transcription. Epigenetics 6: 4–8

Franceschini A, Szklarczyk D, Frankild S, Kuhn M, Simonovic M, Roth A, Lin J, Minguez P, Bork P, Von Mering C & Jensen LJ (2013) STRING v9.1: Protein-protein interaction networks, with increased coverage and integration. Nucleic Acids Res. 41: 808–815

Franzén O, Ermel R, Cohain A, Akers NK, Di Narzo A, Talukdar HA, Foroughi-Asl H, Giambartolomei C, Fullard JF, Sukhavasi K, Köks S, Gan L-M, Giannarelli C, Kovacic JC, Betsholtz C, Losic B, Michoel T, Hao K, Roussos P, Skogsberg J, et al (2016) Cardiometabolic risk loci share downstream cis- and trans-gene regulation across tissues and diseases. Science 353: 827–30

Freigang S (2016) The regulation of inflammation by oxidized phospholipids. Eur. J. Immunol. 46: 1818–1825

French JB, Jones SA, Deng H, Pedley AM, Kim D, Chan CY, Hu H, Pugh RJ, Zhao H, Zhang Y, Huang TJ, Fang Y, Zhuang X & Benkovic SJ (2016) Spatial colocalization and functional link of purinosomes with mitochondria. Science. 351: 733–737

Furnkranz A, Schober A, Bochkov VN, Bashtrykov P, Kronke G, Kadl A, Binder BR, Weber C & Leitinger N (2005) Oxidized phospholipids trigger atherogenic inflammation in murine arteries. Arterioscler. Thromb. Vasc. Biol. 25: 633–638

Gargalovic PS, Gharavi NM, Clark MJ, Pagnon J, Yang WP, He A, Truong A, Baruch-Oren T, Berliner JA, Kirchgessner TG & Lusis AJ (2006a) The unfolded protein response is an important regulator of inflammatory genes in endothelial cells. Arterioscler. Thromb. Vasc. Biol. 26: 2490–2496

Gargalovic PS, Imura M, Zhang B, Gharavi NM, Clark MJ, Pagnon J, Yang WP, He A, Truong A, Patel S, Nelson SF, Horvath S, Berliner JA, Kirchgessner TG & Lusis AJ (2006b)

Identification of inflammatory gene modules based on variations of human endothelial cell responses to oxidized lipids. Proc Natl Acad Sci U S A 103: 12741–12746

Gimbrone MA & García-Cardeña G (2016) Endothelial Cell Dysfunction and the Pathobiology of Atherosclerosis. Circ. Res. 118: 620–636

Godecke S, Roderigo C, Rose CR, Rauch BH, Godecke A & Schrader J (2012) Thrombin-induced ATP release from human umbilical vein endothelial cells. Am. J. Physiol. Cell Physiol. 302: C915-23

Gong K, Zhao W, Li N, Barajas B, Kleinman M, Sioutas C, Horvath S, Lusis AJ, Nel A & Araujo JA (2007) Air-pollutant chemicals and oxidized lipids exhibit genome-wide synergistic effects on endothelial cells. Genome Biol. 8: R149 1-13

Gu L, Hitzel J, Moll F, Kruse C, Malik RA, Preussner J, Looso M, Leisegang MS, Steinhilber D, Brandes RP & Fork C (2016) The histone demethylase PHF8 Is essential for endothelial cell migration. PLoS One 11: 1–15

Gustafsson R, Jemth A-S, Gustafsson NMS, Färnegårdh K, Loseva O, Wiita E, Bonagas N, Dahllund L, Llona-Minguez S, Häggblad M, Henriksson M, Andersson Y, Homan E, Helleday T & Stenmark P (2017) Crystal Structure of the Emerging Cancer Target MTHFD2 in Complex with a Substrate-Based Inhibitor. Cancer Res. 77: 937–948

Gustafsson Sheppard N, Jarl L, Mahadessian D, Strittmatter L, Schmidt A, Madhusudan N, Tegnér J, Lundberg EK, Asplund A, Jain M & Nilsson R (2015) The folate-coupled enzyme MTHFD2 is a nuclear protein and promotes cell proliferation. Sci. Rep. 5: 15029 1-11

Hahn BH & McMahon M (2008) Atherosclerosis and systemic lupus erythematosus: the role of altered lipids and of autoantibodies. Lupus 17: 368–370

Hancock RL, Dunne K, Walport LJ, Flashman E & Kawamura A (2015) Epigenetic regulation by histone demethylases in hypoxia. Epigenomics 7: 1–21

Hao S (2005) Uncharged tRNA and Sensing of Amino Acid Deficiency in Mammalian Piriform Cortex. Science. 307: 1776–1778

Hara T, Monguchi T, Iwamoto N, Akashi M, Mori K, Oshita T, Okano M, Toh R, Irino Y, Shinohara M, Yamashita Y, Shioi G, Furuse M, Ishida T & Hirata K (2017) Targeted Disruption of JCAD (Junctional Protein Associated With Coronary Artery Disease)/KIAA1462, a Coronary Artery Disease–Associated Gene Product, Inhibits Angiogenic Processes In Vitro and In Vivo. Arterioscler. Thromb. Vasc. Biol. 37: 1667–1673

Harding HP, Novoa I, Zhang Y, Zeng H, Wek R, Schapira M & Ron D (2000) Stress-Induced Gene Expression in Mammalian Cells. Mol. Cell 6: 1099–1108

Harding HP, Zhang Y, Zeng H, Novoa I, Lu PD, Calfon M, Sadri N, Yun C, Popko B, Paules R, Stojdl DF, Bell JC, Hettmann T, Leiden JM & Ron D (2003) An integrated stress response regulates amino acid metabolism and resistance to oxidative stress. Mol. Cell 11: 619–33

Hitzel J, Lee E, Zhang Y, Bibli SI, Li X, Zukunft S, Pflüger B, Hu J, Schürmann C, Vasconez AE, Oo JA, Kratzer A, Kumar S, Rezende F, Josipovic I, Thomas D, Giral H, Schreiber Y, Geisslinger G, Fork C, Yang X, Sigala F, Romanoski CE, Kroll J, Jo H, Landmesser U, Lusis AJ, Namgaladze D, Fleming I, Leisegang MS, Zhu J, Brandes RP (2018) Oxidized phospholipids regulate amino acid metabolism through MTHFD2 to facilitate nucleotide release in endothelial cells. Nat. Commun. 9: 2292

Hong S, Cho Y-W, Yu L-R, Yu H, Veenstra TD & Ge K (2007) Identification of JmjC domain-containing UTX and JMJD3 as histone H3 lysine 27 demethylases. Proc. Natl. Acad. Sci. U. S. A. 104: 18439–44

Horton JR, Upadhyay AK, Qi HH, Zhang X, Shi Y & Cheng X (2010) Enzymatic and structural insights for substrate specificity of a family of jumonji histone lysine demethylases. Nat. Struct. Mol. Biol. 17: 38–43

Huan T, Meng Q, Saleh M a., Norlander a. E, Joehanes R, Zhu J, Chen BH, Zhang B, Johnson a. D, Ying S, Courchesne P, Raghavachari N, Wang R, Liu P, O'Donnell CJ, Vasan R, Munson PJ, Madhur MS, Harrison DG, Yang X, et al (2015) Integrative network analysis reveals molecular mechanisms of blood pressure regulation. Mol. Syst. Biol. 11: 799–799

Huang C, Chen J, Zhang T, Zhu Q, Xiang Y, Chen CD & Jing N (2010a) The dual histone demethylase KDM7A promotes neural induction in early chick embryos. Dev. Dyn. 239: 3350–7

Huang C, Xiang Y, Wang Y, Li X, Xu L, Zhu Z, Zhang T, Zhu Q, Zhang K, Jing N & Chen CD (2010b) Dual-specificity histone demethylase KIAA1718 (KDM7A) regulates neural differentiation through FGF4. Cell Res. 20: 154–65

Hung T, Pratt GA, Sundararaman B, Townsend MJ, Chaivorapol C, Bhangale T, Graham RR, Ortmann W, Criswell LA, Yeo GW & Behrens TW (2015) The Ro60 autoantigen binds endogenous retroelements and regulates inflammatory gene expression. Science. 350: 455–459

Hurley D, Araki H, Tamada Y, Dunmore B, Sanders D, Humphreys S, Affara M, Imoto S, Yasuda K, Tomiyasu Y, Tashiro K, Savoie C, Cho V, Smith S, Kuhara S, Miyano S, Charnock-Jones DS, Crampin EJ & Print CG (2012) Gene network inference and visualization tools for biologists: Application to new human transcriptome datasets. Nucleic Acids Res. 40: 2377–2398

Inouye M, Ripatti S, Kettunen J, Lyytikäinen LP, Oksala N, Laurila PP, Kangas AJ, Soininen P, Savolainen MJ, Viikari J, Kähönen M, Perola M, Salomaa V, Raitakari O, Lehtimäki T, Taskinen MR, Järvelin MR, Ala-Korpela M, Palotie A & de Bakker PIW (2012) Novel Loci for Metabolic Networks and Multi-Tissue Expression Studies Reveal Genes for Atherosclerosis. PLoS Genet. 8: e1002907 1-11

Iwase S, Lan F, Bayliss P, de la Torre-Ubieta L, Huarte M, Qi HH, Whetstine J, Bonni A, Roberts TM & Shi Y (2007) The X-Linked Mental Retardation Gene SMCX/JARID1C Defines a Family of Histone H3 Lysine 4 Demethylases. Cell 128: 1077–1088

Jain M, Nilsson R, Sharma S, Madhusudhan N, Kitami T, Souza AL, Kafri R, Kirschner MW, Clish CB & Mootha VK (2012) Metabolite Profiling Identifies a Key Role for Glycine in Rapid Cancer Cell Proliferation. Science. 336: 1040–1044

Jenuwein T (2001) Translating the Histone Code. Science. 293: 1074–1080

Jewell JL, Russell RC & Guan K-L (2013) Amino acid signalling upstream of mTOR. Nat. Rev. Mol. Cell Biol. 14: 133–9

Jostins L, Ripke S, Weersma RK, Duerr RH, McGovern DP, Hui KY, Lee JC, Schumm LP, Sharma Y, Anderson CA, Essers J, Mitrovic M, Ning K, Cleynen I, Theatre E, Spain SL, Raychaudhuri S, Goyette P, Wei Z, Abraham C, et al (2012) Host-microbe interactions have shaped the genetic architecture of inflammatory bowel disease. Nature 491: 119–24

Jyrkkanen H-K, Kansanen E, Inkala M, Kivela AM, Hurttila H, Heinonen SE, Goldsteins G, Jauhiainen S, Tiainen S, Makkonen H, Oskolkova O, Afonyushkin T, Koistinaho J, Yamamoto M, Bochkov VN, Yla-Herttuala S & Levonen A-L (2008) Nrf2 Regulates Antioxidant Gene Expression Evoked by Oxidized Phospholipids in Endothelial Cells and Murine Arteries In Vivo. Circ. Res. 103: e1–e9

Katada S, Imhof A & Sassone-Corsi P (2012) Connecting threads: Epigenetics and metabolism. Cell 148: 24–28

Khachigian LM (2006) Early growth response-1 in cardiovascular pathobiology. Circ. Res. 98: 186–91

Kidd B a, Peters L a, Schadt EE & Dudley JT (2014) Unifying immunology with informatics and multiscale biology. Nat. Immunol. 15: 118–27

Klose RJ, Yamane K, Bae Y, Zhang D, Erdjument-Bromage H, Tempst P, Wong J & Zhang Y (2006) The transcriptional repressor JHDM3A demethylates trimethyl histone H3 lysine 9 and lysine 36. Nature 442: 312–316

Klose RJ, Yan Q, Tothova Z, Yamane K, Erdjument-Bromage H, Tempst P, Gilliland DG, Zhang Y & Kaelin WG (2007) The Retinoblastoma Binding Protein RBP2 Is an H3K4 Demethylase. Cell 128: 889–900

Klose RJ & Zhang Y (2007) Regulation of histone methylation by demethylimination and demethylation. Nat Rev Mol Cell Biol 8: 307–318

Kondo A, Nonaka A, Shimamura T, Yamamoto S, Yoshida T, Kodama T, Aburatani H & Osawa T (2017) Long Noncoding RNA JHDM1D-AS1 Promotes Tumor Growth by Regulating Angiogenesis in Response to Nutrient Starvation. Mol. Cell. Biol. 37: e00125 1-17

Kooistra SM & Helin K (2012) Molecular mechanisms and potential functions of histone demethylases. Nat. Publ. Gr. 13: 297–311

Kottakis F, Polytarchou C, Foltopoulou P, Sanidas I, Kampranis SC & Tsichlis PN (2011) FGF-2 Regulates Cell Proliferation, Migration, and Angiogenesis through an NDY1/KDM2B-miR-101-EZH2 Pathway. Mol. Cell 43: 285–298

Krupenko NI, Dubard ME, Strickland KC, Moxley KM, Oleinik N V. & Krupenko SA (2010) ALDH1L2 is the mitochondrial homolog of 10-formyltetrahydrofolate dehydrogenase. J. Biol. Chem. 285: 23056–23063

Langfelder P & Horvath S (2008) WGCNA: an R package for weighted correlation network analysis. BMC Bioinformatics 9: 559

Lee A-H, Iwakoshi NN & Glimcher LH (2003) XBP-1 regulates a subset of endoplasmic reticulum resident chaperone genes in the unfolded protein response. Mol. Cell. Biol. 23: 7448–59

Lee E, de Ridder J, Kool J, Wessels LF a & Bussemaker HJ (2014) Identifying regulatory mechanisms underlying tumorigenesis using locus expression signature analysis. Proc. Natl. Acad. Sci. U. S. A. 111: 5747–52

Lee MG, Norman J, Shilatifard A & Shiekhattar R (2007a) Physical and Functional Association of a Trimethyl H3K4 Demethylase and Ring6a/MBLR, a Polycomb-like Protein. Cell 128: 877–887

Lee MS, Bonner JR, Bernard DJ, Sanchez EL, Sause ET, Prentice R, Burgess SM & Brody LC (2012a) Disruption of the folate pathway in zebrafish causes developmental defects. BMC Dev. Biol. 12: 12 1-11

Lee N, Zhang J, Klose RJ, Erdjument-Bromage H, Tempst P, Jones RS & Zhang Y (2007b) The trithorax-group protein Lid is a histone H3 trimethyl-Lys4 demethylase. Nat. Struct. Mol. Biol. 14: 341–3

Lee S, Birukov KG, Romanoski CE, Springstead JR, Lusis AJ & Berliner JA (2012b) Role of phospholipid oxidation products in atherosclerosis. Circ. Res. 111: 778–799

Levitan I & Shentu T-P (2011) Impact of oxLDL on Cholesterol-Rich Membrane Rafts. J. Lipids 2011: 1–11

Lewis CA, Parker SJ, Fiske BP, McCloskey D, Gui DY, Green CR, Vokes NI, Feist AM, Vander Heiden MG & Metallo CM (2014) Tracing Compartmentalized NADPH Metabolism in the Cytosol and Mitochondria of Mammalian Cells. Mol. Cell 55: 253–263

Li D & Mehta JL (2000) Upregulation of Endothelial Receptor for Oxidized LDL (LOX-1) by Oxidized LDL and Implications in Apoptosis of Human Coronary Artery Endothelial Cells. Arter. Thromb Vasc Biol 20: 1116–1122

Li D, Yang B & Mehta JL (1998) Ox-LDL induces apoptosis in human coronary artery endothelial cells: role of PKC, PTK, bcl-2, and Fas. Am. J. Physiol. 275: H568–H576

Li Q, Shi L, Gui B, Yu W, Wang J, Zhang D, Han X, Yao Z & Shang Y (2011) Binding of the JmjC demethylase JARID1B to LSD1/NuRD suppresses angiogenesis and metastasis in breast cancer cells by repressing chemokine CCL14. Cancer Res. 71: 6899–6908

Li R, Mouillesseaux KP, Montoya D, Cruz D, Gharavi N, Dun M, Koroniak L & Berliner JA (2006) Identification of prostaglandin E2 receptor subtype 2 as a receptor activated by OxPAPC. Circ. Res. 98: 642–650

Lim H-J, Dimova N V, Tan M-KM, Sigoillot FD, King RW & Shi Y (2013) The G2/M regulator histone demethylase PHF8 is targeted for degradation by the anaphase-promoting complex containing CDC20. Mol. Cell. Biol. 33: 4166–80

Liu W, Tanasa B, Tyurina O V, Zhou TY, Gassmann R, Liu WT, Ohgi KA, Benner C, Garcia-Bassets I, Aggarwal AK, Desai A, Dorrestein PC, Glass CK & Rosenfeld MG (2010) PHF8 mediates histone H4 lysine 20 demethylation events involved in cell cycle progression. Nature 466: 508–12

Lohman AW, Billaud M & Isakson BE (2012) Mechanisms of ATP release and signalling in the blood vessel wall. Cardiovasc. Res. 95: 269–280

Lohman AW & Isakson BE (2014) Differentiating connexin hemichannels and pannexin channels in cellular ATP release. FEBS Lett. 588: 1379–1388

Loscalzo J (2006) Homocysteine trials--clear outcomes for complex reasons. N. Engl. J. Med. 354: 1629–1632

Ma Y, Brewer JW, Alan Diehl J & Hendershot LM (2002) Two distinct stress signaling pathways converge upon the CHOP promoter during the mammalian unfolded protein response. J. Mol. Biol. 318: 1351–1365

Madigan D, York J & Allard D (1995) Bayesian graphical models for discrete data. Int. Stat. Rev. 63: 215–232

Magnusson M, Lewis GD, Ericson U, Orho-Melander M, Hedblad B, Engström G, Östling G, Clish C, Wang TJ, Gerszten RE & Melander O (2013) A diabetes-predictive amino acid score and future cardiovascular disease. Eur. Heart J. 34: 1982–1989

Mäkinen V-P, Civelek M, Meng Q, Zhang B, Zhu J, Levian C, Huan T, Segrè A V, Ghosh S, Vivar J, Nikpay M, Stewart AFR, Nelson CP, Willenborg C, Erdmann J, Blakenberg S, O'Donnell CJ, März W, Laaksonen R, Epstein SE, et al (2014) Integrative Genomics Reveals Novel Molecular Pathways and Gene Networks for Coronary Artery Disease. PLoS Genet. 10: e1004502 1-14

Malmberg SE & Adams CM (2008) Insulin signaling and the general amino acid control response: Two distinct pathways to amino acid synthesis and uptake. J. Biol. Chem. 283: 19229–19234

Marbach D, Prill RJ, Schaffter T, Mattiussi C, Floreano D & Stolovitzky G (2010) Revealing strengths and weaknesses of methods for gene network inference. Proc. Natl. Acad. Sci. U. S. A. 107: 6286–91

Mardinoglu A, Bjornson E, Zhang C, Klevstig M, Söderlund S, Ståhlman M, Adiels M, Hakkarainen A, Lundbom N, Kilicarslan M, Hallström BM, Lundbom J, Vergès B, Barrett PHR, Watts GF, Serlie MJ, Nielsen J, Uhlén M, Smith U, Marschall H, et al (2017) Personal model-assisted identification of NAD+ and glutathione metabolism as intervention target in NAFLD. Mol. Syst. Biol. 13: 1–17

Marinou K, Antoniades C, Tousoulis D, Pitsavos C, Goumas G & Stefanadis C (1995) Homocysteine: a risk factor for coronary artery disease? Hellenic J. Cardiol. 46: 59–67

Martinet W, De Loof H & De Meyer GRY (2014) MTOR inhibition: A promising strategy for stabilization of atherosclerotic plaques. Atherosclerosis 233: 601–607

McDonough MA, Loenarz C, Chowdhury R, Clifton IJ & Schofield CJ (2010) Structural studies on human 2-oxoglutarate dependent oxygenases. Curr. Opin. Struct. Biol. 20: 659–672

Medvedeva YA, Lennartsson A, Ehsani R, Kulakovskiy I V., Vorontsov IE, Panahandeh P, Khimulya G, Kasukawa T & Drabløs F (2015) EpiFactors: A comprehensive database of human epigenetic factors and complexes. Database 2015: 1–10

Mehrmohamadi M, Liu X, Shestov AA & Locasale JW (2014) Characterization of the Usage of the Serine Metabolic Network in Human Cancer. Cell Rep. 9: 1507–1519

Miller YI & Shyy JY-J (2017) Context-Dependent Role of Oxidized Lipids and Lipoproteins in Inflammation. Trends Endocrinol. Metab. 28: 143–152

Mittermayer F, Krzyzanowska K, Exner M, Mlekusch W, Amighi J, Sabeti S, Minar E, Müller M, Wolzt M & Schillinger M (2006) Asymmetric dimethylarginine predicts major adverse cardiovascular events in patients with advanced peripheral artery disease. Arterioscler. Thromb. Vasc. Biol. 26: 2536–2540

Morera L, Lübbert M & Jung M (2016) Targeting histone methyltransferases and demethylases in clinical trials for cancer therapy. Clin. Epigenetics 8: 57

Mueller MA, Beutner F, Teupser D, Ceglarek U & Thiery J (2008) Prevention of atherosclerosis by the mTOR inhibitor everolimus in LDLR-/- mice despite severe hypercholesterolemia. Atherosclerosis 198: 39–48

Myoishi M, Hao H, Minamino T, Watanabe K, Nishihira K, Hatakeyama K, Asada Y, Okada KI, Ishibashi-Ueda H, Gabbiani G, Bochaton-Piallat ML, Mochizuki N & Kitakaze M (2007) Increased endoplasmic reticulum stress in atherosclerotic plaques associated with acute coronary syndrome. Circulation 116: 1226–1233

Naj AC, Beecham GW, Martin ER, Gallins PJ, Powell EH, Konidari I, Whitehead PL, Cai G, Haroutunian V, Scott WK, Vance JM, Slifer MA, Gwirtsman HE, Gilbert JR, Haines JL, Buxbaum JD & Pericak-Vance MA (2010) Dementia Revealed: Novel Chromosome 6 Locus for Late-Onset Alzheimer Disease Provides Genetic Evidence for Folate-Pathway Abnormalities. PLoS Genet. 6: e1001130 1-10

Narayanan M, Huynh JL, Wang K, Yang X, Yoo S, McElwee J, Zhang B, Zhang C, Lamb JR, Xie T, Suver C, Molony C, Melquist S, Johnson AD, Fan G, Stone DJ, Schadt EE, Casaccia P, Emilsson V & Zhu J (2014) Common dysregulation network in the human prefrontal cortex underlies two neurodegenerative diseases. Mol. Syst. Biol. 10: 743 1-16

Nègre-Salvayre A, Augé N, Camaré C, Bacchetti T, Ferretti G & Salvayre R (2017) Dual signaling evoked by oxidized LDLs in vascular cells. Free Radic. Biol. Med. 106: 118–133

Neph S, Stergachis AB, Reynolds A, Sandstrom R, Borenstein E & Stamatoyannopoulos JA (2012) Circuitry and dynamics of human transcription factor regulatory networks. Cell 150: 1274–1286

Ng SS, Yue WW, Oppermann U & Klose RJ (2009) Dynamic protein methylation in chromatin biology. Cell. Mol. Life Sci. 66: 407–422

Nicholls SJ & Hazen SL (2009) Myeloperoxidase, modified lipoproteins, and atherogenesis: Fig. 1. J. Lipid Res. 50: S346–S351

Nikpay M, Goel A, Won H-H, Hall LM, Willenborg C, Kanoni S, Saleheen D, Kyriakou T, Nelson CP, Hopewell JC, Webb TR, Zeng L, Dehghan A, Alver M, Armasu SM, Auro K, Bjonnes A, Chasman DI, Chen S, Ford I, et al (2015) A comprehensive 1000 Genomes–based genome-wide association meta-analysis of coronary artery disease. Nat. Genet. 47: 1121–1130

Nilsson R, Jain M, Madhusudhan N, Sheppard NG, Strittmatter L, Kampf C, Huang J, Asplund A & Mootha VK (2014) Metabolic enzyme expression highlights a key role for MTHFD2 and the mitochondrial folate pathway in cancer. Nat. Commun. 5: 3128 1-10

Le Novère N (2015) Quantitative and logic modelling of molecular and gene networks. Nat. Rev. Genet. 16: 146–58

Nowak RP, Tumber A, Johansson C, Che KH, Brennan P, Owen D & Oppermann U (2016a) Advances and challenges in understanding histone demethylase biology. Curr. Opin. Chem. Biol. 33: 151–159

Okada T, Yoshida H, Akazawa R, Negishi M & Mori K (2002) Distinct roles of activating transcription factor 6 (ATF6) and double-stranded RNA-activated protein kinase-like endoplasmic reticulum kinase (PERK) in transcription during the mammalian unfolded protein response. Biochem. J. 366: 585–94

Osawa T, Muramatsu M, Wang F, Tsuchida R, Kodama T, Minami T & Shibuya M (2011) Increased expression of histone demethylase JHDM1D under nutrient starvation suppresses tumor growth via down-regulating angiogenesis. Proc. Natl. Acad. Sci. U. S. A. 108: 20725–9

Outinen P a, Sood SK, Pfeifer SI, Pamidi S, Podor TJ, Li J, Weitz JI & Austin RC (1999) Homocysteine-induced endoplasmic reticulum stress and growth arrest leads to specific changes in gene expression in human vascular endothelial cells. Blood 94: 959–967

Pan M-R, Hsu M-C, Chen L-T & Hung W-C (2016) G9a orchestrates PCL3 and KDM7A to promote histone H3K27 methylation. Sci. Rep. 5: 18709 1-8

Peden JF, Hopewell JC, Saleheen D, Chambers JC, Hager J, Soranzo N, Collins R, Danesh J, Elliott P, Farrall M, Stirrups K, Zhang W, Hamsten A, Parish S, Lathrop M, Watkins H, Clarke R, Deloukas P, Kooner JS, Goel A, et al (2011) A genome-wide association study in Europeans and South Asians identifies five new loci for coronary artery disease. Nat. Genet. 43: 339–344

Peri S, Navarro JD, Kristiansen TZ, Amanchy R, Surendranath V, Muthusamy B, Gandhi TKB, Chandrika KN, Deshpande N, Suresh S, Rashmi BP, Shanker K, Padma N, Niranjan V, Harsha HC, Talreja N, Vrushabendra BM, Ramya M a, Yatish a J, Joy M, et al (2004) Human protein reference database as a discovery resource for proteomics. Nucleic Acids Res. 32: D497–D501

Peters LA, Perrigoue J, Mortha A, Iuga A, Song W, Neiman EM, Llewellyn SR, Di Narzo A, Kidd BA, Telesco SE, Zhao Y, Stojmirovic A, Sendecki J, Shameer K, Miotto R, Losic B, Shah H, Lee E, Wang M, Faith JJ, et al (2017) A functional genomics predictive network model identifies regulators of inflammatory bowel disease. Nat. Genet. 49: 1437–1449

Pidkovka NA, Cherepanova OA, Yoshida T, Alexander MR, Deaton RA, Thomas JA, Leitinger N & Owens GK (2007) Oxidized phospholipids induce phenotypic switching of vascular smooth muscle cells in vivo and in vitro. Circ. Res. 101: 792–801

Di Pietro E, Sirois J, Tremblay ML & MacKenzie RE (2002) Mitochondrial NAD-dependent methylenetetrahydrofolate dehydrogenase-methenyltetrahydrofolate cyclohydrolase is essential for embryonic development. Mol. Cell. Biol. 22: 4158–66

Pikman Y, Puissant A, Alexe G, Furman A, Chen LM, Frumm SM, Ross L, Fenouille N, Bassil CF, Lewis CA, Ramos A, Gould J, Stone RM, DeAngelo DJ, Galinsky I, Clish CB, Kung AL, Hemann MT, Vander Heiden MG, Banerji V, et al (2016) Targeting MTHFD2 in acute myeloid leukemia. J. Exp. Med. 213: 1285–1306

Piper MK, Raza K, Nuttall SL, Stevens R, Toescu V, Heaton S, Gardner-Medwin J, Hiller L, Martin U, Townend J, Bacon PA & Gordon C (2007) Impaired endothelial function in systemic lupus erythematosus. Lupus 16: 84–88

Pircher A, Treps L, Bodrug N & Carmeliet P (2016) Endothelial cell metabolism : A novel player in atherosclerosis ? Basic principles and therapeutic opportunities. Atherosclerosis 253: 247–257

Podrez EA, Byzova T V, Febbraio M, Salomon RG, Ma Y, Valiyaveettil M, Poliakov E, Sun M, Finton PJ, Curtis BR, Chen J, Zhang R, Silverstein RL & Hazen SL (2007) Platelet CD36 links hyperlipidemia, oxidant stress and a prothrombotic phenotype. Nat. Med. 13: 1086–95

Potente M, Gerhardt H & Carmeliet P (2011) Basic and therapeutic aspects of angiogenesis. Cell 146: 873–887

Qi HH, Sarkissian M, Hu G, Wang Z, Bhattacharjee A, Gordon DB, Gonzales M, Lan F, Ongusaha PP, Huarte M, Yaghi NK, Lim H, Garcia BA, Brizuela L, Zhao K, Roberts TM & Shi Y (2010) Histone H4K20/H3K9 demethylase PHF8 regulates zebrafish brain and craniofacial development. Nature 466: 503–7

Richards NGJ & Kilberg MS (2006) Asparagine Synthetase Chemotherapy. Annu. Rev. Biochem. 75: 629–654

Riteau N, Baron L, Villeret B, Guillou N, Savigny F, Ryffel B, Rassendren F, Le Bert M, Gombault a & Couillin I (2012) ATP release and purinergic signaling: a common pathway for particle-mediated inflammasome activation. Cell Death Dis. 3: e403 1-10

Robinson MD, McCarthy DJ & Smyth GK (2009) edgeR: A Bioconductor package for differential expression analysis of digital gene expression data. Bioinformatics 26: 139–140

Romanoski CE, Che N, Yin F, Mai N, Pouldar D, Civelek M, Pan C, Lee S, Vakili L, Yang W-P, Kayne P, Mungrue IN, Araujo JA, Berliner JA & Lusis AJ (2011) Network for Activation of Human Endothelial Cells by Oxidized Phospholipids: A Critical Role of Heme Oxygenase 1. Circ. Res. 109: e27–e41

Ron-Harel N, Santos D, Ghergurovich JM, Sage PT, Reddy A, Lovitch SB, Dephoure N, Satterstrom FK, Sheffer M, Spinelli JB, Gygi S, Rabinowitz JD, Sharpe AH & Haigis MC (2016) Mitochondrial Biogenesis and Proteome Remodeling Promote One-Carbon Metabolism for T Cell Activation. Cell Metab. 24: 104–117

Sanson M, Auge N, Vindis C, Muller C, Bando Y, Thiers JC, Marachet MA, Zarkovic K, Sawa Y, Salvayre R & Negre-Salvayre A (2009) Oxidized low-density lipoproteins trigger endoplasmic reticulum stress in vascular cells: Prevention by oxygen-regulated protein 150 expression. Circ. Res. 104: 328–336

Schadt EE (2009) Molecular networks as sensors and drivers of common human diseases. Nature 461: 218–223

Schadt EE, Lamb J, Yang X, Zhu J, Edwards S, Guhathakurta D, Sieberts SK, Monks S, Reitman M, Zhang C, Lum PY, Leonardson A, Thieringer R, Metzger JM, Yang L, Castle J, Zhu H, Kash SF, Drake TA, Sachs A, et al (2005) An integrative genomics approach to infer causal associations between gene expression and disease. Nat. Genet. 37: 710–7

Schadt EE, Molony C, Chudin E, Hao K, Yang X, Lum PY, Kasarskis A, Zhang B, Wang S, Suver C, Zhu J, Millstein J, Sieberts S, Lamb J, GuhaThakurta D, Derry J, Storey JD, Avila-Campillo I, Kruger MJ, Johnson JM, et al (2008) Mapping the genetic architecture of gene expression in human liver. PLoS Biol. 6: 1020–1032

Schisler JC, Grevengoed TJ, Pascual F, Cooper DE, Ellis JM, Paul DS, Willis MS, Patterson C, Jia W & Coleman R a. (2015) Cardiac energy dependence on glucose increases metabolites related to glutathione and activates metabolic genes controlled by mechanistic target of rapamycin. J. Am. Heart Assoc. 4: e001136–e001136

Schnabel R, Lackner KJ, Rupprecht HJ, Espinola-Klein C, Torzewski M, Lubos E, Bickel C, Cambien F, Tiret L, Münzel T & Blankenberg S (2005) Glutathione peroxidase-1 and homocysteine for cardiovascular risk prediction: Results from the atherogene study. J. Am. Coll. Cardiol. 45: 1631–1637

Schwarz G (1978) Estimating the Dimension of a Model. Ann. Stat. 6: 461–464

Scull CM & Tabas I (2011) Mechanisms of ER stress-induced apoptosis in atherosclerosis. Arterioscler. Thromb. Vasc. Biol. 31: 2792–2797

Seye CI, Kong Q, Erb L, Garrad RC, Krugh B, Wang M, Turner JT, Sturek M, González FA & Weisman GA (2002) Functional P2Y2 nucleotide receptors mediate uridine 5′-triphosphate-induced intimal hyperplasia in collared rabbit carotid arteries. Circulation 106: 2720–2726

Shen L, Song C-X, He C & Zhang Y (2014) Mechanism and function of oxidative reversal of DNA and RNA methylation. Annu. Rev. Biochem. 83: 585–614

Shi Y, Lan F, Matson C, Mulligan P, Whetstine JR, Cole PA, Casero RA & Shi Y (2004) Histone demethylation mediated by the nuclear amine oxidase homolog LSD1. Cell 119: 941–953

Shi Y & Whetstine JR (2007) Dynamic Regulation of Histone Lysine Methylation by Demethylases. Mol. Cell 25: 1–14

Shin M, Bryant JD, Momb J & Appling DR (2014a) Mitochondrial MTHFD2L is a dual redox cofactor-specific methylenetetrahydrofolate dehydrogenase/methenyltetrahydrofolate cyclohydrolase expressed in both adult and embryonic tissues. J. Biol. Chem. 289: 15507–15517

Shin S, Fauman EB, Petersen A, Krumsiek J, Santos R, Huang J, Arnold M, Erte I, Forgetta V, Yang T, Walter K, Menni C, Chen L, Vasquez L, Valdes AM, Hyde CL, Wang V, Ziemek D, Roberts P, Xi L, et al (2014b) An atlas of genetic influences on human blood metabolites. Nat. Genet. 46: 543–550

Shirodaria C, Antoniades C, Lee J, Jackson CE, Robson MD, Francis JM, Moat SJ, Ratnatunga C, Pillai R, Refsum H, Neubauer S & Channon KM (2007) Global improvement of vascular function and redox state with low-dose folic acid: Implications for folate therapy in patients with coronary artery disease. Circulation 115: 2262–2270

Sieberts SK & Schadt EE (2007) Moving toward a system genetics view of disease. Mamm. Genome 18: 389–401

Singh KK, Shukla PC, Quan A, Al-Omran M, Lovren F, Pan Y, Brezden-Masley C, Ingram AJ, Stanford WL, Teoh H & Verma S (2013) BRCA1 is a novel target to improve endothelial dysfunction and retard atherosclerosis. J. Thorac. Cardiovasc. Surg. 146: 949–960

Siu F, Bain PJ, Leblanc-Chaffin R, Chen H & Kilberg MS (2002) ATF4 is a mediator of the nutrient-sensing response pathway that activates the human asparagine synthetase gene. J. Biol. Chem. 277: 24120–24127

Smith AD & Refsum H (2016) Homocysteine, B Vitamins, and Cognitive Impairment. Annu. Rev. Nutr. 36: 211–239

Springstead JR, Gugiu BG, Lee S, Cha S, Watson AD & Berliner J a (2012) Evidence for the importance of OxPAPC interaction with cysteines in regulating endothelial cell function. J. Lipid Res. 53: 1304–1315

Stelzl U, Worm U, Lalowski M, Haenig C, Brembeck FH, Goehler H, Stroedicke M, Zenkner M, Schoenherr A, Koeppen S, Timm J, Mintzlaff S, Abraham C, Bock N, Kietzmann S, Goedde A, Toksöz E, Droege A, Krobitsch S, Korn B, et al (2005) A human protein-protein interaction network: A resource for annotating the proteome. Cell 122: 957–968

Subramanian A, Tamayo P, Mootha VK, Mukherjee S & Ebert BL (2005) Gene set enrichment analysis : A knowledge-based approach for interpreting genome-wide. Proc Natl Acad Sci U S A 102: 15545–15550

Sun L, Huang Y, Wei Q, Tong X, Cai R, Nalepa G & Ye X (2015) Cyclin E-CDK2 protein phosphorylates plant homeodomain finger protein 8 (PHF8) and regulates its function in the cell cycle. J. Biol. Chem. 290: 4075–4085

Talukdar HA, Foroughi Asl H, Jain RK, Ermel R, Ruusalepp A, Franzen O, Kidd BA, Readhead B, Giannarelli C, Kovacic JC, Ivert T, Dudley JT, Civelek M, Lusis AJ, Schadt EE, Skogsberg J, Michoel T & Björkegren JLM (2016) Cross-Tissue Regulatory Gene Networks in Coronary Artery Disease. Cell Syst. 2: 196–208

Tang Y, Hong Y-Z, Bai H-J, Wu Q, Chen CD, Lang J-Y, Boheler KR & Yang H-T (2016) Plant Homeo Domain Finger Protein 8 Regulates Mesodermal and Cardiac Differentiation of Embryonic Stem Cells Through Mediating the Histone Demethylation of pmaip1. Stem Cells 34: 1527–1540

Tedeschi PM, Markert EK, Gounder M, Lin H, Dvorzhinski D, Dolfi SC, Chan LL-Y, Qiu J, DiPaola RS, Hirshfield KM, Boros LG, Bertino JR, Oltvai ZN & Vazquez a (2013) Contribution of serine, folate and glycine metabolism to the ATP, NADPH and purine requirements of cancer cells. Cell Death Dis. 4: e877 1-12

Tedeschi PM, Vazquez A, Kerrigan JE & Bertino JR (2015) Mitochondrial Methylenetetrahydrofolate Dehydrogenase (MTHFD2) Overexpression Is Associated with Tumor Cell Proliferation and Is a Novel Target for Drug Development. Mol. Cancer Res. 13: 1361–6

Thiel G, Mayer SI, Müller I, Stefano L & Rössler OG (2010) Egr-1-A Ca(2+)-regulated transcription factor. Cell Calcium 47: 397–403

Thomas D, Herold N, Keppler OT, Geisslinger G & Ferreirós N (2015) Quantitation of endogenous nucleoside triphosphates and nucleosides in human cells by liquid chromatography tandem mass spectrometry. Anal. Bioanal. Chem. 407: 3693–3704

Thomson MJ, Puntmann V & Kaski JC (2007) Atherosclerosis and oxidant stress: The end of the road for antioxidant vitamin treatment? Cardiovasc. Drugs Ther. 21: 195–210

Thorp E, Iwawaki T, Miura M & Tabas I (2011) A reporter for tracking the UPR in vivo reveals patterns of temporal and cellular stress during atherosclerotic progression. J. Lipid Res. 52: 1033–1038

Tibbetts AS & Appling DR (2010) Compartmentalization of Mammalian folate-mediated one-carbon metabolism. Annu. Rev. Nutr. 30: 57–81

Tousoulis D, Böger RH, Antoniades C, Siasos G, Stefanadi E & Stefanadis C (2007) Mechanisms of disease: L-arginine in coronary atherosclerosis - A clinical perspective. Nat. Clin. Pract. Cardiovasc. Med. 4: 274–283

Trapnell C, Pachter L & Salzberg SL (2009) TopHat: discovering splice junctions with RNA-Seq. Bioinformatics 25: 1105–1111

Tsimikas S, Mallat Z, Talmud PJ, Kastelein JJP, Wareham NJ, Sandhu MS, Miller ER, Benessiano J, Tedgui A, Witztum JL, Khaw KT & Boekholdt SM (2010) Oxidation-specific biomarkers, lipoprotein(a), and risk of fatal and nonfatal coronary events. J. Am. Coll. Cardiol. 56: 946–955

Tsukada Y -i., Ishitani T & Nakayama KI (2010) KDM7 is a dual demethylase for histone H3 Lys 9 and Lys 27 and functions in brain development. Genes Dev. 24: 432–437

Tsukada Y, Fang J, Erdjument-Bromage H, Warren ME, Borchers CH, Tempst P & Zhang Y (2006) Histone demethylation by a family of JmjC domain-containing proteins. Nature 439: 811–816

Tucker EJ, Hershman SG, Köhrer C, Belcher-Timme CA, Patel J, Goldberger OA, Christodoulou J, Silberstein JM, McKenzie M, Ryan MT, Compton AG, Jaffe JD, Carr SA, Calvo SE, RajBhandary UL, Thorburn DR & Mootha VK (2011) Mutations in MTFMT Underlie a Human Disorder of Formylation Causing Impaired Mitochondrial Translation. Cell Metab. 14: 428–434

Walport LJ, Hopkinson RJ & Schofield CJ (2012) Mechanisms of human histone and nucleic acid demethylases. Curr. Opin. Chem. Biol. 16: 525–534

Wang I-M, Zhang B, Yang X, Zhu J, Stepaniants S, Zhang C, Meng Q, Peters M, He Y, Ni C, Slipetz D, Crackower M a., Houshyar H, Tan CM, Asante-Appiah E, O'Neill G, Jane Luo M, Thieringer R, Yuan J, Chiu C-S, et al (2014) Systems analysis of eleven rodent disease models reveals an inflammatome signature and key drivers. Mol. Syst. Biol. 8: 594–594

Wang Q, Ma S, Song N, Li X, Liu L, Yang S, Ding X, Shan L, Zhou X, Su D, Wang Y, Zhang Q, Liu X, Yu N, Zhang K, Shang Y, Yao Z & Shi L (2016a) Stabilization of histone demethylase PHF8 by USP7 promotes breast carcinogenesis. J Clin Invest 126: 2205–2220

Wang S, Chennupati R, Kaur H, Iring A, Wettschureck N & Offermanns S (2016b) Endothelial cation channel PIEZO1 controls blood pressure by mediating flow-induced ATP release. J. Clin. Invest. 126: 1–10

Watson A, Leitinger N & Navab M (1997) Structural identification by mass spectrometry of oxidized phospholipids in minimally oxidized low density lipoprotein that induce monocyte/endothelial interactions. J. Biol. Chem. 272: 13597–13607

Weismann D & Binder CJ (2012) The innate immune response to products of phospholipid peroxidation. Biochim. Biophys. Acta - Biomembr. 1818: 2465–2475

Wu J & Kaufman RJ (2006) From acute ER stress to physiological roles of the Unfolded Protein Response. Cell Death Differ 13: 374–384

Wurtz P, Raiko JR, Magnussen CG, Soininen P, Kangas AJ, Tynkkynen T, Thomson R, Laatikainen R, Savolainen MJ, Laurikka J, Kuukasjarvi P, Tarkka M, Karhunen PJ, Jula A, Viikari JS, Kahonen M, Lehtimaki T, Juonala M, Ala-Korpela M & Raitakari OT (2012) High-throughput quantification of circulating metabolites improves prediction of subclinical atherosclerosis. Eur. Heart J. 33: 2307–2316

Yan MS-C, Matouk CC & Marsden PA (2010) Epigenetics of the vascular endothelium. J. Appl. Physiol. 109: 916–926

Yang X, Deignan JL, Qi H, Zhu J, Qian S, Zhong J, Torosyan G, Majid S, Falkard B, Kleinhanz RR, Karlsson J, Castellani LW, Mumick S, Wang K, Xie T, Coon M, Zhang C, Estrada-Smith D, Farber CR, Wang SS, et al (2009) Validation of candidate causal genes for obesity that affect shared metabolic pathways and networks. Nat. Genet. 41: 415–423

Yeh M, Cole AL, Choi J, Liu Y, Tulchinsky D, Qiao JH, Fishbein MC, Dooley AN, Hovnanian T, Mouilleseaux K, Vora DK, Yang WP, Gargalovic P, Kirchgessner T, Shyy JYJ & Berliner JA (2004) Role for sterol regulatory element-binding protein in activation of endothelial cells by phospholipid oxidation products. Circ. Res. 95: 780–788

Yokoyama A, Okuno Y, Chikanishi T, Hashiba W, Sekine H, Fujiki R & Kato S (2010) KIAA1718 is a histone demethylase that erases repressive histone methyl marks. Genes Cells 15: 867–73

Yoo S, Takikawa S, Geraghty P, Argmann C, Campbell J, Lin L, Huang T, Tu Z, Feronjy R, Spira A, Schadt EE, Powell C a & Zhu J (2015) Integrative Analysis of DNA Methylation and

Gene Expression Data Identifies EPAS1 as a Key Regulator of COPD. PLoS Genet. 11: e1004898 1-16

Yu S, Wong SL, Lau CW, Huang Y & Yu CM (2011) Oxidized LDL at low concentration promotes in-vitro angiogenesis and activates nitric oxide synthase through PI3K/Akt/eNOS pathway in human coronary artery endothelial cells. Biochem. Biophys. Res. Commun. 407: 44–48

Zhang B, Gaiteri C, Bodea L-G, Wang Z, McElwee J, Podtelezhnikov A a, Zhang C, Xie T, Tran L, Dobrin R, Fluder E, Clurman B, Melquist S, Narayanan M, Suver C, Shah H, Mahajan M, Gillis T, Mysore J, MacDonald ME, et al (2013) Integrated systems approach identifies genetic nodes and networks in late-onset Alzheimer's disease. Cell 153: 707–20

Zhang B & Horvath S (2005) A General Framework for Weighted Gene Co-Expression Network Analysis. Stat. Appl. Genet. Mol. Biol. 4: Article17 1-43

Zhang Q-J & Liu Z-P (2015) Histone methylations in heart development, congenital and adult heart diseases. Epigenomics 7: 321–330

Zhou J, Lhoták Š, Hilditch BA & Austin RC (2005) Activation of the unfolded protein response occurs at all stages of atherosclerotic lesion development in apolipoprotein E-deficient mice. Circulation 111: 1814–1821

Zhu J, Lum PY, Lamb J, GuhaThakurta D, Edwards SW, Thieringer R, Berger JP, Wu MS, Thompson J, Sachs AB & Schadt EE (2004) An integrative genomics approach to the reconstruction of gene networks in segregating populations. Cytogenet. Genome Res. 105: 363–374

Zhu J, Sova P, Xu Q, Dombek KM, Xu EY, Vu H, Tu Z, Brem RB, Bumgarner RE & Schadt EE (2012) Stitching together Multiple Data Dimensions Reveals Interacting Metabolomic and Transcriptomic Networks That Modulate Cell Regulation. PLoS Biol. 10: e1001301 1-19

Zhu J, Wiener MC, Zhang C, Fridman A, Minch E, Lum PY, Sachs JR & Schadt EE (2007) Increasing the power to detect causal associations by combining genotypic and expression data in segregating populations. PLoS Comput. Biol. 3: 692–703

Zhu J, Zhang B, Smith EN, Drees B, Brem RB, Kruglyak L, Bumgarner RE & Schadt EE (2008) Integrating large-scale functional genomic data to dissect the complexity of yeast regulatory networks. Nat. Genet. 40: 854–61

8 Apppendix

8.1 Selected key driver associated subnetworks

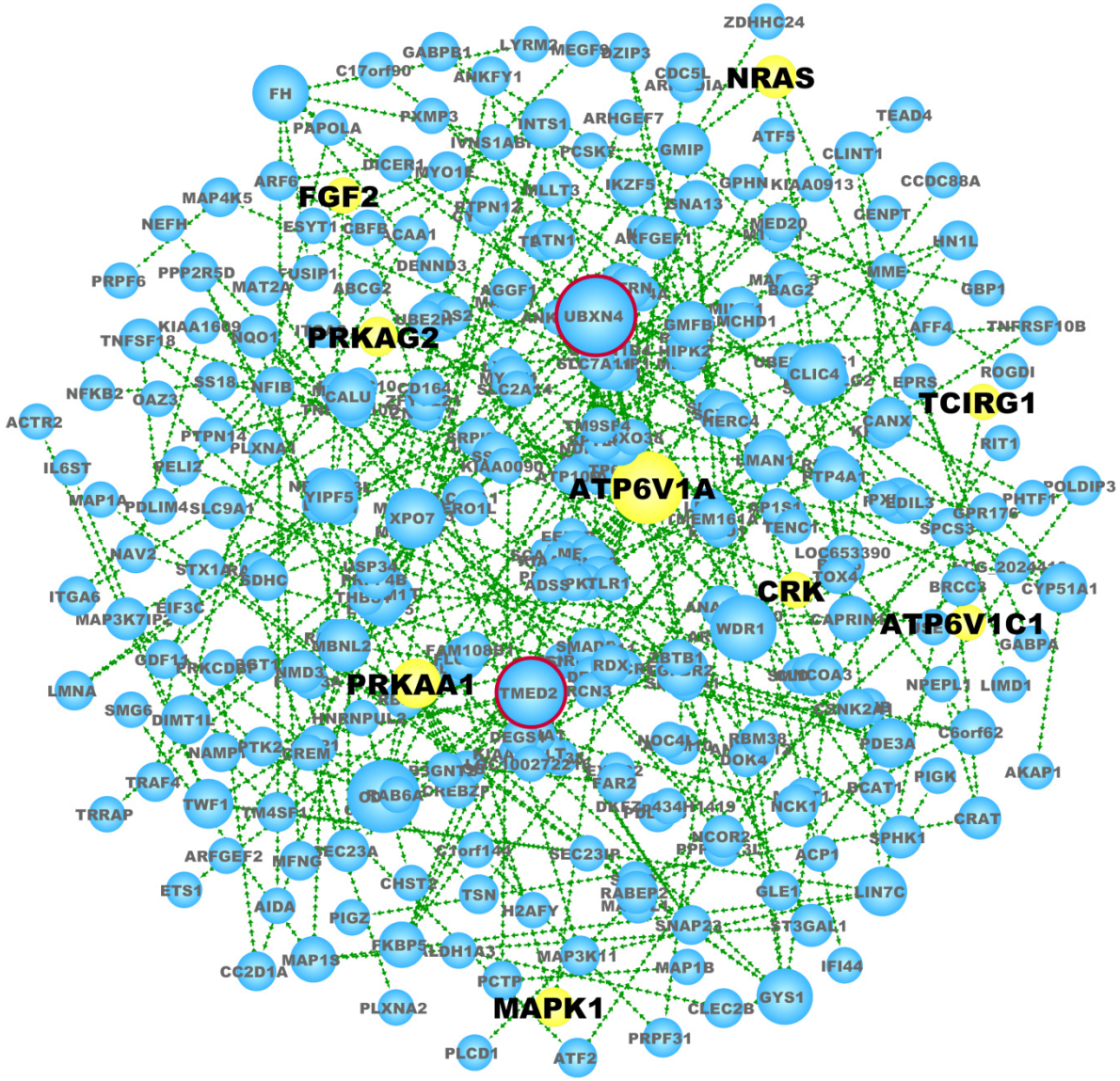

Figure 33: UBXN4 associated BN_{ox}.

Key drivers UBXN4 and TMED2 are highlighted in red. Genes which belong to the gene set category GO_GOLGI_ORGANIZATION are colored in yellow.

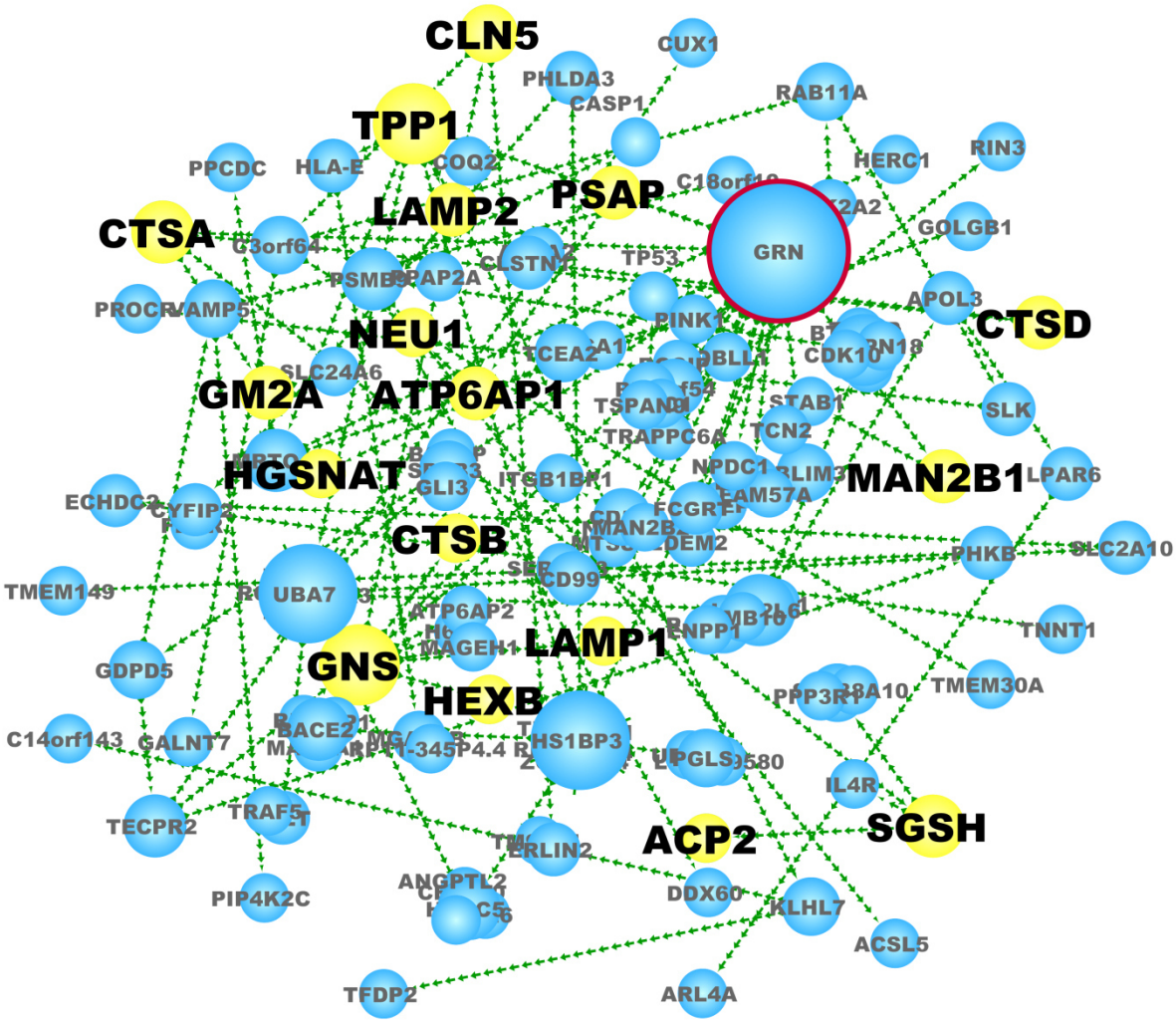

Figure 34: GRN associated BN_{ox}.

Key drvier GRN is highlighted in red. Genes which belong to the gene set category KEGG_LYSOSOME are colored in yellow.

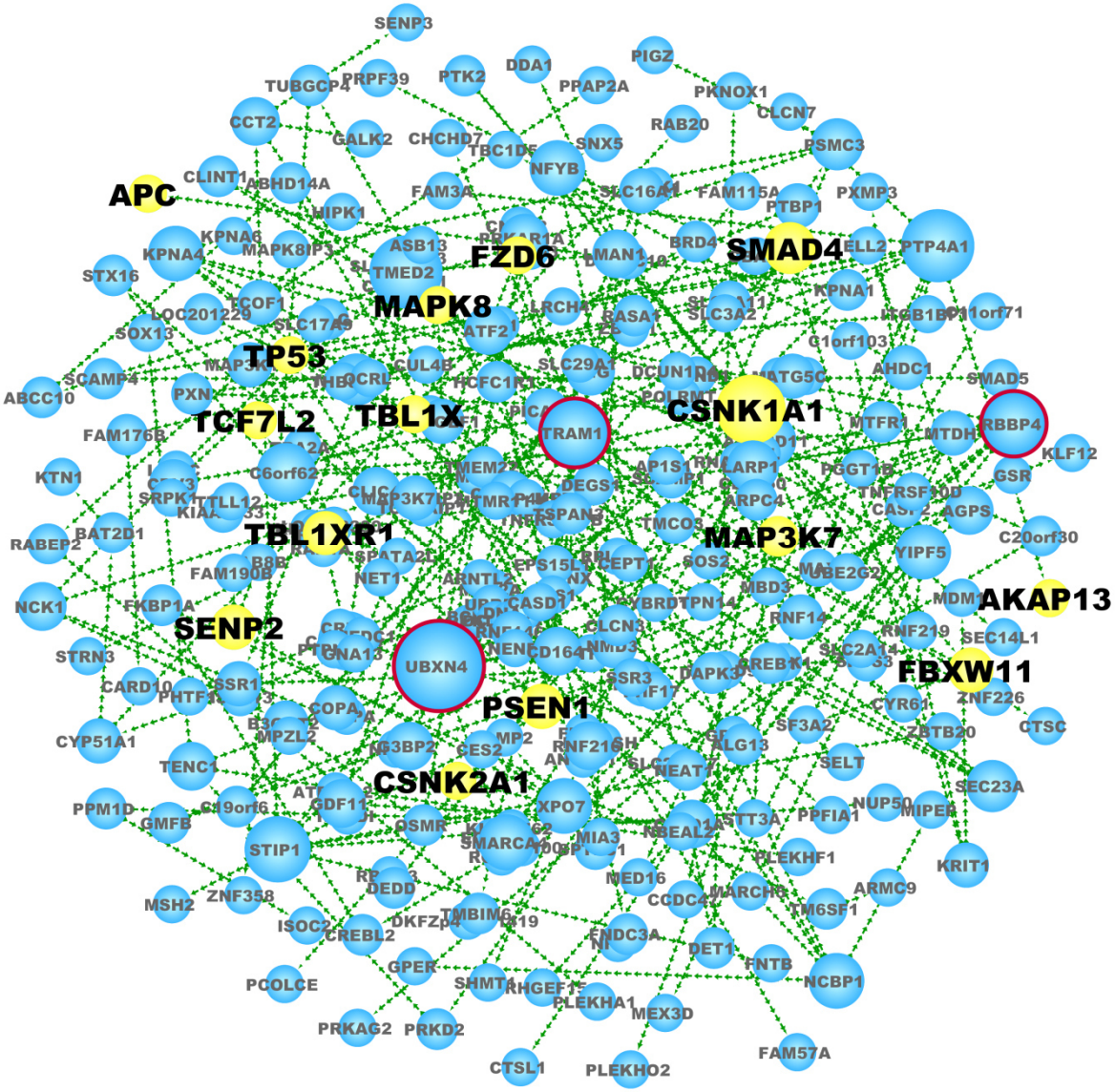

Figure 35: TRAM1 associated BN_{ct}.

Key drviers TRAM1, UBXN4 and RBBP4 are highlighted in red. Genes which belong to the gene set category KEGG_WNT_SIGNALING_PATHWAY are colored in yellow.

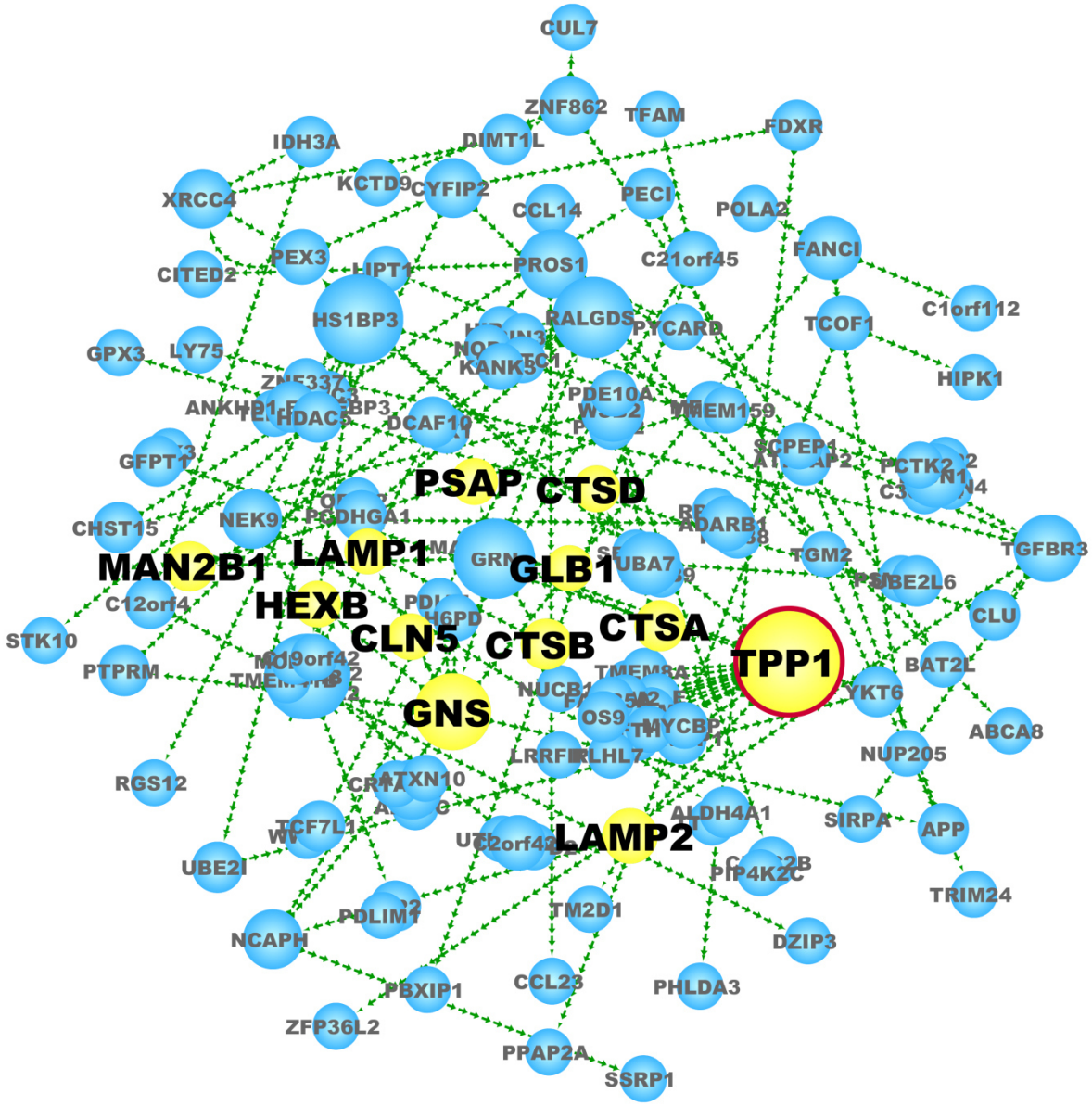

Figure 36: TPP1 associated BN_{ct}.

Key drvier TPP1 is highlighted in red. Genes which belong to the gene set category GO_VACUOLAR_LUMEN are colored in yellow.

8.2 Tables

Table 13: Genetic variances in genes in BN_{MTHFD2} associated with CAD risk.

List of genes in BN_{MTHFD2} with SNPs (meta-analysis p-value < $1x10^{-4}$) associated with Coronary artery disease (CAD) and myocardial infarction based on the CARDIoGRAMplusC4D consortium.

GeneSymbol	TxStart	TxEnd	markername	p_dgc
SORT1	1.1E+08	1.1E+08	rs7528419	7.05E-08
SLC7A1	30083550	30169825	rs9551751	7.93E-08
SORT1	1.1E+08	1.1E+08	rs12740374	1.25E-07
SORT1	1.1E+08	1.1E+08	rs4970834	1.04E-06
SORT1	1.1E+08	1.1E+08	rs611917	1.45E-06
SHMT2	57623827	57628718	rs11172113	1.72E-06
DDIT3	57910370	57914300	rs11172113	1.72E-06
MARS	57881735	57910438	rs11172113	1.72E-06
CEBPB	48807119	48809227	rs6095611	9.14E-06
CEBPB	48807119	48809227	rs1034056	1.38E-05
TUFT1	1.52E+08	1.52E+08	chr1:151745545:D	1.48E-05
CEBPB	48807119	48809227	rs6067199	1.59E-05
CEBPB	48807119	48809227	chr20:48333314:D	1.65E-05
FOXO1	41129800	41240734	rs9594389	1.68E-05
CEBPB	48807119	48809227	rs6091031	1.75E-05
FOXO1	41129800	41240734	rs7323896	1.78E-05
CEBPB	48807119	48809227	rs6067190	1.97E-05
CEBPB	48807119	48809227	rs913477	2.05E-05
CEBPB	48807119	48809227	rs3787327	2.17E-05
CEBPB	48807119	48809227	rs12329570	2.20E-05
CEBPB	48807119	48809227	rs6063420	2.29E-05
CEBPB	48807119	48809227	rs6095616	2.30E-05
GJA4	35258598	35261348	rs1336624	2.42E-05
CEBPB	48807119	48809227	rs6095618	2.47E-05
CEBPB	48807119	48809227	rs13044772	2.62E-05
TUFT1	1.52E+08	1.52E+08	rs6683364	2.87E-05
CEBPB	48807119	48809227	rs6067189	2.95E-05
CEBPB	48807119	48809227	rs6012717	3.13E-05
CEBPB	48807119	48809227	rs4810977	3.37E-05
CEBPB	48807119	48809227	rs913476	3.40E-05
TUFT1	1.52E+08	1.52E+08	rs3790514	3.54E-05
CEBPB	48807119	48809227	rs4809751	3.60E-05
CEBPB	48807119	48809227	rs1927781	3.62E-05
TUFT1	1.52E+08	1.52E+08	rs1054479	3.64E-05
CEBPB	48807119	48809227	rs4809753	3.66E-05
CEBPB	48807119	48809227	rs4810980	3.67E-05
CEBPB	48807119	48809227	rs4810979	3.68E-05
CEBPB	48807119	48809227	rs13043361	3.80E-05
CEBPB	48807119	48809227	rs35854666	3.83E-05
TUFT1	1.52E+08	1.52E+08	rs7542898	3.84E-05
CEBPB	48807119	48809227	rs74462005	3.88E-05
CEBPB	48807119	48809227	rs4810981	3.92E-05
FOXO1	41129800	41240734	rs7328137	4.06E-05
FOXO1	41129800	41240734	rs9603683	4.71E-05
FOSL1	65659691	65667997	rs12419237	4.82E-05
CDC42EP2	65082288	65089900	rs12419237	4.82E-05
PIK3C2B	2.04E+08	2.04E+08	rs16854023	5.57E-05
CEBPB	48807119	48809227	rs6012716	5.72E-05
FOXO1	41129800	41240734	rs9549073	5.88E-05
WASF3	27131839	27263082	rs9512451	6.89E-05
TUFT1	1.52E+08	1.52E+08	rs6673917	7.00E-05
MET	1.16E+08	1.16E+08	rs184476308	7.11E-05
TUFT1	1.52E+08	1.52E+08	rs6681093	7.34E-05
SLC47A1	19437166	19482346	rs7502682	7.47E-05

SLC47A1	19437166	19482346	rs2233072	7.62E-05
ARHGEF2	1.56E+08	1.56E+08	rs822509	7.92E-05
ARHGEF2	1.56E+08	1.56E+08	rs822505	8.13E-05
ARHGEF2	1.56E+08	1.56E+08	rs2948071	8.18E-05
GARS	30634180	30673648	rs142982771	8.26E-05
PPARD	35310334	35395968	rs10484578	8.37E-05
GARS	30634180	30673648	chr7:30374648:I	8.40E-05
MET	1.16E+08	1.16E+08	rs6951060	8.63E-05
SLC47A1	19437166	19482346	rs973649	8.93E-05
GARS	30634180	30673648	rs35295500	9.21E-05
SLC47A1	19437166	19482346	rs973650	9.33E-05
ARHGEF2	1.56E+08	1.56E+08	rs822527	9.39E-05
RCOR3	2.11E+08	2.11E+08	rs7540109	9.44E-05
FOXO1	41129800	41240734	rs4943737	9.59E-05

Table 14: Association between genes in BN_{MTHFD2} and plasma metabolites.

List of genes in BN_{MTHFD2} with SNPs (meta-analysis p-value < $1x10^{-4}$) associated with metabolites in human blood with physical locations of the variant within ±5 kb of gene bodies.

Gene	metabolonID	metabolonDescription	SNPs	p-value
SETX	M33801	ADpSGEGDFXAEGGGVR*	rs612169	9.66E-14
SETX	M33801	ADpSGEGDFXAEGGGVR*	rs644234	1.43E-13
SETX	M33801	ADpSGEGDFXAEGGGVR*	rs643434	1.45E-13
SETX	M33801	ADpSGEGDFXAEGGGVR*	rs514659	2.63E-13
SETX	M33801	ADpSGEGDFXAEGGGVR*	rs545971	3.33E-13
SETX	M33801	ADpSGEGDFXAEGGGVR*	rs674302	3.56E-13
SETX	M33801	ADpSGEGDFXAEGGGVR*	rs529565	5.41E-13
SETX	M33801	ADpSGEGDFXAEGGGVR*	rs505922	7.76E-13
SETX	M33801	ADpSGEGDFXAEGGGVR*	rs630014	3.53E-09
AARS	M01299	tyrosine	rs9936903	1.89E-08
AARS	M02734	gamma-glutamyltyrosine	rs9936903	9.21E-08
SETX	M32740	X-11423	rs643434	1.53E-07
SETX	M32740	X-11423	rs644234	1.54E-07
SETX	M32740	X-11423	rs529565	6.02E-07
SETX	M32740	X-11423	rs505922	6.02E-07
SETX	M32740	X-11423	rs674302	6.05E-07
SETX	M32740	X-11423	rs545971	6.13E-07
SETX	M32740	X-11423	rs514659	6.56E-07
SETX	M32740	X-11423	rs612169	7.99E-07
GJA4	M32654	3-dehydrocarnitine*	rs4609395	2.19E-06
SETX	M33084	ADSGEGDFXAEGGGVR*	rs529565	2.75E-06
SETX	M33084	ADSGEGDFXAEGGGVR*	rs505922	3.48E-06
SETX	M33084	ADSGEGDFXAEGGGVR*	rs514659	3.87E-06
SETX	M33084	ADSGEGDFXAEGGGVR*	rs612169	3.96E-06
SETX	M33084	ADSGEGDFXAEGGGVR*	rs545971	4.35E-06
SETX	M33084	ADSGEGDFXAEGGGVR*	rs674302	4.38E-06
SETX	M32808	X-11491	rs514659	6.61E-06
SETX	M32808	X-11491	rs545971	6.66E-06
SETX	M32808	X-11491	rs674302	6.99E-06
SETX	M32808	X-11491	rs612169	7.99E-06
GJA4	M32654	3-dehydrocarnitine*	rs4604660	1.20E-05
GJA4	M32654	3-dehydrocarnitine*	rs12725080	1.20E-05
SETX	M33801	ADpSGEGDFXAEGGGVR*	rs568203	1.24E-05
SETX	M32808	X-11491	rs505922	1.25E-05
SETX	M32808	X-11491	rs529565	1.26E-05
CBS	M32709	X-03056	rs4819388	1.40E-05
MTHFD2	M27710	N-acetylglycine	rs10174907	1.43E-05
SETX	M32808	X-11491	rs500498	1.60E-05
CBS	M32709	X-03056	rs7278940	1.62E-05
GJA4	M32654	3-dehydrocarnitine*	rs12058538	1.92E-05
GJA4	M32654	3-dehydrocarnitine*	rs7526321	1.92E-05

SETX	M32808	X-11491	rs644234	2.10E-05
SETX	M32808	X-11491	rs643434	2.10E-05
HERPUD1	M32616	X-11299	rs7185970	2.22E-05
CBS	M32709	X-03056	rs4818887	2.23E-05
PPARD	M37202	4-androsten-3beta,17beta-diol	rs6938138	2.35E-05
SETX	M33084	ADSGEGDFXAEGGGVR*	rs644234	2.52E-05
SETX	M33084	ADSGEGDFXAEGGGVR*	rs643434	2.53E-05
LYST	M22030	2-hydroxyisobutyrate	rs12136895	2.55E-05
SPRED2	M01645	laurate (12:0)	rs1344891	2.57E-05
PCK2	M15365	glycerol 3-phosphate (G3P)	rs1062230	2.60E-05
THG1L	M27273	X-10506	rs1052926	2.78E-05
GLDC	M32338	glycine	rs2297442	2.94E-05
HSPA13	M32489	caproate (6:0)	rs1297269	2.95E-05
NPC1	M31555	pyridoxate	rs13381663	3.71E-05
HERPUD1	M32616	X-11299	rs16960143	3.84E-05
CBS	M33587	eicosenoate (20:1n9 or 11)	rs3746963	4.02E-05
SPRED2	M01645	laurate (12:0)	rs7562559	4.15E-05
SPRED2	M01645	laurate (12:0)	rs1437461	4.15E-05
CBS	M32709	X-03056	rs3746963	4.85E-05
ARMC9	M01558	4-acetamidobutanoate	rs6734039	4.94E-05
ARMC9	M01558	4-acetamidobutanoate	rs12988432	4.95E-05
SHMT2	M36776	7-alpha-hydroxy-3-oxo-4-	rs11172833	4.95E-05
LTA4H	M01302	methionine	rs12579455	4.99E-05
TRIB3	M34350	X-12740	rs6051957	5.24E-05
STC2	M32867	X-11550	rs11134792	5.44E-05
FOSL2	M33230	1-	rs1881253	5.70E-05
SETX	M02132	citrulline	rs612169	5.91E-05
NAV3	M12017	3-methoxytyrosine	rs10746103	5.95E-05
SETX	M32740	X-11423	rs500498	6.33E-05
SETX	M02132	citrulline	rs545971	6.35E-05
SETX	M02132	citrulline	rs674302	6.39E-05
STC2	M32867	X-11550	rs11134793	6.66E-05
SETX	M02132	citrulline	rs514659	6.86E-05
TUFT1	M33422	gamma-glutamylphenylalanine	rs10888547	6.88E-05
FOSL2	M33960	1-oleoylglycerophosphocholine	rs1881253	6.99E-05
GJA4	M34481	X-12798	rs12058538	6.99E-05
GJA4	M34481	X-12798	rs7526321	6.99E-05
HERPUD1	M32616	X-11299	rs7203177	7.11E-05
ARMC9	M22649	X-09108	rs12988432	7.31E-05
CBS	M33587	eicosenoate (20:1n9 or 11)	rs4818887	7.35E-05
ARMC9	M22649	X-09108	rs6734039	7.36E-05
KIF3A	M18369	gamma-glutamylleucine	rs2243211	7.50E-05
KIF3A	M18369	gamma-glutamylleucine	rs2243210	7.57E-05
SETX	M36230	X-14304	rs643434	7.67E-05
SETX	M36230	X-14304	rs644234	7.70E-05
FOSL2	M33230	1-	rs13017378	7.81E-05
SETX	M31548	DSGEGDFXAEGGGVR*	rs529565	7.88E-05
EPAS1	M00054	tryptophan	rs1530628	8.13E-05
ANKRD46	M32838	X-11521	rs7007746	8.30E-05
SPRED2	M27718	creatine	rs2118304	8.31E-05
DAPK1	M01712	cortisol	rs11142238	8.33E-05
TRIB3	M36673	X-14745	rs2295495	8.43E-05
EPAS1	M27710	N-acetylglycine	rs1530628	8.69E-05
SETX	M31548	DSGEGDFXAEGGGVR*	rs612169	8.81E-05
HERPUD1	M33163	X-11818	rs16960143	8.86E-05
CBS	M33587	eicosenoate (20:1n9 or 11)	rs4819388	9.04E-05
NFIL3	M03127	hypoxanthine	rs1152759	9.13E-05
SETX	M31548	DSGEGDFXAEGGGVR*	rs514659	9.20E-05
TUFT1	M34420	bradykinin, des-arg(9)	rs10788864	9.29E-05
FOSL2	M33230	1-	rs11127162	9.39E-05
SETX	M31548	DSGEGDFXAEGGGVR*	rs545971	9.43E-05
EPAS1	M27710	N-acetylglycine	rs2197698	9.45E-05

FOSL2	M33821	1-	rs11127164	9.49E-05
SETX	M31548	DSGEGDFXAEGGGVR*	rs674302	9.52E-05
SETX	M31548	DSGEGDFXAEGGGVR*	rs505922	9.59E-05
SLC7A5	M33961	1-stearoylglycerophosphocholine	rs4785651	9.75E-05
EPAS1	M27710	N-acetylglycine	rs1530627	9.76E-05

8.3 List of figures

8.4 List of tables

8.5 Abbreviations

°C	Degree Celsius
µg	Mikrogramm
µl	Mikroliter
µM	Mikromolar
10-fTHF	10-Formyl tetrahydrofolate
5,10-meTHF	5,10-methylene tetrahydrofolate
5-meTHF	5-methylene tetrahydrofolate
AARs	Aminoacyl tRNA synthetases
ALDH1L1/2	Aldehyde dehydrogenase 1 family member L1/2
AMPS	Ammonium peroxodisulfate
ARMCX2	Armadillo repeat containing, X-linked 2
ASNS	Asparagine synthetase
ASPM	Abnormal spindle microtubule assembly
ATF4	Activating transcription factor 4
ATIC	5-Aminoimidazole-4-carboxamide ribonucleotide formyltransferase / IMP cyclohydrolase
ATP	Adenosine triphosphate
BIC	Bayesian information criterion
BIM-I	Bisindolmaleimide I
BN	Bayesian network
BN_{ct}	control Bayesian network
BN_{MTHFD2}	MTHFD2 Bayesian subnetwork
BN_{ox}	oxPAPC Bayesian network
BRCA1	DNA Repair Associated 1
CAD	Coronary artery disease
CARDIoGRAMplusC4D	Coronary artery disease genome wide replication and meta-analysis plus the coronary artery disease genetics consortium
CARS	Cysteinyl-tRNA synthetase
CBS	cystathionine-beta-synthase
CCCP	carbonyl cyanide-3-chlorophenylhydrazone
CCNB1/2	Cyclin B1/2
CDC20	Cell division cycle 20
CDCA3	Cell division cycle associated 3
CDF	Cumulative distribution function
CDKN3	Cyclin dependent kinase inhibitor 3
CEBPB	CCAAT/enhancer binding protein beta

CEP	2-(ω-car-boxyethyl)Pyrrole
CHAC1	ChaC glutathione specific gamma-glutamylcyclotransferase 1
CKS1B	CDC28 protein kinase regulatory subunit 1B
COPD	Chronic obstructive pulmonary disease
C_t	Cycle threshold
CTH	Cystathionine gamma-lyase
CVD	Cardiovascular disease
Cyclo-EC	Epoxycyclopentenones
DC	Differential connectivity
DDIT3/CHOP	DNA damage inducible transcript 3
DE	Differential expression
DEG	Differentially expressed genes
DHFR	Dihydrofolate reductase
DMSO	Dimethylsulfoxide
DNA	Deoxyribonucleic acid
DNAJB1	DnaJ heat shock protein family member B1
dNTP	Desoxy nucleotide triphosphate
DOCK9	Dedicator of cytokinesis 9
DPBS	Dulbecco`s phosphate buffered saline
DPYSL2	Dihydropyrimidinase like 2
DTT	Dithiothreitol
DUT	Deoxyuridine triphosphatase
EBM	Endothelial basal medium
EBNA1BP2	EBNA1 binding protein 2
EC	Endothelial cell
ECGS-H	bovine hypotha-lamic extract
EDTA	Ethylenediaminetetraacetic acid
EGF	Epidermal growth factor
EGM	Endothelial growth medium
EGR1	Early growth response 1
EGTA	Ethylene glycol tetraacetic acid
EHHADH	Enoyl-CoA hydratase and 3-hydroxyacyl CoA dehydrogenase
EMG1	EMG1, N1-specific pseudouridine methyltransferase
eNOS	endothelial nitric oxide synthase
eQTL	Expression quantitative trait loci
ER	Endoplasmic reticulum
EtOH	Ethanol

F3	Coagulation factor III, tissue factor
FCS	Fetal calf serium
FDR	False discovery rate
FET	Fisher’s exact test
FFA	Flufenamic acid
fMET	N-formyl methionine
g	Gramm
G6PD	Glucose-6-phosphate dehydrogenase
GARS	Glycyl-tRNA Synthetase
GART	Phosphoribosylglycinamide formyltransferase, phosphoribosylglycinamide synthetase, phosphoribosylaminoimidazole synthetase
GCLM	Glutamate-cysteine ligase modifier subunit
GEO	Gene expression omnibus
GINS1	GINS complex subunit 1
GLDC	Glycine decarboxylase
GMNN	Geminin, DNA replication inhibitor
GO	Gene ontology
GOC	Gain of connectivity
GOC-AA	Gain of connectivity cluster 6 (amino acid)
GOT1	Glutamic oxaloacetic transaminase 1
GRN	Granulin precursor
GSEA	Gene set enrichment analysis
GSS	Glutathione synthetase
GTP	Guanosine triphosphate
GWAS	Genome wide association study
H3K4me2	Histone 3 Lysine 4 dimethylation
HAEC	Human aortic endothelial cells
HASMC	Human aortic smooth muscle cells
HCl	Hydrochloric acid
hEGF	human epidermal growth factor
HEK293	Human embryonic kidney cells 293
HEPES	N-2-Hydroxyethylpiperazin-N'-2-ethansulfonsäure
HisOH	L-Histidinol
HO1/HMOX1	Heme oxygenase 1
HPRD	Human protein reference database
HSPA1A	Heat shock protein family A member 1A

HUVEC	Human umbilical vein endothelial cell
IFIH1	Interferon induced with helicase C domain 1
IFIT1/3	Interferon induced protein with tetratricopeptide repeats 1/3
IFNβ	Interferon beta
IL1β	Interleukin 1 beta
ITGAV	Integrin subunit alpha V
JHDM1D-AS1	JHDM1D antisense RNA 1
JmjC	Jumonji C
JMJD	Jumonji domain containing
kb	kilobase
K_{cat}	catalytic rate
KCl	Potassium chloride
kDa	Kilodalton
KDM7A	Lysine demethylase 7A
KDR	Kinase insert domain receptor
KIF4A	Kinesin family member 4A
K_M	Michaelis constant
KOdiAPC	1-palmitoyl-2-(5-keto-6-octene-dioyl)-sn-glycero-3-phosphocholine
L	Liter
LDL	Low density lipoprotein
LDLR	Low density lipoprotein receptor
lncRNA	long non coding RNA
LOC	Loss of connectivity
LPS	Lipopolysaccharide
LSD1/2	Lysine-specific histone demethylase 1/2
mA	Milliampere
MARS	Methionyl-tRNA synthetase
MCMC	Monte Carlo Markov chain
MDA	Malondialdehyde
MEM	Minimum essential medium
mg	milligramm
min	minute
ml	milliliter
mM	millimolar
mmol	millimol
mRNA	messenger RNA

MRTO4	MRT4 homolog, ribosome maturation factor
MSigDB	Molecular signatures databse
MTFMT	Mitochondrial methionyl-tRNA formyltransferase
MTHFD1	Methylenetetrahydrofolate dehydrogenase, cyclohydrolase and formyltetrahydrofolate synthetase 1
MTHFD1L/2L	Methylenetetrahydrofolate dehydrogenase ($NADP^+$ dependent) 1/2-like
MTHFD2	Methylenetetrahydrofolate dehydrogenase ($NADP^+$ dependent) 2, methenyltetrahydrofolate cyclohydrolase
MTHFR	Methylenetetrahydrofolate reductase
mTOR	Mechanistic target of rapamycin
mTORC1/2	Mechanistic target of rapamycin complex 1/2
MTR	5-Methyltetrahydrofolate-homocysteine methyltransferase
NAC	N-Acetyl-L-cysteine
NaCl	Sodium chloride
NAD	Nicotinamide adenine dinucleotide
NADPH	Nicotinamide adenine dinucleotide phosphat
NAT	Natural antisense transcript
NDC80	NDC80, kinetochore complex component
NEK2	NIMA related kinase 2
NHDN	N-hob downstream nodes
NISCH	Nischarin
nm	nanometer
nM	nanomolar
NO	Nitric oxide
NP	nondeterministic polynomial
NUSAP1	Nucleolar and spindle associated protein 1
OA	Ocadaic acid
OV	Orthovanadate
oxCE	oxidized cholesteryl ester
oxLDL	oxidized low density lipoproteins
oxPAPC	oxidized PAPC
oxPC	oxidized phosphatidylcholine
oxPE	oxidized phosphatidylethanolamine
oxPL	oxidized phospholipid
PAGE	Polyacrylamide gel electrophoresis
OCR	Oxygen consumption rate

PAPC	1-palmitoyl-2-arachidonoyl-sn-glycero-3-phosphocholine
PBK	PDZ binding kinase
PBMC	Peripheral blood mononuclear cell
PBS	Phosphate buffered saline
PCDH12	Protocadherin 12
PCK2	Phosphoenolpyruvate carboxykinase 2
PDSS1	Decaprenyl diphosphate synthase subunit 1
PECPC	1-palmitoyl-2-(5,6-epoxyisoprostane A2)-sn-glycero-3-phosphocholine
PEIPC	1-palmitoyl-2-(5,6-epoxyisoprostanoyl)-sn-glycero-3-phosphocholine
PFA	Paraformaldehyde
PFKFB3	6-Phosphofructo-2-kinase/fructose-2,6-biphosphatase 3
PGF	Placental growth factor
PGPC	1-Palmitoyl-2-glutaryl-sn-glycero-3-phosphocholine
PHD	Plant homeo domain
PHF8	PHD finger protein 8
PHGDH	Phosphoglycerate dehydrogenase
PKC	Protein kinase C
PLK1/4	Polo like kinase 1/4
PMA	Phorbol-12-myristate-13-acetate
PMSF	Phenylmethylsulfonylfluoride
PNMA2	Paraneoplastic Ma antigen 2
POVPC	1-Palmitoyl-2-(5-oxovaleroyl)-sn-glycero-3-phospho-choline
PPM1F	Protein phosphatase Mg^{2+}/Mn^{2+} dependent 1F
PSAT1	Phosphoserine aminotransferase 1
PSPH	Phosphoserine phosphatase
PUFA	polyunsaturated fatty acid
qPCR	Quantitative polymerase chain reaction
RAD51AP1	RAD51 associated protein 1
RBBP4	RB binding protein 4 chromatin remodeling factor
RGN	Regulatory gene network
RNA	Ribonucleic acid
RNAseq	RNA sequencing
ROS	Reactive oxygen species
Rpm	Rounds per minutes
RT	Reverse transkriptase

SAM	S-adenosyl methionine
SBC/SBIC	Schwarz criterion
SC4MOL	Sterol-C4-methyl oxidase-like
SDS	Sodium dodecylsulfate
SEM	Standard error of the mean
SERPINE1	Serpin family E member 1
SFRS1	Serine and arginine rich splicing factor 1
SGSM2	Small G protein signaling modulator 2
SHMT1/2	Serine hydroxymethyltransferase 1
siRNA	Small interfering ribonucleic acid
SLC1A5	Solute carrier family 1 member 5
SLC3A2	Solute carrier family 3 member 2
SLC7A1	Solute carrier family 7 member 1
SLC7A5	Solute carrier family 7 member 5
SLE	Systemic lupus erythematodes
SMURF2	SMAD specific E3 ubiquitin protein ligase 2
SNP	Single nucleotide polymorphism
SQLE	Squalene epoxidase
STC2	Stanniocalcin 2
sXBP1	spliced x-box binding protein 1
SYPL1	Synaptophysin like 1
TAF9B	TATA-Box binding protein associated factor 9b
TBC1D8	TBC1 domain family member 8
TCF7L2	Transcription factor 7 like 2
TEMED	Tetramethylethylendiamine
THF	Tetrahydrofolate
TIPIN	TIMELESS interacting protein
TMED2	Transmembrane P24 trafficking protein 2
TMOD3	Tropomodulin 3
TNFSF10	TNF superfamily member 10
TOP	topological overlap matrix
TPP1	Tripeptidyl peptidase 1
TRAM1	Translocation associated membrane protein 1
TRIB3	Tribbles pseudokinase 3
TRIS	Tris (hydroxymethyl) aminomethane
tRNA	transfer ribonucleic acid
TSPAN7	Tetraspanin 7

TSS	Transcriptional start site
TXNRD1	Thioredoxin reductase 1
TYMS	Thymidylate synthetase
UBXN4	UBX domain protein 4
UCHL5	Ubiquitin C-terminal hydrolase L5
UPGMA	Unweighted pair group method with arithmetic mean
UPR	Unfolded protein response
VEGFA	Vascular endothelial growth factor A
WGCNA	weighted gene co-expression network analysis
YARS	Tyrosyl-tRNA synthetase
YWHAZ	Tyrosine 3-monooxygenase/tryptophan 5-monooxygenase activation protein zeta
YY1	YY1 transcription factor
ZWILCH	Zwilch kinetochore protein

8.6 Declaration

Except where stated otherwise by reference or acknowledgement, the work presented was generated by myself under the supervision of my advisors Prof. Ralf Brandes and Prof. Jun Zhu during my doctoral studies. All contributions obtained from colleagues and in the context of collaborative research are explicitly listed below:

Figure 11: Differential connectivity clusters of HAEC exposed to oxPAPC. Yi Zhang; Department of Mathematics, Hebei University of Science and Technology, Shijiazhuang Hebei, China; computation of DC clusters. Eunjee Lee; Icahn Institute of Genomics and Multiscale Biology, Mount Sinai Icahn School of Medicine, New York; DC cluster visualization. Juliane Hitzel; GSEA and figure preparation

Figure 12: Validation of HAEC Bayesian networks. Eunjee Lee; Icahn Institute of Genomics and Multiscale Biology, Mount Sinai Icahn School of Medicine, New York; assistance with computation. Juliane Hitzel; processing of endothelial signatures and figure preparation

Figure 13: HAEC Bayesian networks. Jun Zhu; Icahn Institute of Genomics and Multiscale Biology, Mount Sinai Icahn School of Medicine, New York; construction and provision of the Bayesian networks. Eunjee Lee; Icahn Institute of Genomics and Multiscale Biology, Mount Sinai Icahn School of Medicine, New York; assistance with visualization. Juliane Hitzel; network visualization, key driver analysis, subnetwork extraction, GSEA

Figure 16: RNAseq validation of MTHFD2 Bayesian subnetwork. Eunjee Lee; Icahn Institute of Genomics and Multiscale Biology, Mount Sinai Icahn School of Medicine, New York; processing of RNAseq data. Juliane Hitzel; HAEC treatment, heatmap creation, DEG projection onto network, network visualization, venn diagram

Figure 18: Expression of genes in the BNMTHFD2 in human aortic plaques. Eunjee Lee; Icahn Institute of Genomics and Multiscale Biology, Mount Sinai Icahn School of Medicine, New York; assistance with computation. Juliane Hitzel; assistance with data processing and figure preparation

Figure 19: Heatmap of amino acid profile in HAEC. Sven Zukunft; Institute for Vascular Signalling, Centre for Molecular Medicine, Goethe University, Frankfurt am Main; mass spectrometry measurement. Juliane Hitzel; HAEC treatment, data analysis, heatmap creation

Figure 20: A: MTHFD2 is required for glycine synthesis in human aortic smooth muscle cells. Sven Zukunft; Institute for Vascular Signalling, Centre for Molecular Medicine, Goethe University, Frankfurt am Main; mass spectrometry measurement. Beatrice Pflüger; Institute for Cardiovascular Physiology, Goethe University, Frankfurt am Main; smooth muscle cell treatment. Juliane Hitzel; data analysis, heatmap creation

Figure 21: Glycine, but not serine or asparagine prevents the induction of the Bayesian amino acid subnetwork. Sven Zukunft; Institute for Vascular Signalling, Centre for Molecular

Medicine, Goethe University, Frankfurt am Main; mass spectrometry measurement. Juliane Hitzel; HAEC treatment, qPCR, data analysis

Figure 22: Glycine prevents the impairment of spheroid outgrowth in response to MTHFD2 knockdown. Matthias Leisegang; Institute for Cardiovascular Physiology, Goethe University, Frankfurt am Main; spheroid outgrowth assay. Juliane Hitzel; migration assay

Figure 23: OxPAPC elicits ATP release. Dominique Thomas; Institute of Clinical Pharmacology, Pharmazentrum Frankfurt/ZAFES, Faculty of Medicine, Goethe University, Frankfurt am Main; mass spectrometry measurement. Dmitry Namgaladze; Institute of Biochemistry I, Goethe University, Frankfurt am Main; OCR measurement. Juliane Hitzel; HAEC treatment, qPCR, ATP measurement

Figure 30: KDM7A is associated with interferon signaling. Eunjee Lee; Icahn Institute of Genomics and Multiscale Biology, Mount Sinai Icahn School of Medicine, New York; assistance with computation. Juliane Hitzel; SLE data processing

Figure 31: KDM7A is associated with PKC activity. Eunjee Lee; Icahn Institute of Genomics and Multiscale Biology, Mount Sinai Icahn School of Medicine, New York; assistance with computation. Juliane Hitzel; HUVEC treatment, qPCR, WB

Figure 32: The PKC-EGR1-KDM7A axis. Eunjee Lee; Icahn Institute of Genomics and Multiscale Biology, Mount Sinai Icahn School of Medicine, New York; assistance with computation; Beatrice Pflüger; Institute for Cardiovascular Physiology, Goethe University, Frankfurt am Main; ChIP experiment. Juliane Hitzel; HUVEC experiments

Table 8: Association between genes in the BNMTHFD2 and CAD risk loci. Genetic variances in genes in the BNMTHFD2 associated with CAD risk. Eunjee Lee; Icahn Institute of Genomics and Multiscale Biology, Mount Sinai Icahn School of Medicine, New York; assistance with computation. Juliane Hitzel; figure preparation

Table 9: Association between genes in the BNMTHFD2 and plasma metabolites. Eunjee Lee; Icahn Institute of Genomics and Multiscale Biology, Mount Sinai Icahn School of Medicine, New York; assistance with computation; figure preparation

Table 11: Significantly enriched gene set categories in KDM7A signature. Wei Chen; Max-Delbrück-Center for Molecular Medicine, Berlin; Mario Looso; Max Planck Institute for Heart and Lung Research, Bad Nauheim; RNAseq measurement and pre-processing. Juliane Hitzel; RNAseq analysis, GSEA

Whenever a figure or table or text is identical to a previous publication, it is referenced explicitly. Copyright permission and co-author agreement has been obtained.

The following parts of the thesis have been previously published:

- Figures 10-19, 21-24
- Tables 1-9

8.9 Publications

Hitzel J, Lee E, Zhang Y, Bibli SI, Li X, Zukunft S, Pflüger B, Hu J, Schürmann C, Vasconez AE, Oo JA, Kratzer A, Kumar S, Rezende F, Josipovic I, Thomas D, Giral H, Schreiber Y, Geisslinger G, Fork C, Yang X, Sigala F, Romanoski CE, Kroll J, Jo H, Landmesser U, Lusis AJ, Namgaladze D, Fleming I, Leisegang MS, Zhu J, Brandes RP. Oxidized phospholipids regulate amino acid metabolism through MTHFD2 to facilitate nucleotide release in endothelial cells. *Nat Commun.* 2018 Jun 12;9(1):2292. doi: 10.1038/s41467-018-04602-0

Josipovic I, Pflüger B, Fork C, Vasconez AE, Oo JA, **Hitzel J**, Seredinski S, Gamen E, Heringdorf DMZ, Chen W, Looso M, Pullamsetti SS, Brandes RP, Leisegang MS. Long noncoding RNA LISPR1 is required for S1P signaling and endothelial cell function. *J Mol Cell Cardiol.* 2018 Jan 31;116:57-68; doi: 10.1016/j.yjmcc.2018.01.015

Gu L, **Hitzel J**, Moll F, Kruse C, Malik RA, Preussner J, Looso M, Leisegang MS, Steinhilber D, Brandes RP, Fork C. The Histone Demethylase PHF8 Is Essential for Endothelial Cell Migration. *PLoS One*. 2016 Jan 11;11(1):1-15

Fork C, Gu L, **Hitzel J**, Josipovic I, Hu J, SzeKa Wong M, Ponomareva Y, Albert M, Schmitz SU, Uchida S, Fleming I, Helin K, Steinhilber D, Leisegang MS, Brandes RP. Epigenetic Regulation of Angiogenesis by JARID1B-Induced Repression of HOXA5. *Arterioscler Thromb Vasc Biol.* 2015 Jul;35(7):1645-1652

Fork C, **Hitzel J**, Nichols BJ, Tikkanen R, Brandes RP. Flotillin-1 facilitates toll-like receptor 3 signaling in human endothelial cells. *Basic Res Cardiol.* 2014;109(6):4391-13